EJBCS

Eurasian Journal of Biological and Chemical Sciences (Eurasian J. Bio. Chem. Sci.)

Cilt: 5 Volume: 1 Year: 2022

e-ISSN 2651-5237

EJBCS
Eurasian Journal of Biological and Chemical Sciences

Cilt: 5 Volume: 1 Year: 2022

Published Biannually

Corresponding Address
Gaziantep University, Faculty of Arts and Sciences, Department of Biology, Gaziantep, Turkey
E-mail: mtdogan1@gmail.com
Web: http://www.dergipark.org.tr/ejbcs

Owner / Publisher
Muhammet DOĞAN
This journal is peer-reviewed and published twice (June, December) a year.

e-ISSN 2651-5237

EJBCS
Eurasian Journal of Biological and Chemical Sciences

Cilt: 5 Volume: 1 Year: 2022

Contents / İçindekiler

RESEARCH ARTICLE
Eurasian J Bio Chem Sci, 5(1):1-4, 2022
https://doi.org/10.46239/ejbcs.1003863

EJBCS

Eurasian Journal of Biological and Chemical Sciences

Journal homepage: www.dergipark.org.tr/ejbcs

Effect of vitamin B3 supplementation on glutathione redox cycle

Adem Keskin[1*]

[*1]*Aydın Adnan Menderes University, Institute of Health Sciences, Department of Biochemistry (Medicine), Aydın, Turkey*

*Corresponding author : ademkeskin78@gmail.com
Orcid No: https://orcid.org/0000-0003-1921-2583

Received : 02/10/2021
Accepted : 14/01/2022

Abstract: In this study, the effect of vitamin B3 supplement given to rats was investigated on glutathione redox cycle by looking at glutathione peroxidase and glutathione s transferase activities. 20 Wistar albino male rats were used. Vitamin B3 supplement was given to one of the two groups that were formed. The other group was determined as the control group. 360 mg/kg/day vitamin B3 supplement was given by oral gavage method for 10 days. At the end of 10 days, intracardiac blood samples were taken. Glutathione peroxidase activity level was determined as 1033.44±198.05 U/L in the vitamin B3 supplement group and 526.00±99.54 U/L in the control group. The glutathione peroxidase activity level of the vitamin B3 supplemented group was found to be statistically significantly higher than the glutathione peroxidase activity level of the control group ($p<0.001$, $t=7.239$). This difference has huge impact size ($d=3.24$). Glutathione s transferase activity level was determined as 6.50±0.97 U/mL in the vitamin B3 supplement group and 7.50±0.67 U/mL in the control group. The glutathione s transferase activity level of the group given vitamin B3 supplementation was found to be statistically significantly lower than the glutathione s transferase activity level of the control group ($p=0.015$, $t=2.698$). This difference has a very large effect size ($d=1.20$). As a result, vitamin B3 supplementation led to an increase in glutathione peroxidase activity at a huge effect size and a decrease in glutathione s transferase activity at a very large effect size.

Keywords: Vitamin B3, Glutathione peroxidase, Glutathione s transferase, Glutathione redox cycle

1. Introduction

Glutathione is a simple sulfur compound that is non-protein and consists of three amino acids. The functions of glutathione are very diverse. In particular, redox and homeostatic buffering are in the foreground. Glutathione status is modulated by oxidants as well as nutrition and other factors. Changes in the thiol-disulfide balance can affect its structure and activity (Noctor et al. 2011).

Glutathione's functions include detoxifying electrophilic xenobiotics such as chemical carcinogens, environmental pollutants, and antitumor agents (Hayes et al. 2005). The classical activity of glutathione transferases is the conjugation of compounds with electrophilic centers to the tripeptide glutathione (Oakley 2011).

Selenium-containing glutathione peroxidase, which has an important role in redox reactions and is involved in the glutathione cycle, protects against oxidative damage, inhibits inflammation and oxidant-induced regulated cell death (Brigelius-Flohe and Flohe 2020). Oxidized glutathione is formed by glutathione peroxidase, which is involved in the redox cycle of glutathione. Glutathione reductase, which is involved in the conversion of this oxidized glutathione to reduced glutathione, is responsible for maintaining the reduced glutathione supply (Couto et al. 2016). Glutathione reductase catalyzes the reduction of glutathione disulfide, dependent on nicotinamide adenine dinucleotide phosphate, for the supply of reduced glutathione (Belorgey et al. 2013).

The functional cofactors derived from vitamin B3 are nicotinamide adenine dinucleotide (NAD^+), its phosphorylated form, nicotinamide adenine dinucleotide phosphate ($NADP^+$), and their reduced forms (NAD(P)H). These cofactors, called the NAD(P)(H) pool, are closely related in all major bioenergetic, anabolic and catabolic pathways in all life forms. This pool also contributes to post-translational protein modifications and second messenger generation (Makarov et al. 2019).

Vitamin B3 is the precursor of NADPH, a cofactor in the glutathione redox cycle, which has an important role in redox, homeostatic buffering and xenobiotic detoxification. In this study, the effect of vitamin B3 supplementation on the activities of glutathione peroxidase and glutathione transferase enzymes involved in the glutathione redox cycle was investigated.

2. Materials and Method

The study is qualitatively an experimental animal study. The ethics committee decision required for the study was obtained from the Animal Experiments Local Ethics Committee of Aydın Adnan Menderes University. In the study, 20 Wistar Albino male rats weighing between 380-465 grams were used. Two groups of ten were formed. One group was given a vitamin B3 supplement. The other group was determined as the control group.

2.1. Operations on rats

The study was planned as 10 days. During this time frame, one group was given a daily vitamin B3 supplement. Vitamin B3 was obtained from Sigma-Aldrich as a powder preparation of 100 grams. A solution was prepared from the powder preparation in order to give it to the rats by oral gavage method. Determination of solution dose; It was determined based on the study of Kwon et al. (2018). Each animal was weighed every day and 360 mg/kg/day vitamin B3 supplement was given by oral gavage method. Both groups exercised 30 minutes after vitamin B3 supplementation. The purpose of exercise was to activate the glutathione cycle more by increasing the oxidative stress level in rats. One day after the tenth day of vitamin B3 supplementation, blood samples were taken by intracardiac route.

2.2. Biochemical processes

Approximately seven ml of blood samples were taken intracardiacly and centrifuged at 3000 rpm for five minutes. Serum samples were taken. The method of Paglia and Valentina (1967) was used for glutathione peroxidase activity analysis. In this method, glutathione peroxidase activity is calculated by monitoring the decrease in the absorbance value of NADPH, which is oxidized per minute at a wavelength of 340 nm. The glutathione s transferase colorimetric analysis kit, which is the kit of the Elabscience brand, was used for glutathione s transferase activity analysis,. Biotek Epoch (Canada) device was used for these analyses.

2.3. Statistical analysis

SPSS for Windows 22.0 program was used for statistical analysis. Data obtained from the study were given as mean±standard deviation (X±SD), and P values below 0.05 were considered statistically significant. The groups were compared with an independent sample t-test. The effect sizes were calculated based on the t values obtained and the studies of Cohen (1988) and Sawilowsky (2009).

3. Results

In this study, glutathione peroxidase activity level was determined as 1033.44±198.05 U/L in the vitamin B3 supplement group and 526.00±99.54 U/L in the control group (Table 1). Glutathione peroxidase activity levels of the groups were compared with an independent sample t test. As a result of this comparison, the glutathione peroxidase activity level of the group given vitamin B3 supplementation was found to be statistically significantly higher than the glutathione peroxidase activity level of the control group ($p<0.001$ $t=7.239$). According to the effect size calculation based on Cohen (1988) and Sawilowsky (2009) studies on effect size, a significant difference with a huge effect size ($d=3.24$) was found between the groups.

In this study, glutathione s transferase activity level was determined as 6.50±0.97 U/mL in the vitamin B3 supplement group and 7.50±0.67 U/mL in the control group (Table 1). Glutathione s transferase activity levels of the groups were compared with independent sample t test. As a result of this comparison, the glutathione s transferase activity level of the vitamin B3 supplemented group was found to be statistically significantly lower than the glutathione s transferase activity level of the control group ($p=0.015$ $t=2.698$). According to the effect size calculation based on Cohen (1988) and Sawilowsky (2009) studies on effect size, a significant difference with a very large effect size ($d=1.20$) was found between the groups.

Table 1. Glutathione Peroxidase and Glutathione S Transferase enzyme activity level mean and standard deviations of the groups

Enzyme	Vitamin B3 Group	Control Group	p	d
Glutathione Peroxidase (U/L)	1033.44± 198.05	526.00± 99.54	<0.001	3.24
Glutathione S Transferase (U/mL)	6.50± 0.97	7.50± 0.67	0.015	1.20

4. Discussion

Vitamin B3 and its derivatives, nicotinamide adenine dinucleotides, play important roles in the cellular redox state, Ca^{+2} stores, DNA damage and repair, stress responses, cell cycle timing, and lipid and energy conservation and regulation. It is stated that the metabolism associated with them occupies a central place in the aging processes of mammals (Xu and Sauve 2010). One of these associated sites of metabolism is the glutathione redox cycle. Glutathione is at the center of the glutathione redox cycle, has a thiol tripeptide structure. Glutathione is found in almost every compartment of the cell, including the nucleus. Transport between different intracellular compartments is crucial for the regulation of cell proliferation (Vivancos et al. 2010).

Glutathione is involved in many other reactions such as glutathionylation of proteins, neutralization of superoxides, and detoxification of metabolites through conjugation (Bachhawat and Yadav 2018). The basic and earliest known function of glutathione is thiol-disulfide interactions, where it is converted back to reduced glutathione by NADPH-dependent glutathione reductase. The central role of glutathione in defense metabolism in animals has long been established as selenium-dependent glutathione peroxidase is a central pillar of animal antioxidant metabolism (Noctor et al. 2012).

Glutathione s transferase plays a multifunctional role in the detoxification mechanism, including the activation of

cytochrome P450 as well as the conjugation of phase two system oxidants (Jones et al. 2007).

Many studies have been conducted on the link between glutathione and vitamins. Liang et al. (1999) investigated the effect of vitamin B2 deficiency on glutathione levels in their study with rats. In this study, glutathione levels were found to be low in rats fed a diet devoid of vitamin B2 for 6 weeks. Another study with a diet deprived of vitamin B2 for 12 weeks found a decrease in glutathione levels (Huang et al. 2010). In a study conducted with rats infected with Trichinella spiralis, a decrease in glutathione peroxidase activity was found with vitamin B2 deficiency (Tumkiratiwong et al. 2003). A similar conclusion was reached in a another study on vitamin B2 and beta carotene, precursor of vitamin A (Shenhu et al. 1999). A review on vitamin B2 states that vitamin B2 has an antioxidant effect as a component of the glutathione redox cycle (Ashoori and Saedisomeolia 2014). In the study of Ponce et al. (2011), they concluded that the daily release of the glutathione redox cycle decreases in vitamin A deficiency. They stated that they found retinoid- as well as clock-responsive sites on regulatory regions of glutathione reductase and glutathione peroxidase genes. Vitamin D has also been found to increase glutathione in the brain by upregulating brain gamma-glutamyl transpeptidase, an enzyme involved in the glutathione cycle (Garcion et al. 2002). Van Haaften et al. (2003), stated that antioxidants such as vitamin E have protective effects on glutathione-dependent enzymes. In addition, it has been stated that vitamin E, together with glutathione and a heat-sensitive membrane-bound factor, can prevent the harmful effects of reactive oxygen species on polyunsaturated fatty acids in biomembranes. In the study of Waly et al. (2015), it was determined that the consumption of glutathione increased in healthy young people who were fed low in vitamin C, and as a result, it induced oxidative stress.

In our study, glutathione peroxidase activity was found to be significantly higher in the vitamin B3 given group compared to the control group. The effect size of this result has been found to be huge. This is due to NADPH, a derivative of vitamin B3. At the same time, NADPH is the cofactor of the glutathione reductase enzyme. In addition, glutathione reductase is an enzyme involved in the glutathione redox cycle. The Meyer-Ficca et al. (2016) study confirms this result. Meyer-Ficca et al. (2016) stated that there is a intimate connection between dietary vitamin B3 intake and resulting NAD concentrations. In a study conducted with rats, it was stated that retinal NAD levels decrease with aging and this causes a tendency to glaucoma. In the same study, it was stated that glaucoma did not develop with oral vitamin B3 administration (Williams et al. 2017). Lappas et al. (2011) found that nicotinamide (a vitamin B3 derivative) treatment of human placenta caused an increase in glutathione peroxidase gene expression. Overdose of acetaminophen causes severe oxidative stress. In a study with rats whose liver was damaged by acetaminophen, they determined the prophylactic and therapeutic effects of vitamin B3 (Mahmoud and Mahmoud 2016).

In our study, Glutathione s transferase activity was found to be significantly lower in the vitamin B3 given group compared to the control group. The effect size of this result has been found to be very large. This is because reduced glutathione is a substrate for both glutathione s transferase and glutathione peroxidase. Therefore, an increase in glutathione peroxidase enzyme activity at a huge effect size led to a very large effect size decrease in glutathione s transferase activity.

5. Conclusion

As a result, vitamin B3 supplementation in rats caused an increase in glutathione peroxidase activity at a huge effect size and a decrease in glutathione s transferase activity at a very large effect size. In cases where oxidative stress increases (exercise, infection, excessive drug use, etc.), glutathione levels decrease. In addition, glutathione levels decrease in old age and long-term vitamin deficiency. In these cases, vitamin B3 supplementation can be used to continue the Glutathione redox cycle in order to reduce the damage caused by oxidative stress.

References

Ashoori M, Saedisomeolia A. 2014. Riboflavin (vitamin B2) and oxidative stress: a review. Br J Nutr. 111(11):1985-1991.

Bachhawat AK, Yadav S. 2018. The glutathione cycle: Glutathione metabolism beyond the γ-glutamyl cycle. IUBMB Life. 70(7):585-592.

Belorgey D, Antoine Lanfranchi D, Davioud-Charvet E. 2013. 1,4-Naphthoquinones and Other NADPH-Dependent Glutathione Reductase- Catalyzed Redox Cyclers as Antimalarial Agents. Curr Pharm Des. 19(14):2512-2528.

Brigelius-Flohe R, Flohe L. 2020. Regulatory Phenomena in the Glutathione Peroxidase Superfamily. Antioxid Redox Signal. 33(7):498-516.

Cohen J. 1988. Statistical Power Analysis for the Behavioral Sciences. 2nd edn. Lawrence Erlbaum Associates. New York.

Couto N, Wood J, Barber J. 2016. The role of glutathione reductase and related enzymes on cellular redox homoeostasis network. Free Radic Biol Med. 95:27-42.

Garcion E, Wion-Barbot N, Montero-Menei C, Berger F, Wion D. 2002. New clues about vitamin D in the nervous system. Trends Endocrinol Metab. 13:100-105.

Hayes JD, Flanagan JU, Jowsey IR. 2005. Glutathione Transferases. Annu Rev Pharmacol Toxicol. 45:51-88.

Huang, J, Tian, L, Wu, X, Yang H, Liu Y. 2010. Effects of dietary riboflavin levels on antioxidant defense of the juvenile grouper Epinephelus coioides . Fish Physiol Biochem. 36:55-62.

Jones CI, Zhu H, Martin SF, Han Z, Li Y, Alevriadou BR. 2007. Regulation of antioxidants and phase 2 enzymes by shear-induced reactive oxygen species in endothelial cells. Ann Biomed Eng. 35:683-693.

Kwon WY, Suh GJ, Kim KS, Jung YS, Kim SH, Lee R, et al. 2018. Niacin And Selenium Attenuates Brain Injury After Cardiac Arrest By Upregulatıng Dj-1-Akt Signaling. Crit Care Med. 46(1):125.

Lappas M, Permezel M. 2011. The anti-inflammatory and antioxidative effects of nicotinamide, a vitamin B3

derivative, are elicited by FoxO3 in human gestational tissues: implications for preterm birth. J Nutr Biochem. 22(12):1195-1201.

Liang H, Liu Q, Xu, J. 1999. The effect of riboflavin on lipid peroxidation in rats. Wei Sheng Yan Jiu. 28:370–371.

Makarov MV, Trammell SAJ, Migaud ME. 2019. The chemistry of the vitamin B3 metabolome. Biochem Soc Trans. 47(1):131–147.

Mahmoud YI, Mahmoud AA. 2016. Role of nicotinamide (vitamin B3) in acetaminophen-induced changes in rat liver: Nicotinamide effect in acetaminophen-damged liver. Exp Toxicol Pathol. 68(6):345-354.

Meyer-Ficca M, Kirkland JB. 2016. Niacin. Adv Nutr. 7(3):556-558

Noctor G, Queval G, Mhamdi A, Chaouch S, Foyer CH. 2011. Glutathione. TAB. 9:e0142.

Noctor G, Mhamdi A, Chaouch S, Han Y, Neukermans J, Marquez-Garcia B, Queval G, Foyer CH. 2012. Glutathione in plants: an integrated overview. Plant Cell Environ. 35(2):454-484.

Oakley A. 2011. Glutathione transferases: a structural perspective. Drug Metab Rev. 43(2):138-151.

Paglia DE, Valentine WN. 1967. Studies on the quantitative and qualitative characterization of erythrocyte glutathione peroxidase. J Lab Clin Med. 70(1):158-169.

Ponce IT, Rezza IG, Delgado SM, Navigatore LS, Bonomi MR, Golini RL, Gimenez MS, Anzulovich AC. 2011. Daily oscillation of glutathione redox cycle is dampened in the nutritional vitamin A deficiency. Biol Rhythm Res. 43(4):351-372.

Sawilowsky S. 2009. New effect size rules of thumb. J Mod Appl Stat Methods. 8(2): 467-474.

Shenhu W, Jie M, Qixuan C, Yuechu X, Yuming C, Huilian Z. 1999. Effect of beta-carotene and riboflavin on lipid peroxidation in rats. Acta Nutr Sin. 21:22-27.

Tumkiratiwong, P, Tungtrongchitr, R, Migasena, P, Pongpaew P, Rojekittikhun W, Vudhivai N. 2003. Antioxidant enzyme levels in the erythrocytes of riboflavin-deficient and Trichinella spiralis-infected rats. Southeast Asian J Trop Med Public Health. 34:480-485.

Van Haaften RIM, Haenen GRMM, Evelo CTA, Bast A. 2003. Effect of Vitamin E on Glutathione-Dependent Enzymes. Drug Metab Rev. 35(2-3):215-253.

Vivancos PD, Wolff T, Markovic J, Pallardo FV, Foyer CH. 2010. A nuclear glutathione cycle within the cell cycle. Biochem. 431(2):169-178.

Waly M, Al-Attabi Z, Guizani N. 2015. Low Nourishment of Vitamin C Induces Glutathione Depletion and Oxidative Stress in Healthy Young Adults. Prev Nutr Food Sci. 20(3):198-203.

Williams PA, Harder JM, Foxworth NE, Cochran KE, Philip VM, Porciatti V, et al. 2017. Vitamin B3 modulates mitochondrial vulnerability and prevents glaucoma in aged mice. Science. 355(6326):756-760.

Xu P, Sauve AA. 2010. Vitamin B3, the nicotinamide adenine dinucleotides and aging. Mech Ageing Dev. 131(4):287-298.

RESEARCH ARTICLE
Eurasian J Bio Chem Sci, 5(1):5-8, 2022
https://doi.org/10.46239/ejbcs.1034194

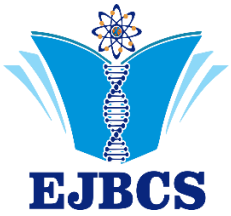

Eurasian Journal of Biological and Chemical Sciences

Journal homepage: www.dergipark.org.tr/ejbcs

Diphenylcarbazone and tartrazine as sensitizer metal complex dyes for dye sensitized solar cells

Burak Ünlü[1,2*], Serbülent Türk[1,2], Mahmut Özacar[2,3]

*[*1]Sakarya University, Biomedical, Magnetic and Semiconductor Materials Application and Research Center (BIMAS-RC), 54187, Sakarya, Turkey.*
[2]Sakarya University, Biomaterials, Energy, Photocatalysis, Enzyme Technology, Nano & Advanced Materials, Additive Manufacturing, Environmental Applications and Sustainability Research & Development Group, (BIOENAMS R & D Group), 54187, Sakarya, Turkey.
[3]Sakarya University, Department of Chemistry, Faculty of Science & Arts, 54187, Sakarya, Turkey.

*Corresponding author : burakunlu@sakarya.edu.tr
Orcid No: https://orcid.org/ 0000-0001-5109-9686

Received : 08/12/2021
Accepted : 10/04/2022

Abstract: Dye sensitized solar cells (DSSCs) are photovoltaic devices that produce electricity from the photon energy of sunlight using dyes. Dyes used DSSCs should have a broad absorption spectrum at the UV-Vis region and should be strongly bound to the photoanode surface. Dyes are used in DSSCs can be classified into three types: metal complex dyes, metal-free organic dyes and natural dyes. For metal complex dyes, ruthenium is usually used as metal centers. While most Ru complex dyes have high efficiency, Ru is a rare metal. To decrease the cost of Ru complex dyes, transition metals are widely investigated. In this work, diphenylcarbazone and tartrazine with different metal complexes were synthesized and investigated for their suitability for DSSCs. UV-Vis was used for the characterization of dyes and linear sweep voltammetry and electrochemical impedance spectroscopy were used to investigate the performance of DSSCs.

Keywords: Dye sensitized solar cells, metal complex dyes, diphenyl carbazone, tartrazine

1. Introduction

Dye sensitized solar cells (DSSCs) are classified in 3. Generation solar cells that convert sunlight to electricity by the photovoltaic effect. After Gratzel published the first paper about DSSCs (Oregan and Gratzel 1991), dye sensitized solar cells have attracted scientists' attention because of their easy preparation and use of low-cost materials. However, DSSCs cannot compete with other solar cells by the aspect of light conversion efficiency (Sharma et al. 2017). Therefore, intensive research has been done on DSSCs.

DSSCs consist of four main parts: photoanode, dye, electrolyte and counter electrode (Jena et al. 2012). As photoanode, semiconductor metal oxide coated transparent conductive oxide substrates (FTO or ITO) are usually used. TiO_2, ZnO, SnO_2 are usually used as semiconductor metal oxide photoanode materials (Kumar et al. 2017). The main roles of photoanodes in DSSCs are collection of the excited electrons from the dye LUMO and carry forward to these electrons through an external circuit to counter electrode (Jung and Lee 2013). As electrolyte usually redox couple including organic solvents are used. In this regard, I^-/I_3^- is usually used as a liquid electrolyte (Wu et al. 2015). Electrolytes are collected electrons from the counter electrode and give an electron to the excited dye molecule to regenerate it simultaneously (Gong et al. 2017). Counter electrodes used in DSSCs are generally platinum coated FTO and collect electrons from the external circuit and regenerate redox couple in the electrolyte (Sugathan et al. 2015).

Dyes are one of the essential components of DSSCs because electron excitation/movement starts with dye molecules. Dyes used in DSSCs can be categorized as Metal complex dyes, metal-free organic dyes and natural dyes (Mishra et al. 2009). Although metal-free organic dyes have a high molar absorption coefficient and can be manipulated to change suitable molecular geometry or HOMO-LUMO energy levels, solar cells' efficiency using this type of dye is low. Natural dyes are cheap sensitizers obtained from

plants, herbs, vegetables etc., but they have very poor stability (Richhariya et al. 2017). Metal complex dyes have high stability and broad light absorption at the UV-VIS region. However, rare and expensive ruthenium metal is used as metal center at metal complex dyes at dye sensitized solar cells.

Tartrazine (trisodium 1-(4-sulfonatophenyl)-4-(4-sulfonatophenylazo)-5-pyrazolone-3-carboxylate)) is a yellow-colored synthetic azo dye that is used for food or drinks coloring. Tartrazine has two sulfonic acid and one carboxylic acid group on its structure, so it can change molecular form with pH change (Saleh et al. 2016). Diphenylcarbazone (1-anilino-3-phenyliminourea) is a molecule from the carbazone family. Diphenylcarbazone is used as a chelating agent to determine the presence of metal ions because it can form metal complexes with intense colors (Deshmukh and Bokil 1956).

In this study, it was aimed to prepare tartrazine (TART) or diphenylcarbazone (DPC) metal complexes with cobalt and zinc metals to find a cheap alternative to Ru complexes. While Ru metal is rare and expensive, using cheap and easily accessible transition metal complexes as sensitizers might eliminate the low efficiency of DSSCs for low-cost technologies or applications. Therefore, these dyes were used as sensitizers at DSSCs and investigated how they affect the efficiency of DSSCs.

2. Materials and Method

All chemicals that were used in this study were purchased from Sigma Aldrich. $ZnCl_2$ and $CoCl_2.6H_2O$ were entirely dissolved with the proper amount in ethanol to prepare 0.3 mM Co^{2+} and Zn^{2+} solution. Same as metal solutions, tartrazine and diphenylcarbazone were dissolved in ethanol with the proper amount to prepare 0.3 mM ligand solutions. While vigorously stirring, 10 mL ligand solutions were added to 5 mL metal solutions dropwise to prevent precipitation. After adding process was completed, solutions were stirred for 10 min. Then, prepared metal complexes were put in the dark and observed to see whether precipitation occurred or not. Prepared metal complexes were named Co-TART, Zn-TART for tartrazine complexes and Co-DPC, Zn-DPC for diphenylcarbazone complexes.

Dye-Sensitized Solar Cells were prepared as in our previous study (Ünlü and Özacar 2020). TiO_2 photoanodes were immersed in prepared dye solutions for 24 h in the dark.

3. Results and Discussion

UV-VIS Spectroscopy was used to characterize prepared dyes and obtained spectra can be seen in Figure 1. For TART, Co-TART and Zn-TART, all spectra are nearly the same. Although there is a slight shift at n-π* transition band between 425-475 nm, there are no disappearing or new bands. That means there is some interaction between TART and Co or Zn, but complexation was not completely occurred. For DPC and its Co and Zn complexes, the situation is different than TART and TART complexes. Zn-DPC shows a new broad absorption band at nearly 525 nm, which means the formation of Zn-DPC complex was successful. Therefore, even though there is no new band for Co-DPC, the band seen at 290 nm for DPC disappeared. It also shows that the synthesis of Co-DPC was successful.

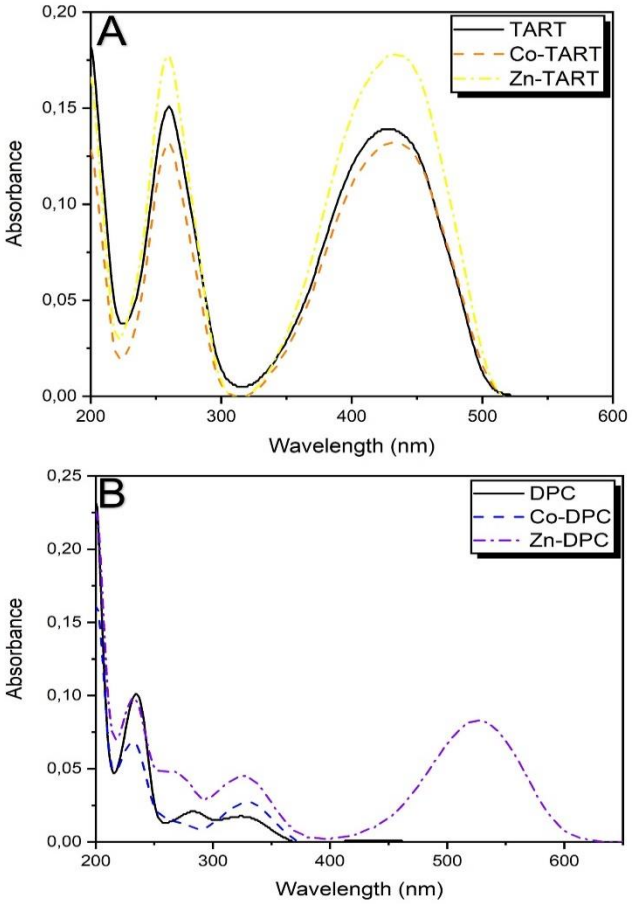

Fig. 1 UV-VIS spectra of A) TART, Co-TART, Zn-TART and B) DPC, Co-DPC, Zn-DPC

Linear sweep voltammetry was used to characterize DSSCs sensitized with TART, DPC and their metal complexes. FF and solar conversion efficiency (η) were calculated with the Equation 1 and Equation 2:

$$FF = \frac{Jmax * Vmax}{Jsc * Voc} \quad (1)$$

$$\eta = \frac{Jsc * Voc * FF}{Pin} \quad (2)$$

where Jsc is short current density, Voc is open-circuit voltage, Jmax and Vmax are maximum current density and maximum voltage and Pin is the power of the light source. The J-V curves of the prepared DSSCs can be seen in Figure 2. and electrochemical values and efficiencies of DSSCs can be seen in Table 1. DSSC that was sensitized with TART was showed the highest efficiency among all TART dyes. While TART and TART metal complexes have the same light absorption property, unreacted metal ions were caused to decrease at the efficiency. For DPC dyes, it can be seen that Zn-DPC has the highest efficiency and Co-DPC is following it. Zn-DPC has the highest efficiency because it can absorb light between 450-600 nm, so it can absorb

more photons from sunlight to produce excited electrons. Co-DPC can absorb more light than bare DPC dye, but it does not have a broad light absorption like Zn-DPC dye. That's why its efficiency is lower than Zn-DPC.

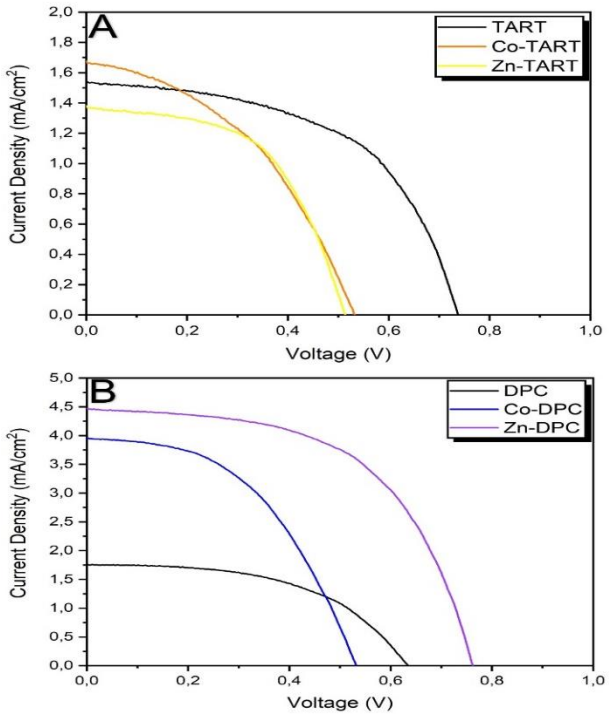

Fig. 2 J-V curves of DSSCs that were sensitized with A) TART, Co-TART, Zn-TART and B) DPC, Co-DPC, Zn-DPC

Table 1. Photoelectrochemical Values of Prepared DSSCs

Dye	Jsc (mA/cm^2)	Voc (V)	FF	η (%)
TART	1,54	0,74	0,54	0,61
Co-TART	1,68	0,53	0,43	0,38
Zn-TART	1,38	0,51	0,55	0,39
DPC	1,76	0,63	0,52	0,58
Co-DPC	3,96	0,53	0,48	1,01
Zn-DPC	4,47	0,76	0,56	1,91

Electrochemical Impedance Spectroscopy (EIS) was used to investigate solar cell characteristics such as resistance and electron lifetime. Nyquist and Bode plots of prepared DSSCs can be seen in Figure 3. For TART, Co-TART and Zn-TART sensitized solar cells, Zn-TART has the highest resistance among them all. This high resistance value can be explained with unreacted Zn^{2+} ions at the dye solution. While there are unreacted Co^{2+} ions for Co-TART dyes, it has the lowest resistance value than all TART dyes. However, Co-TART dye has the lowest electron lifetime value that can be seen at the Bode plot. That can explain the low efficiency that Co-TART sensitized DSSC has. For DPC dyes, all resistance and electron lifetime value are in good harmony with the efficiency of DSSCs. Both Co-DPC and Zn-DPC dyes have less resistance value than DPC and it can explain the high efficiency of these dyes.

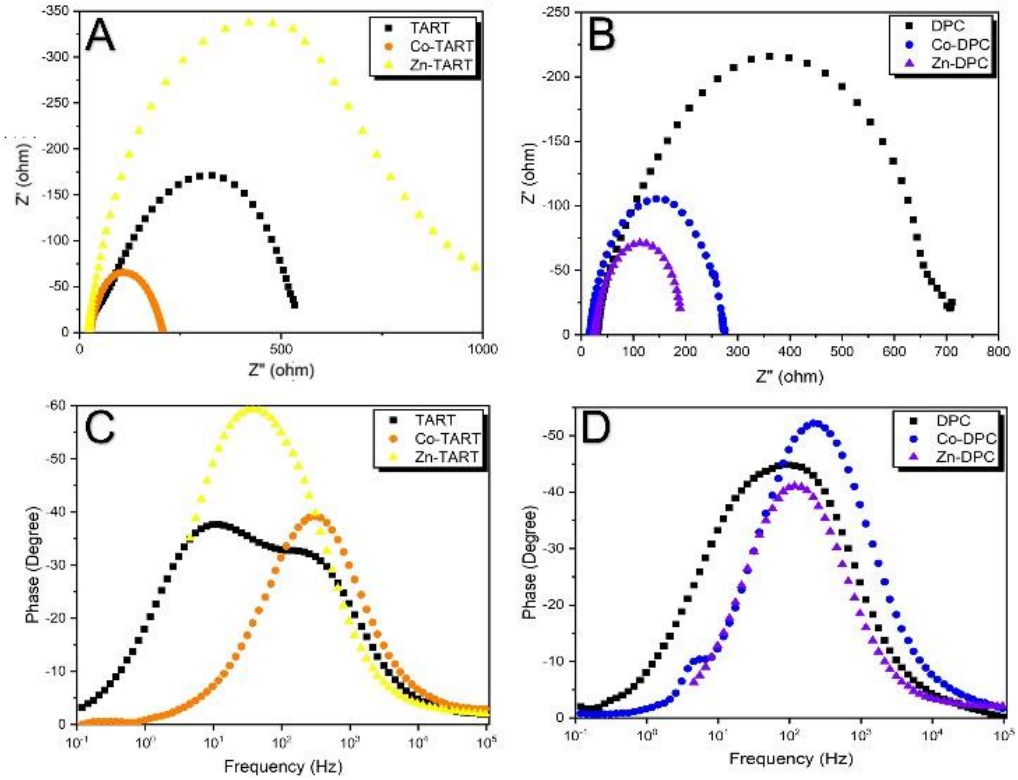

Fig. 3 Nyquist Plots for A) TART, Co-TART, Zn-TART and B) DPC, Co-DPC, Zn-DPC and Bode Plots for C) TART, Co-TART, Zn-TART and D) DPC, Co-DPC, Zn-DPC dyes

4. Conclusion

The new TART and DPC dyes and their metal complexes were developed and were used as a sensitizer in DSSCs. For TART dyes, complexations were a failure. However, we believed that Co or Zn complexes could be prepared by adjusting pH or using heat. Co and Zn complex with DPC were prepared successfully and showed high-efficiency value than DPC as expected. Finally, by mixing with TART and Zn-DPC to prepare cocktail dyes, we think that efficiency can be improved because of broadening the light absorption at the UV-VIS region.

Acknowledgements

This research did not receive any specific grant from funding agencies in the public, commercial, or not-for-profit sectors

References

Deshmukh GS, Bokil I. 1956. Diphenylcarbazone as an Internal Indicator in Volumetric Analysis. III. Volumetric Determination of Thorium by Ammonium Molybdate. Bull Chem Soc Jpn. 29:449–450

Gong J, Sumathy K, Qiao Q, Zhou Z. 2017. Review on dye-sensitized solar cells (DSSCs): Advanced techniques and research trends. Renew Sustain Energy Rev. 68:234–246

Jena A, Mohanty SP, Kumar P, Naduvath J, Lekha P, Das J, Narula HK, Mallick S, Bhargava P, Gondane V. 2012. Dye Sensitized Solar Cells: A Review. Trans Indian Ceram Soc. 71:1–16

Jung HS, Lee J. 2013. Dye Sensitized Solar Cells for Economically Viable Photovoltaic Systems. J Phys Chem Lett. 10:1682–1693

Kumar R, Umar A, Kumar G, Nalwa HS, Kumar A, Akhtar M.S. 2017. Zinc oxide nanostructure-based dye-sensitized solar cells. J Mater Sci. 52:4743–4795

Mishra A, Fischer MKR, Büuerle P. 2009. Metal-Free organic dyes for dye-Sensitized solar cells: From structure: Property relationships to design rules. Angew Chemie Int Ed. 48:2474–2499

Oregan B, Gratzel M. 1991. a Low-Cost, High-Efficiency Solar-Cell Based on Dye-Sensitized Colloidal TiO_2 Films. Nature. 353:737–740

Richhariya G, Kumar A, Tekasakul P, Gupta, B. 2017. Natural dyes for dye sensitized solar cell: A review. Renew Sustain Energy Rev. 69:705–718

Saleh M, Hashem E, Salahi N. 2016. Oxidation and Complexation-Based Spectrophotometric Methods for Sensitive Determination of Tartrazine E102 in Some Commercial Food Samples. Comput Chem. 04:51–64

Sharma S, Bulkesh S, Ghoshal SK, Mohan D. 2017. Dye sensitized solar cells: From genesis to recent drifts. Renew Sustain Energy Rev. 70:529–537

Sugathan V, John E, Sudhakar K. 2015. Recent improvements in dye sensitized solar cells : A review. Renew Sustain Energy Rev. 52:54–64

Ünlü B, Özacar M. 2020. Effect of Cu and Mn amounts doped to TiO_2 on the performance of DSSCs. Sol Energy. 196:448-456

Wu J, Lan Z, Lin J, Huang M, Huang Y, Fan L, Luo G. 2015. Electrolytes in dye-sensitized solar cells. Chem Rev 115:2136–2173

RESEARCH ARTICLE
Eurasian J Bio Chem Sci, 5(1):9-14, 2022
https://doi.org/10.46239/ejbcs.1038373

EJBCS

Eurasian Journal of Biological and Chemical Sciences

Journal homepage: www.dergipark.org.tr/ejbcs

Fe_3O_4@κ-KRG-aşı-PDMAEMA manyetik nanopartiküllerden pH kontrollü doksorubisin salımı

Gülcan Geyik[1*], Nuran Işıklan[2]

*[*1]Hitit Üniversitesi, Alaca Avni Çelik Meslek Yüksekokulu, Mülkiyet Koruma ve Güvenlik Bölümü, Çorum, Türkiye*
[2]Kırıkkale Üniversitesi, Fen Edebiyat Fakültesi, Kimya Bölümü, Kırıkkale, Türkiye

*Corresponding author : gulcan_gyk@hotmail.com
Orcid No: https://orcid.org/0000-0003-4558-9288

Received : 19/12/2021
Accepted : 14/04/2022

Özet: Son yıllarda manyetik yapılı biyouyumlu nanoparçacıkların kanser tedavisinde etkinliği artmaktadır. Hedefli ilaç salım sistemi, geleneksel kanser tedavi yöntemlerinin yan etkilerini azaltmakta ve tedavi etkinliğini artırması sebebiyle yakın zamanda umut verici kanser tedavisi olarak ortaya çıkmaktadır. Çalışmamızda hibrit yapılı manyetik nanopartiküller sentezlenmiştir. Nanopartiküller anorganik yapılı demir oksit çekirdeği (Fe_3O_4) ve organik yapılı kopolimerden (κ-KRG-aşı-PDMAEMA) oluşmaktadır. Manyetik nanopartiküllerin yapısı UV ve Zeta-sizer ile karakterize edilmiştir. Sentezlenen Fe_3O_4@κ-KRG-aşı-PDMAEMA nanopartiküllerine anti-tümör etkiye sahip kanser ilacı doksorubisin (DOX) yüklenerek Fe_3O_4@κ-KRG-aşı-PDMAEMA@DOX manyetik nanopartikülleri elde edilmiştir. İlaç yüklü manyetik nanopartiküllerin fosfat tamponunda (pH 7,4), asetat tamponunda (pH 5,5) ve asidik ortamda (pH 1,2) 37 ºC'de *in vitro* salımı incelenmiştir. Sentezlenen Fe_3O_4@κ-KRG-aşı-PDMAEMA@DOX manyetik nanopartiküllerin pH'ya duyarlı olduğu ve yüksek salım performansına sahip olduğu gösterildi. Fe_3O_4@κ-KRG-aşı-PDMAEMA@DOX nanopartiküllerin DOX salımı pH 7,4, pH 5,5 ve pH 1,2 ortamlarında sırası ile %66,53, %70,08 ve %90,47 bulunmuştur. Manyetik nanopartiküllerin kinetik hesaplamaları yapılmıştır. Manyetik nanopartiküllerin demir içeriği %66,77 bulunmuştur.

Anahtar Kelimeler: Manyetik nanopartikül, doksorubisin, kopolimer, demir oksit

pH controlled release of doxorubicin from Fe_3O_4@κ-CRG-graft-PDMAEMA magnetic nanoparticles

Abstract: In recent years, the effectiveness of magnetically biocompatible nanoparticles in cancer treatment has been increased. Targeted drug delivery system has recently emerged as a promising cancer treatment because it reduces the side effects of traditional cancer treatment methods and increases the effectiveness of treatment. In our study, hybrid magnetic nanoparticles were synthesized. Nanoparticles consist of an inorganic iron oxide core (Fe_3O_4) and an organic copolymer (κ-CRG-graft-PDMAEMA). The magnetic nanoparticles' structure was characterized by UV and Zeta-sizer techniques. Fe_3O_4@κ-CRG-graft-PDMAEMA@DOX magnetic nanoparticles were obtained by loading the anti-tumor cancer drug doxorubicin (DOX) on the synthesized Fe_3O_4@κ-CRG-graft-PDMAEMA nanoparticles. The *in vitro* release of drug-loaded magnetic nanoparticles in phosphate buffer (pH 7.4), acetate buffer (pH 5.5) and acidic medium (pH 1.2) at 37 °C was investigated. It has been shown that the synthesized Fe_3O_4@κ-CRG-graft-PDMAEMA@DOX magnetic nanoparticles are pH sensitive and have high release performance. The DOX release of Fe_3O_4@κ-CRG-graft-PDMAEMA@DOX nanoparticles in pH 7.4, pH 5.5 and pH 1.2 mediums was found to be 66.53%, 70.08% and 90.47% s, respectively. Kinetic calculations of magnetic nanoparticles were made. The iron content of magnetic nanoparticles was found to be 66.77%.

Anahtar Kelimeler: Manyetik nanopartikül, doksorubisin, kopolimer, demir oksit

1. Giriş

Nanoteknoloji kimya, biyoloji, fizik, mühendislik ve tıbbi alanları birleştiren geniş kapsamlı bir araştırma alanıdır (Gao ve ark. 2012; Jabir ve ark. 2012). Bu araştırma alanı nanometre boyutundaki malzemelerin yapısını, davranışını ve uygulamalarını kapsamaktadır (Alexis ve ark. 2008). Hızla gelişmekte olan nanoteknoloji, dünya çapında bilim dünyasının ilgisini kazanmıştır (Jabir ve ark. 2012). Son

yıllarda kanser hastalığının tedavisine yenilikçi çözümler sunma potansiyeline sahiptir. Nano ölçekli materyallerin en önemli biyomedikal uygulamaları, moleküler görüntüleme, ilaç dağıtım, gen iletim, hedefli ilaç serbestleştirme, biyomarkır haritalama ve fototerapi alanlarını içermektedir (Bae ve ark. 2011).

Manyetik nanoparçacıklar genellikle geçiş metali demir, nikel ve mangan gibi manyetik elementlerden oluşur. Günümüzde manyetik nanoparçacıklar biyoteknoloji alanında örneğin; kanser hipertermia, hedefli ve kontrollü ilaç salımı, NMR görüntüleme, in vivo ve in vitro uygulamalarda geniş yer tutmaktadır (Akbarzadeh ve ark. 2012; Nene ve ark. 2016; Singamaneni ve ark. 2011). Manyetik hedefli ilaç dağıtım sistemi günümüzde çokça uygulanmakta ve etkili bir sistem olarak kabul görmektedir. Oral veya enjeksiyon yoluyla hastaya verilen manyetik materyal taşıyan ilaç, dış manyetik alanla kanser alanlarına yönlendirilebilecektir (Yang ve ark. 2014). Manyetik alan tarafından yönlendirilme, ilaç taşıyıcılarını etkili bir şekilde tümör dokularına sürükleyerek ilaç verme verimliliğini artıracaktır (Yang ve ark. 2008).

Kontrollü ilaç salımı; ilacı belirli dozda, belirli süre vücutta tutabilme prensibine dayanmaktadır (Danckwerts ve Fassihi 1991). Etken madde salımı konvansiyonel dozaj şekillerine göre uzun bir süreçte devam etmektedir (Tüylek 2017). Kanser tedavisinde kullanılan birçok ilaç kanserli hücrelere özel olmadığı için sağlıklı hücrelere de zarar verebilmektedir. Bu sorunu aşmak için, manyetik nanopartiküller terapötik maddeleri istenilen hedef bölgeye iletmede kullanılabilir. Manyetik nanoparçacıklar dışardan uygulanan bir dış manyetik alan ile spesifik bölgede tutulabilir (Indira ve Lakshmi 2010). Kontrollü ilaç salımının avantajları manyetik nanopartiküllerin üstün özellikleri ile birleşince yan etkileri azaltılmış olur, doz aşımı engellenmiş ve tedavi için gerekli konsantrasyon aralığında ilaç seviyesi sağlanmış olmaktadır (Ruuge ve Rusetski 1993).

Doksorubisin (DOX), kanser tedavisinde kullanılan anti-tümör etkiye sahip bir ilaçtır (Huang ve ark. 2017; Zhang ve ark. 2017). Kanser tedavisinde etkinliği oldukça yüksektir (Patil ve ark. 2012). Meme kanseri, yumurtalık kanseri, akciğer kanseri, nöroblastoma kanseri, lösemi gibi kanserin tedavisinde en çok kullanılan ilaçlardan biridir.

Bu çalışmanın amacı kanser tedavisinde kullanılmak üzere hibrit yapılı nanopartikül tasarlamaktır. Çekirdek (Fe_3O_4)-kabuk (kappa-karagenan-aşı-dimetilaminoetil metakrilat) yapılı hibrit nanopartiküller sentezlenerek doksorubisinin yan etkilerinin azaltılması ve böylece terapötik etkinliğinin artırılması hedeflendi. Bu amaca ulaşmak için ilk olarak κ-karagenan-aşı-poli(dimetilaminoetil metakrilat) kopolimeri serbest radikalik katılma polimerizasyon yöntemi ile sentezlendi. Daha sonra kopolimer kaplı manyetik nanopartiküller mikrodalgada ikili çöktürme yöntemi ile sentezlenerek doksorubisin yüklendi. İlaç yüklü manyetik nanopartiküllerin tutuklanma verimi ve ilaç yükleme kapasiteleri hesaplandı ve nanopartiküllerin pH duyarlılığı araştırıldı.

2. Materyal ve Metod

2.1. Materyal

κ-Karagenan (KRG, %98), N,N-dimetilaminoetil metakrilat (DMAEMA, %98), $FeCl_3.6H_2O$ (%99), $FeS0_4.7H_2O$ (%99), etanol (≥ %99,8) Sigma-Aldrich firmasından temin edildi. Doksorubisin (DOX) Santa Cruz Biotechnology Inc. firmasından temin edildi. N,N-dimetilaminoetil metakrilat 65 °C'de destillendikten sonra kullanıldı ve diğer kimyasalların hepsi alındığı halleriyle kullanılmıştır.

2.2. κ-KRG-aşı-PDMAEMA Kopolimerin Sentezi

Aşılama işlemi azot gazı atmosferinde, üç boyunlu balonda, geri soğutucu altında ve mikrodalga fırında gerçekleştirildi. Karagenan çözeltisi saf su içerisinde, 70 ^oC sıcaklığında 3 saat karıştırılarak elde edildi. Çözeltiye destillenmiş farklı miktarlarda N,N dimetilaminoetil metakrilat ilave edildi. Mikrodalga fırında 500 watta, 70 ^oC'de 30 dakika süreyle azot gazı geçirilerek ve daha sonra karışıma başlatıcısı 4,4'-Azobis (4-siyanovalerik asit) ilave edilerek tepkime başlatıldı. Tepkime süresince ortamdan azot gazı geçirilmeye devam edildi. Oluşan ürünler metanolde (500 mL) çöktürüldü ve süzülerek elde edilen ürün, homopolimerin uzaklaştırılması amacıyla Soxalet içerisinde tetrahedrafuranda (120 mL) yıkandı. Homopolimeri uzaklaştırılan aşı kopolimer 40 ^oC'de vakum etüvünde sabit tartıma gelene kadar kurutuldu. Aşı yüzdesi aşağıdaki Eşitlik 1 yardımıyla kütle artışından hesaplanmıştır. Elde edilen kopolimerin karakterizasyonu daha önceki çalışmamızda sunulmuştur (Geyik ve Işıklan 2022).

Aşı yüzdesi = (kopolimer kütlesi-polimer kütlesi) / polimer kütlesi x 100 (1)

2.3. κ-KRG-aşı-PDMAEMA Kopolimerinden Manyetik Nanopartikül Sentezi

κ-KRG-aşı-PDMAEMA kopolimerleri deoksijene suda 70 ^oC'de manyetik karıştırıcı yardımıyla 1 saatte çözüldü. Çift boyunlu balonda kopolimer çözeltisi 70 ^oC, asitlendirilmiş $FeCl_3.6H_2O$ tuzundan 5 mL, $FeSO_4.7H_2O$ tuzundan 1 (nFe^{+2}/nFe^{+3} = 0,625/1 olacak şekilde) ilave edilerek azot atmosferinde, mikrodalgada 500 watta, yarım saat karıştırıldı. Çözeltiye KOH (1 M) ilave edildi. Çözelti azot atmosferinde, 70 °C'de, 500 watta 1 saat mikrodalgada karıştırıldı. Magnet yardımıyla manyetik özelliğe sahip olan nanopartiküllerle olmayan nanopartiküller birbirinden ayrıldıktan sonra manyetik nanopartiküller etanol/deoksijene su karışımı ile yıkandı. Elde edilen Fe_3O_4@κ-KRG-aşı-PDMAEMA nanopartikülleri etüvde 40 °C'de 48 saat kurutuldu. İlaç yüklü nanopartiküller hazırlanırken kopolimer karışımına 5 mg DOX ilave edilerek oluşturuldu. Oluşan nanopartiküller sabit tartıma gelene kadar kurutuldu. Manyetik nanopartiküllerin mıknatıs yardımı ile toplanma görüntüsü Şekil 1'de sunulmuştur.

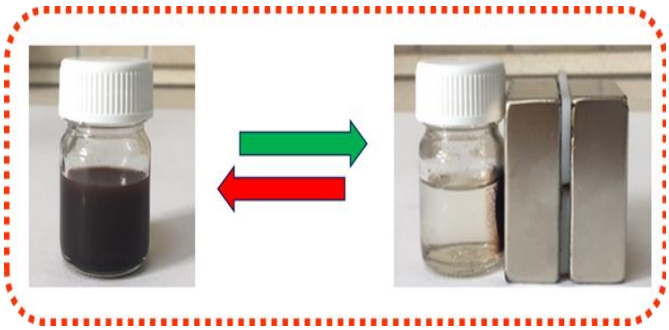

Şekil 1. Manyetik nanopartiküllerin mıknatıs varlığında toplanması

2.4. Tutuklanma Verimi (TV)

Tutuklanma verimi hesaplanması için ilaç yüklü nanopartiküllerden 5 mg alınarak 25 mL pH 7,4 ($H_2PO_4^-$/ HPO_4^{-2}) tamponu ilave edildi ve 25 °C'de 100 rpm hızda çalkalamalı su banyosunda 4 saat boyunca bekletildi. Elde edilen ekstrakt süzülerek DOX içeriği UV spektrofotometresi ile DOX'un maksimum absorpsiyon gösterdiği dalgaboyu olan 499 nm'de tayin edildi. Tutuklanma verimi çalışmaları her bir formülasyondaki ilaç yüklü nanopartiküller için üçer defa tekrarlanarak hesaplandı.

Nanopartiküllerin DOX yükleme kapasitesi Eşitlik 2 ve DOX'un tutuklanma verimi Eşitlik 3 ile hesaplandı.

İlaç Yükleme Kapasitesi (%)= (Nanopartiküldeki deneysel ilaç miktarı)/ (Nanopartikül miktarı)x100 (2)

Tutuklanma Verimi (%)=(Nanopartiküldeki deneysel ilaç miktarı)/(Nanopartiküldeki teorik ilaç miktarı)×100 (3)

2.5. Manyetik Nanopartiküllerin İn Vitro İlaç Salımı

Fe_3O_4@κ-KRG-aşı-PDMAEMA@DOX manyetik nanopartiküllerinden belirli miktarda alınarak, farklı pH ortamlarında (fosfat tamponu (pH 7,4), asetat tamponunda (pH 5,5) ve asidik ortamda (pH 1,2)), 37 ºC'de *in vitro* salımı 24 saat boyunca incelendi. Tüm salım deneyleri çalkalamalı su banyosunda 100 rpm hızda gerçekleştirildi. Belirli zaman aralıklarında 200 µL örnekler alındı ve toplam hacmi korumak için aynı miktarda tampon salım ortamına ilave edildi. Her bir deney 3 kez tekrarlandı ve standart sapmaları hesaplandı.

2.6. Manyetik Nanopartiküllerin Zeta Potansiyeli ve Partikül Boyutu Ölçümü

Fe_3O_4@κ-KRG-aşı-PDMAEMA ve Fe_3O_4@κ-KRG-aşı-PDMAEMA@DOX manyetik nanopartiküllerin zeta potansiyeli, partikül boyutu ve polidispersite indeksleri 1 mg manyetik nanopartikül 2 mL farklı pH ortamlarında (fosfat tamponu (pH 7,4), asetat tamponu (pH 5,5) ve asidik ortamda (pH 1,2)) hazırlanarak 25 °C'de ölçüldü.

2.7. Demir İçeriği Tayini

ICP-OES cihazı kullanılarak elde edilen manyetik nanopartiküllerin Fe_3O_4 miktarı tayin edildi. Numuneler ve 0-1-2-3-5-10-20 ppm'lik kalibrasyon için standart çözeltileri Plasma Power 1435 W, Pump Speed 30 rpm, Coolant Flow 0,80, Nebulizer Flow 0,70 cihaz şartlarında okutularak kalibrasyon eğrileri oluşturulmuştur. (R2:0.9999). Numuneye uygulanan işlemler şu şekildedir; 0,01 g örneğe 10 mL HNO_3 eklendi ve CEM MARS6 mikrodalga cihazında Carbon Metodu kullanılarak; power: 290-1800, ramp time: 20:00, hold time: 15:00 ve sıcaklık:200 °C cihaz koşullarında yıkama işlemi yapılmıştır. Yıkama işlemi sonrası toplam hacim 50 mL olacak şekilde seyreltilerek yukarıda belirlenen ICP-OES cihaz koşulları altında okuma işlemi yapılmıştır.

2.8. İstatistiksel Analiz

İstatistiksel analizi SPSS 16,0 yazılımı, ANOVA testi (IBM, NY, ABD) ile yapıldı. (P) < 0,05 anlamlılık düzeyi istatistiksel olarak farklı kabul edildi. Sonuçlar ortalama ± standart sapma (SS) olarak hesaplandı. Çalışmalarımızda üç bağımsız ölçüm yapılarak hesaplandı.

3. Bulgular ve Tartışma

κ-KRG-aşı-P(DMAEMA) kopolimerinin yapısında bulunan SO_2^{-4} ile Fe_3O_4 nanoyapısında bulunan Fe^{+3} ve Fe^{+2} iyonları ile bağlanarak demir oksit üzerine kaplandığı düşünülmektedir (Jones ve ark. 2007). Sentezlenen Fe_3O_4@κ-KRG-aşı-PDMAEMA manyetik nanopartiküllerine kanser ilacı olarak DOX yüklendi. İlacın yapıya girdiği UV spektrometresi ile kanıtlandı. Şekil 2'de DOX ve Fe_3O_4@κ-KRG-aşı-PDMAEMA@DOX manyetik nanopartiküllerin UV spektrumu sunulmuştur. DOX ve Fe_3O_4@κ-KRG-aşı-PDMAEMA@DOX manyetik nanopartikülleri 200-700 nm dalgaboyu aralığında tarandı. Manyetik nanopartiküllerde ilacın pik noktalarının varlığı DOX'un yapıya girdiğini göstermektedir. Manyetik nanopartiküllerin spektrumunda DOX'un karakteristik pikleri; 233 nm, 253 nm, 291 nm, 474 nm, 499 nm ve 533 nm'de görülmektedir (Ma ve ark. 2016). Bu piklerde şiddet azalması dışında yerlerinde bir kayma olmamıştır.

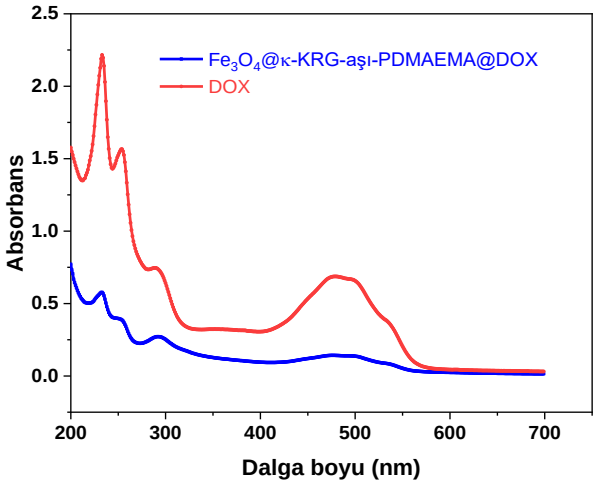

Şekil 2. DOX ve Fe_3O_4@κ-KRG-aşı-PDMAEMA@DOX manyetik nanopartiküllerin UV spektrumu

Fe_3O_4@κ-KRG-aşı-PDMAEMA'nın yüzey morfolojisi TEM ve SAED kullanılarak incelendi. TEM ve SAED görüntüsü Şekil 3'te sunulmuştur. 100 nm'de sunulan TEM görüntüsü nanopartikülleri net olarak göstermektedir. Seçili alan elektron kırınım (SAED) deseni, nanopartiküllerin kristal yapısını karakterize etmek için kullanılan araçlardan

biridir. SAED deseni Fe_3O_4 nanoparçacıların kristal düzlemlerini sunmaktadır. Fe_3O_4@κ-KRG-aşı-PDMAEMA nanopartiküllerinin spesifik kırınım değerlerini (220), (311), (400), (511) ve (440)'de gösterdi. Fe_3O_4 kristalinin kırımın değerleri literatürde mevcuttur ve kübik kristal yapısına sahiptir (Rahimdad ve ark. 2019). SAED deseninde, altı kat desenli net kırınım halkalara sahip olduğu gözlenmiştir. Bu halkalar, partiküllerin yüksek oranda kristallikleri nedeniyle kırınım noktalarının bir araya gelmesinden kaynaklanmaktadır. Bu da nano boyutlu olan Fe_3O_4 parçacıkların yüksek kristalliklerini göstermektedir.

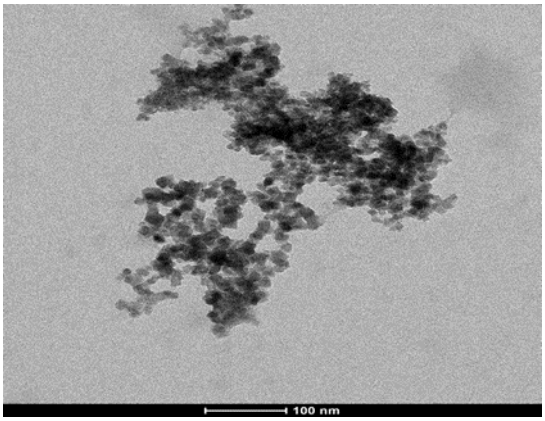

(a)

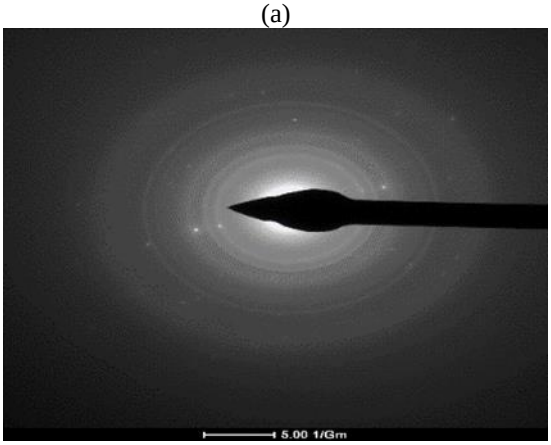

(b)

Şekil 3. Fe_3O_4@κ-KRG-aşı-PDMAEMA'nın TEM (a) ve SAED (b) görüntüsü

Kolloidal kararlılığı karakterize etmek için zeta potansiyeli önemli bir faktördür. Zeta potansiyeli partiküllerin yüzey yükleri hakkında bilgi vermektedir. Genel olarak, yüksek pozitif ve negatif zeta potansiyeli nanopartiküllerin dağılma stabilitesini göstermektedir. Yüksek zeta potansiyeli olan nanopartiküller, partiküller arası yüksek elektrostatik itme kuvvetinden dolayı depolanma süresinde koagüle olmazlar (Shete ve ark. 2013). Fe_3O_4@κ-KRG-aşı-PDMAEMA ve Fe_3O_4@κ-KRG-aşı-PDMAEMA@DOX için farklı pH ortamlarında (1,2, 5,5 ve 7,4) 25 °C'de zeta potansiyeli, hidrodinamik çapı ve polidispersite indeksi ölçümleri yapıldı. Sonuçlar Tablo 1'de sunulmuştur. Nanopartiküllerin pH 5,5 ve pH 7,4 ortamlarında zeta potansiyelleri yüksek çıkmıştır. Nanopartiküllerin yüksek pH'da daha stabil oldukları görülmektedir. Fe_3O_4@κ-KRG-aşı-PDMAEMA ve Fe_3O_4@κ-KRG-aşı-PDMAEMA@DOX nanopartiküllerin yüzey yükü sonuçları incelendiğinde DOX yüklü nanopartiküllerin yüzey yükünde negatif yönlü artış görülmektedir. Fe_3O_4@κ-KRG-aşı-PDMAEMA ve Fe_3O_4@κ-KRG-aşı-PDMAEMA@DOX nanopartiküllerinin hidrodinamik çapı pH'nın artması ile azalmaktadır. Kopolimer yapısında bulunan PDMAEMA yan dalları pH'ya duyarlıdır. Düşük pH'larda PDMAEMA zincirlerinde oluşan kuarterner amin grubunun birbirini itmesinden dolayı şişme artmaktadır. Nanopartiküllerin stabilitesi ve dağılımı hakkında bilgi veren diğer parametre polidispersite indeksi (PDI) değeridir. Polidispersite indeksi, dinamik ışık saçılımı (DLS) ölçümünde önemli bir parametredir. Nanopartiküllerin boyut dağılımındaki değişimi gösterir ve 0,5'in altında olması istenmektedir. PDI değeri 0,1-0,25 aralığında ise nanopartiküller dar dağılıma sahiptir ve istenilende dar dağılıma sahip olmasıdır (Özkahraman ve ark. 2018). Elde edilen PDI değeri 0,5 ve üzerinde ise geniş dağılıma sahiptir. Fe_3O_4@κ-KRG-aşı-PDMAEMA ve Fe_3O_4@κ-KRG-aşı-PDMAEMA@DOX nanopartiküllerinin PDI değeri 0,22 ile 0,27 aralığındadır. Sentezlenen manyetik nanopartiküller dar dağılımına sahiptir.

Tablo 1. Nanopartiküllerin zeta potansiyeli, hidrodinamik çapı ve PDI değerleri

Nanopartikül	pH	Zeta Potansiyeli (mV)	Hidrodinamik Çap (nm)	PDI
Fe_3O_4@κ-KRG-aşı-PDMAEMA	1,2	11,23± 1,10	157,73± 5,50	0,238± 0,09
	5,5	-14,20± 0,36	118,47± 3,84	0,255± 0,12
	7,4	-21,96± 0,51	94,37± 6,51	0,254± 0,10
Fe_3O_4@κ-KRG-aşı-PDMAEMA @DOX	1,2	11,82± 0,70	181,60± 5,21	0,220± 0,03
	5,5	-19,43± 0,50	148,33± 3,65	0,271± 0,06
	7,4	-28,53± 1,40	119,33± 4,09	0,225± 0,03

Manyetik nanopartiküllerin ilaç yüklenme performansını belirlemek için, tutuklanma verimi ve ilaç yükleme kapasitesi hesaplanmıştır. Fe_3O_4@κ-KRG-aşı-PDMAEMA@DOX nanopartiküllerin tutuklanma verimi %66,82 ± 2,23 ve ilaç yükleme kapasitesi %1,63 ± 0,05 olarak hesaplanmıştır. DOX salım çalışmaları 24 saat süreyle pH 1,2, pH 5,5 ve pH 7,4 tamponlarında gerçekleştirilmiştir. Sonuçlar Şekil 4'te sunulmuştur. Fe_3O_4@κ-KRG-aşı-PDMAEMA@DOX nanopartikülleri pH 1,2 ve pH 5,5 tamponunda hızlı salım yaptığı, pH 7,4

tamponunda daha yavaş salım yaptığı görülmüştür. pH 1,2'de ilacı fazla salması yapıda bulunan PDMAEMA'ya bağlıdır. PDMAEMA pH duyarlı bir polimerdir ve düşük pH'larda şişme davranışı gösterir. Şişmenin artması ile nanopartikül içine ve etrafına nüfuz eden ilacın salımı artmıştır. Benzer sonuçlar literatürde rapor edilmiştir (Saha ve ark. 2019).

DOX'un Fe_3O_4@κ-KRG-aşı-PDMAEMA@DOX nanopartiküllerden salım mekanizması Korsmeyer-Peppas kinetik modeli kullanılarak değerlendirildi. Korsmeyer-Peppas modeli Eşitlik 3'te gösterilmektedir (Siepmann ve Peppas 2012):

$$\frac{M_t}{M_\infty} = kt^n \qquad (4)$$

burada M_t/M_∞; t zamanındaki DOX'un salım oranıdır, k; DOX'un salım hız sabitini temsil eder ve n; difüzyon üssüdür (Siepmann ve Peppas 2012; Luo ve ark. 2017). n'nin değeri, salım mekanizmasına bağlı olarak değişir. Küresel partiküller için, n ≤ 0,43, ilacın taşıyıcıdan difüzyon kontrollü salınımını (Fick difüzyonu) belirtirken, n ≥ 0,85, gevşeme kontrollü salımı (Durum II taşıma) gösterir. 0,43 ile 0,85 arasında değişen ara değerler, ilaç salımının hem gevşeme hem de difüzyon tarafından kontrol edildiği anormal taşımanın göstergesidir (Siepmann ve Peppas 2012). Tablo 2, farklı salım ortamlarında Fe_3O_4@κ-KRG-aşı-PDMAEMA@DOX nanopartikülleri için n ve R değerlerini göstermektedir. Tablo 2'de ortam pH'sının 1,2'den 7,4'e değişimi ile DOX salım mekanizmasının değiştiği görülmektedir.

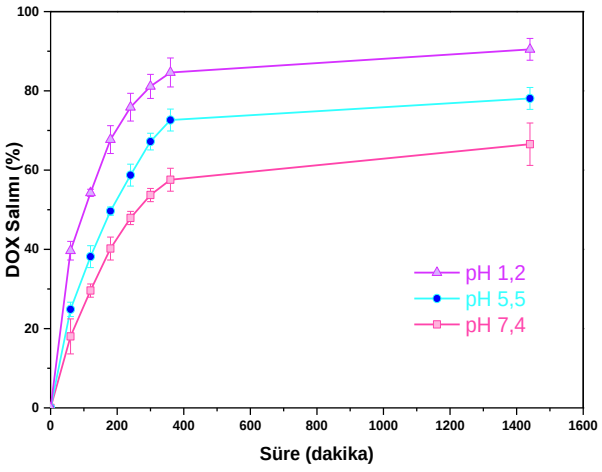

Şekil 4. Fe_3O_4@κ-KRG-aşı-PDMAEMA@DOX manyetik nanopartiküllerden farklı pH ortamlarında ilaç salımı

Tablo 2. Nanopartiküllerin salım kinetiği

pH	n	R	Difüzyon Mekanizması
1,2	0,4247	0,9981	Fick Difüzyonu
5,5	0,6232	0,9998	Fick Yasasına Uymayan
7,4	0,7121	0,9292	Fick Yasasına Uymayan

4. Sonuçlar

Bu çalışmada manyetik alana duyarlı nanopartiküller ikili çöktürme yöntemi ile başarıyla sentezlendi. Mikrodalgada serbest radikalik polimerizasyon yöntemi ile sentezlenen sıcaklık ve pH duyarlı κ-KRG-aşı-PDMAEMA kopolimerinin Fe_3O_4'e kaplanmasıyla çekirdek-kabuk yapılı Fe_3O_4@κ-KRG-aşı-PDMAEMA nanopartikülleri elde edildi. Manyetik nanopartiküller UV, Zeta-Sizer, TEM ve ICP-OES yöntemleri ile karakterize edildi. Sentezlenen bu nanopartiküllere DOX ilacı yüklenerek, ilaç salım çalışmaları *in vitro* farklı pH (7,4, 5,5 ve 1,2) ortamlarında çalışıldı. Fe_3O_4@κ-KRG-aşı-PDMAEMA@DOX nanopartiküllerin DOX salımı pH 7,4, pH 5,5 ve pH 1,2 ortamlarında sırası ile %66,53, %70,08 ve %90,47 bulundu. Nanopartiküllerin asidik ortamda bazik ortama göre daha fazla salım yaptığı görüldü. Süperparamanyetik nanopartiküller pH duyarlı salım ve yüksek DOX tutuklanma verimi gösterdi. Manyetik nanopartiküllerin en düşük hidrodinamik çapı pH 7,4 tamponunda ilaç yüklü olmayan partiküllerde 94,37 nm olarak bulundu. Manyetik nanopartiküllerin pH 7,4 tamponunda daha stabil olduğu görüldü. Manyetik nanopartiküllerin demir içeriği %66,77 bulundu. Sentezlenen nanopartiküller biyouygulamalar için umut vadetmektedir.

Teşekkür

Çalışmamıza maddi destek sağlayan Kırıkkale Üniversitesi Bilimsel Araştırma Projeleri Koordinasyon Birimine (Proje No: 2018/057) teşekkürlerimizi sunuyorum.

Kaynaklar

Akbarzadeh A, Samiei M, Davaran S. 2012. Magnetic nanoparticles: preparation, physical properties, and applications in biomedicine. Nanoscale Res Lett. 7:1-13

Alexis F, Rhee J, Richie JP, Radovic-moreno AF. 2008. New frontiers in nanotechnology for cancer treatment. Urol Oncol: Semin Orig Investig. 26:74-85

Bae K.H, Chung HJ, Park TG. 2011. Nanomaterials for Cancer Therapy and Imaging. Mol Cells. 31:295-302

Danckwerts M, Fassihi A. 1991. Implantable controlled release drug delivery systems: a review. Drug Dev Ind Pharm. 17:1465-1502

Geyik G. Işıklan N. 2022. Multi-stimuli-sensitive superparamagnetic κ-carrageenan based nanoparticles for controlled 5-fluorouracil delivery. Colloids Surf. A: Physicochem Eng Asp. 634:127960

Huang YS, Lu YJ, Chen JP. 2017. Magnetic graphene oxide as a carrier for targeted delivery of chemotherapy drugs in cancer therapy. J Magn Magn Mater. 427:34-40

Indira, T, Lakshmi P. 2010. Magnetic nanoparticles–a review. Int J Pharm Sci Lett. 3:1035-1042

Jabir NR, Tabrez S, Ashraf, GM, Shakil S, Damanhouri GA, Kamal MA. 2012. Nanotechnology-based approaches in anticancer research. Int J Nanomedicine. 7:4391-4408

Jones F, Cölfen H, Antonietti M. 2000. Iron oxyhydroxide colloids stabilized with polysaccharides. Colloid Polym Sci. 278:491-501

Luo H, Ao H, Li G, Li W, Xiong G, Zhu Y, Wan Y. 2017. Bacterial cellulose/graphene oxide nanocomposite as a novel drug delivery system. Curr Appl Phys. 17:249-254

Ma HL, Zhang YW, Zhang L, Wang LC, Sun C, Liu PG, Zhai ML. 2016. Radiation-induced graft copolymerization of dimethylaminoethyl methacrylate onto graphene oxide for Cr(VI) removal. Radiat Phys Chem. 124:159-163

Nene AG, Takahashi M, Wakita K, Umeno M. 2016. Size controlled synthesis of Fe_3O_4 nanoparticles by ascorbic acid mediated reduction of Fe(acac)(3) without using capping agent. J Nano Res. 40:8-19

Özkahraman B, Işıl A, Gök MK, Güçlü G. 2014. Poli (N-Vinilkaprolaktam) Mikrojellerinin Sentez Şartlarının Optimizasyonu. Afyon Kocatepe Üniversitesi Fen ve Mühendislik Bilimleri Dergisi. 14:13-21

Patil R, Portilla-Arias J, Ding H, Konda B, Rekechenetskiy A, Inoue S, Ljubimova JY. 2012. Cellular Delivery of Doxorubicin via pH-Controlled Hydrazone Linkage Using Multifunctional Nano Vehicle Based on Poly(beta-L-Malic Acid). Int J Mol Sci. 13:11681-11693

Rahimdad N, Khalaj, A, Azarian G, Nematollahi D. 2019. Electrochemical Device for the Synthesis of Fe_3O_4 Magnetic Nanoparticles. J. Electrochem. 166: 1-6

Ruuge E, Rusetski A. 1993. Magnetic fluids as drug carriers: targeted transport of drugs by a magnetic field. J Magn Magn Mater. 122:335-339

Saha P, Rakshit R, Mandal K. 2019. Enhanced magnetic properties of Zn doped Fe_3O_4 nano hollow spheres for better bio-medical applications. J Magn Magn Mater. 445:130-136

Shete P, Patil R, Ningthoujam R, Ghosh S, Pawar S. 2013. Magnetic core–shell structures for magnetic fluid hyperthermia therapy application. New J Chem. 37:3784-3792

Siepmann J, Peppas NA. 2012. Modeling of drug release from delivery systems based on hydroxypropyl methylcellulose. Adv Drug Deliv Rev. 64:163-174

Singamaneni S, Bliznyuk VN, Binek C, Tsymbal EY. 2011. Magnetic nanoparticles: recent advances in synthesis, self-assembly and applications. J Mater Chem. 21:16819-16845

Tüylek Z. 2017. İlaç Taşıyıcı Sistemler ve Nanoteknolojik Etkileşim. Bozok Tıp Dergisi. 7:89-98

Yang X, Zhang X, Liu Z, Ma Y, Huang Y, Chen Y. 2008. High-efficiency loading and controlled release of doxorubicin hydrochloride on graphene oxide. J Phys Chem C. 112:17554-17558

Yang JH, Ramaraj B, Yoon KR. 2014. Preparation and characterization of superparamagnetic graphene oxide nanohybrids anchored with Fe_3O_4 nanoparticles. J Alloys Compd. 583:128-133

Zhang BM, Yang XY, Wang Y, Zhai GX. 2017. Heparin modified graphene oxide for pH-sensitive sustained release of doxorubicin hydrochloride. Mater Sci Eng C Mater Biol Appl. 75:198-206

RESEARCH ARTICLE
Eurasian J Bio Chem Sci, 5(1):15-21, 2022
https://doi.org/10.46239/ejbcs.1078752

EJBCS

Eurasian Journal of Biological and Chemical Sciences

Journal homepage: www.dergipark.org.tr/ejbcs

PANi/PPy and PANi Films on ZnNi Alloy Coated Carbon Steel; Electrochemical Syntheses and Corrosion Performances

Ibrahim Filazi[1,2], Ali Tuncay Ozyilmaz[1]*

*[*1]Hatay Mustafa Kemal University, Faculty of Arts and Sciences, Department of Chemistry, Hatay, TURKEY*
[2]Cankiri Karatekin University, Central Research Laboratory, Cankiri, TURKEY

*Corresponding author : atuncay@mku.edu.tr
Orcid No: https://orcid.org/0000-0002-3657-8117

Received : 24/02/2022
Accepted : 21/04/2022

Abstract: Zinc–nickel alloy coating (ZnNi) was successfully deposited on carbon steel (CS) applying current density of 47 $mAcm^{-2}$ with galvanostatic technique. The ZnNi alloy coating image showed that CS metal surface was plated with a blue-grey homogeneous layer. Polyaniline film (PANI) film was synthesized with cyclic voltammetry technique from 0.10 M aniline containing 0.20 M sodium oxalate solution on ZnNi coated carbon steel (CS/ZnNi) electrode surface. And then the synthesis of top PPy film was achieved in pyrrole monomer containing acetonitrile + tetrabutyl ammonium perchlorate medium successfully. After the top PPy synthesis, it was observed that both the PANi homopolymer film and the ZnNi coating continued to exist on the CS surface. The corrosion behaviors of uncoated and coated electrodes were investigated in 3.5% NaCl solution. For this aim, the anodic polarization plots and electrochemical impedance spectroscopy technique were used. The results showed that the top PPy homopolymer film provided an effective barrier property on CS/ZnNi/PANi electrode and a remarkable anodic protection to substrate for longer exposure time.

Keywords: Alloy plating, corrosion, conducting polymer, polypyrrole, polyaniline, ZnNi

1. Introduction

The role and importance of technical metals in today's modern world is too great to ignore. Especially the role of steel among these metals is vital for both industries and governments. While approximately 30 million tonnes of crude steel was produced in the world in 1900, this value reached 1864 million tonnes in 2020 (International Iron and Steel Institute 1978; World Steel Association 2021). This increase not only creates the modern world, but also provides an important workforce and economic value. According to the Oxford Economics report, the share of the steel industry in annual global GDP is around 3.8%. (Oxford Economics, 2019). As can be seen from these values, a healthy metal industry is one of the building blocks of a healthy economy and modern world. However, this rapidly increasing steel usage rate also increases the damage caused by corrosion reactions, which in turn causes the metals to wear out. Corrosion is an unstoppable nature event, causing loss of life and property, serious damage to the state and industry directly or indirectly and a loss of 3.5 to 5% per annum of GNP. (Hou et al. 2017; Koch et al. 2002; Üneri 2011).

For many years, researchers in many disciplines are constantly looking for new ways to protect materials from corrosion and thereby reduce damage caused by corrosion (Kilinççeker et al. 2008; Kilinççeker et al. 2013). Alloy coating is one of the techniques used for this purpose. Especially, zinc & zinc group coatings are frequently uses with various coating techniques for cathodic corrosion protection of Fe group materials due to their high corrosion resistance and mechanical strength. Electro deposition is one of the techniques used for zinc & zinc group coatings and has become widely used in many industries with unique advantages over many other coating techniques such as independence from material shape, easy process setup and control, etc. however, electroplating zinc alone is insufficient to protect materials from corrosion in the medium-long term due to the very less noble nature of zinc. Using zinc alloys with elements in the same period with zinc is one of the most commonly used methods to solve this problem in literature. Among these alloys, especially ZnNi alloy is studied more in the literature because of its excellent resistant characteristic to corrosive factors in the atmospheric environment, machining properties, weldability etc. (Abd El-Lateef et al. 2015; Bhat et al. 2021; Chouia et al. 2021; Ozyilmaz et al. 2020;

Tozar and Karahan 2014) Considering the literature studies in recent years, it is seen that conductive polymers are of interest in the field of corrosion protection due to their unique properties such as superior anticorrosive properties, redox reactions in natural environment and catalytic activity. For this aim, polyaniline and polypyrrole among conducting polymers are use for the corrosion protection of metals in a wide range of aggressive environments (Ates 2016; Kaliyannan et al. 2020; Sokolova et al. 2017).

In this study, the surface of the carbon steel (CS) electrode was plated with a zinc-nickel alloy. The obtained CS/ZnNi electrode was coated with thin polyaniline (PANi) film in an aqueous sodium oxalate solution. After that, polypyrrole (PPy) film was coated as top coating on CS/ZnNi/PANi surface in pyrrole containing acetonitrile + tetrabutyl ammonium perchlorate (TBAP) solution medium. The corrosion performances of the uncoated and coated electrodes were evaluated by EIS and anodic polarization techniques in 3.5% NaCl solution.

2. Materials and Method

All electrochemical studies were carried out on the CH Instruments 660B model electrochemical workstation (S/N: A1420) with three electrode technique in one cell. In the experiment cell, cylindrical low carbon steel electrode (CS) which chemical composition by wt.%: 0.056% C, 0.450% Mn, 0.140% Si, 0.004% S, 0.010% P, 99.34% Fe and surface area 0.0531 cm^2 as working electrode. The square platinum plate (99.99%) with surface area 0.50 cm^2 as counter electrode and Ag/AgCl (3M KCl) electrode as reference electrode was used. Working electrode was isolated with a thick polyester block outside the surfaces which was contact with solution and connects to instrument. Shortly before use, working surface was carefully polished with 400 and 1200 grid abrasive paper, respectively, and washed with 1:1 acetone:ethanol mixture and bi-distilled water, respectively. For the alloy coating, the citrate-sulphate aqueous bath containing 0.20 M $ZnSO_4$, 0.20 M $NiSO_4$, 0.20 M $Na_3C_6H_5O_7$, 0.10 M $(NH_4)_2SO_4$ was used (Winiarski et al. 2015) at natural pH of about 5.3. CS surface was coated with approx. 5 µm ZnNi alloy with chronopotentiometry (CP) technique at 47 mA/cm^2 constant current density at room condition. The electropolymerization was carried out with cyclic voltammetry (CV) technique at room condition. For the PANi coating, 0.10 M freshly distilled aniline monomer was added into 0.20 M aqueous sodium oxalate solution. First, alloy coated electrode (CS/ZnNi) was anodically passivated by applying one segment between -1.50 and 1.00 V potential at a scan rate of 10 mV/s. Next, the film growth curves were taken for 333 seconds at a potential range of 0.00 and 1.00 V at a scan rate 150 mV/s without removing CS/ZnNi electrode from sodium oxalate+aniline solution. After that, PPy film was carried out on PANi coated CS/ZnNi electrode (CS/ZnNi/PANi) surface in acetonitrile+0.025 M TBAP medium containing 0.10 M freshly distilled pyrrole between -0.80 and 0.80 V at 150 mV scan rate for 533 sec. For metallic characterization of uncoated and coated electrodes, the linear sweep voltammetry (LSV) technique was used in aqueous 0.05 M EDTA+0.50 M Na_2SO_4 mixture solution a scan rate of 5 mV/s and a potential range of -1.10 and 1.80 V to show the presence of ZnNi alloy coating on the CS electrode. Anodic polarization curves were obtained from open circuit potential (E_{ocp}) to 1.80 V at 5 mVs^{-1} scan rate, after 240 h of immersion time in 3.5% NaCl solution. Electrochemical impedance studies were recorded at measured open circuit potential values applying 7 mV of amplitude in frequency range from 10^5 to 10^{-3} Hz. Real and imaginary components of the EIS in the complex plane and Bode plots were analyzed with the ZView2 software to estimate the parameters of the equivalent electrical circuit. Surface images were taken with Canon EOS5D high resolution digital camera equipped with Canon EF 100mm Ultrasonic Macro Lens.

3. Results and Discussion

In this study, firstly, the surface of the CS was successfully coated with approx. 5 µm thick ZnNi alloy from citrate-sulphate bath with 47 mA × cm^{-2} current density. It was observed that the surface was polarized immediately at this current density and there was no change at the potential values at a large scale in the increasing time. In addition, it was seen that the potential values of the different electrodes were similar to each other (It was not shown here).

After the metallic coating, the CS/ZnNi electrodes were quickly taken into the PANi synthesis medium. In order to obtain the homogenous PANi film, the ZnNi alloy coated CS electrode were polarized by using only anodic scan from −1.50 to 1.00 V potantial range with scan rate of 10 mV/s (It was not shown here). In the second stage, the growth cycle of PANi film was taken at potential range from 0.00 to 1.00 V with 150 mV/s scan rate. Fifty segments were applied to synthesis of the PANI film.

When the voltammograms were examined, the peaks obtained for surface oxidation-passivation and monomer-oxidation were observed at potentials of about -0.10 and 0.65 V, respectively. After monomer-oxidation peak was observed, current values at ongoing potentials were decreased. All these observations showed that the surface was covered with a thin polyaniline film during on anodic passivation process. A shift of the monomer oxidation peak recorded for aniline to around 0.79 V in the film growth voltammogram was seen in Figure 1. This case proved that a conductive polymer layer were formed on the alloy coated surface during the anodic passivation (Özyılmaz, 2005). The current decreases in the continuing peaks showed that the polyaniline film grew on the surface and reduces the surface conductivity. Figure 1b showed electropolymerization voltammograms for PPy synthesis on to MS/ZnNi/PANi surface. Current increases at potentials after 0.20 V in Figure 1b corresponded to oxidation of the pyrrole monomer. The current values recorded for the monomer oxidation increased at the initial scan and then those values decreased. According to this behavior, it was observed that the surface conductivity first

increased with the polypyrrole film, and then the surface conductivity decreased due to the form transformation of the PPy film.

The photographs of the CS, CS/ZnNi, CS/ZnNi/PANi and CS/ZnNi/PANi|PPy electrodes were given in Figure 2. The surface images show that a homogeneous ZnNi alloy layer is coated on the CS electrode surface with a blue-gray color tone. The photographs of the black PANi and PPy top coatings synthesized on CS/ZnNi surface were given in Figure 2. As can be seen from the images, the surface was homogeneously coated with PANi film and the PANi coating surface was covered with a homogeneous top PPy film.

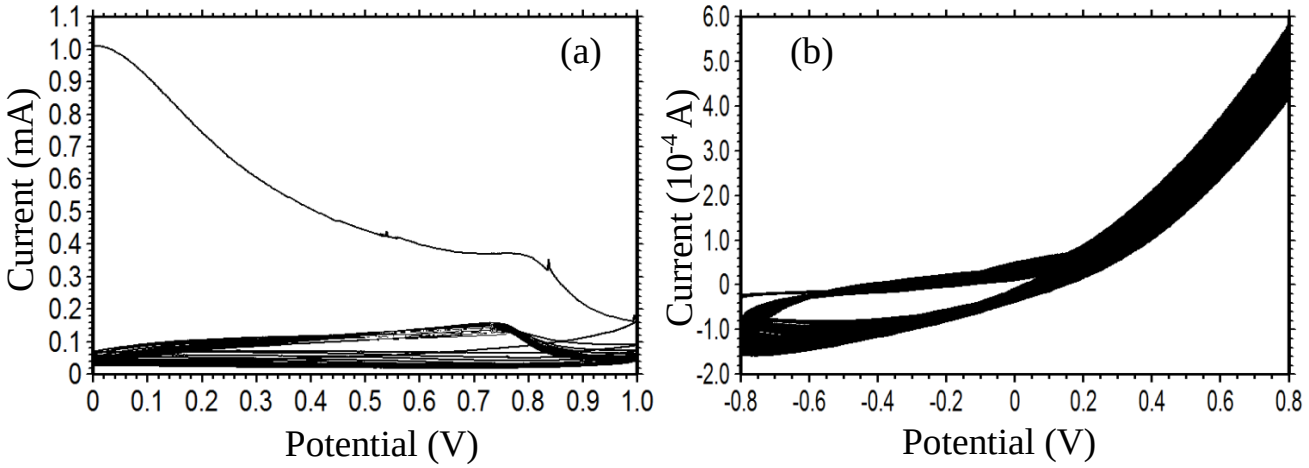

Fig. 1 The voltammograms recorded during the film growth on CS/ZnNi electrode in 0.10 M aniline containing 0.20 M sodium oxalate solution, scan rate: 10 mV/s (a) and on CS/ZnNi/PANi electrode in acetonitrile+0.025 M TBAP containing 0.10 M pyrrole, scan rate: 150 mV s^{-1}(b).

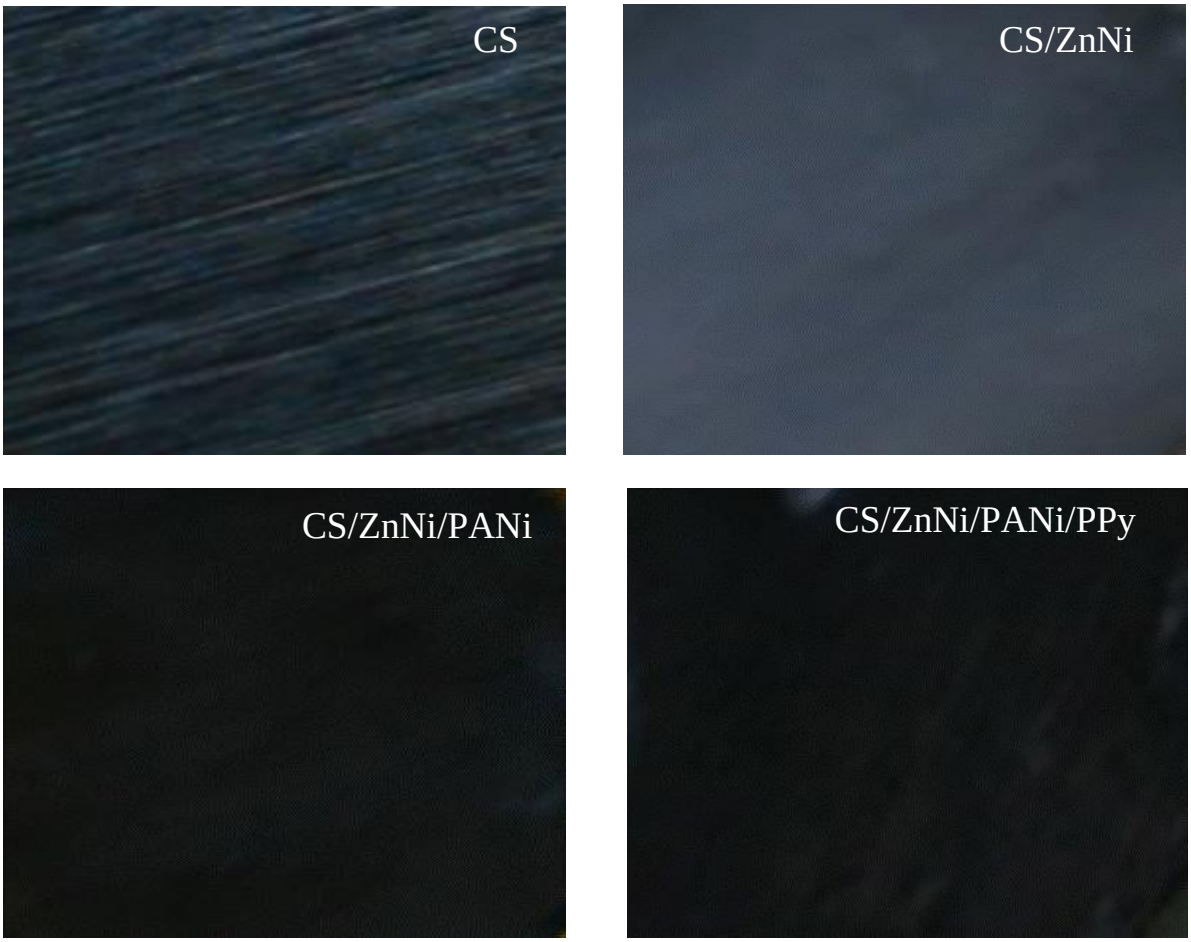

Fig. 2 The photographs of the CS, CS/ZnNi, CS/ZnNi/PANi and CS/ZnNi/PANi|PPy electrodes

Figure 3 shows metallic characterization voltammograms of the CS, CS/ZnNi, CS/ZnNi/PANi and CS/ZnNi/PANi|PPy electrodes. In Figure 3, current increases related to the primary components of the alloy were observed at the CS/ZnNi, CS/ZnNi/PANi and CS/ZnNi/PANi|PPy, unlike CS. For polymer film coated electrodes, these current increases indicated that under polymer films it was a metallic structure that can form complex with EDTA. The current peaks recorded for polymer film coated CS/ZnNi electrodes on the similar potential values of about -0.30 V, which were not recorded for bare CS clearly indicated that the polymer films were synthesized on the ZnNi alloy coated surface. When the current values on the potential values of about 0.10 V obtained for the uncoated and coated electrodes are examined, it is seen that the current values of coated electrodes were lower than the CS electrode. Accordingly, these results showed that the alloy and polymer films formed on the surface created an effective physical barrier and protect the CS electrode from corrosive environment. Besides, the lowest current value recorded for CS/ZnNi/PANi|PPy electrode indicated the presence of effective layers on the CS electrode surface (Akdağ and Özyılmaz 2017).

Anodic polarization results of the CS, CS/ZnNi, CS/ZnNi/PANi and CS/ZnNi/PANi|PPy electrodes after 240h immersion time in 3.5 % NaCl solution are given in Figure 4. The corrosion potential (E_{corr}) values obtained for CS, CS/ZnNi, CS/ZnNi/PANi and CS/ZnNi/PANi|PPy electrodes was found to be -655 mV, -611 mV, -621 mV and -516 mV, respectively. The E_{corr} values of coated electrodes shifted in the anodic region due to anodic protection than that of uncoated electrode. Besides, the most positive E_{corr} value recorded for CS/ZnNi/PANi|PPy electrode, it is easily say that the top PPy film exhibited the most effective physical barrier properties against corrosion products in the corrosive environment when compared with single ZnNi and ZnNi/PANi coatings. This occasion supported the idea that current values of CS/ZnNi/PANi|PPy electrode were significantly lowest when compared with PANi homopolymer film coated ZnNi plated carbon electrode as well as ZnNi plated carbon steel and bare carbon steel electrode. This case showed that PPy film synthesized on CS/ZnNi/PANi electrode had lowest permeability against the attack of corrosive products like dissolved oxygen and chloride ions. These anodic polarization results revealed that top PPy homopolymer film provided important corrosion protection to uncoated and coated CS electrode.

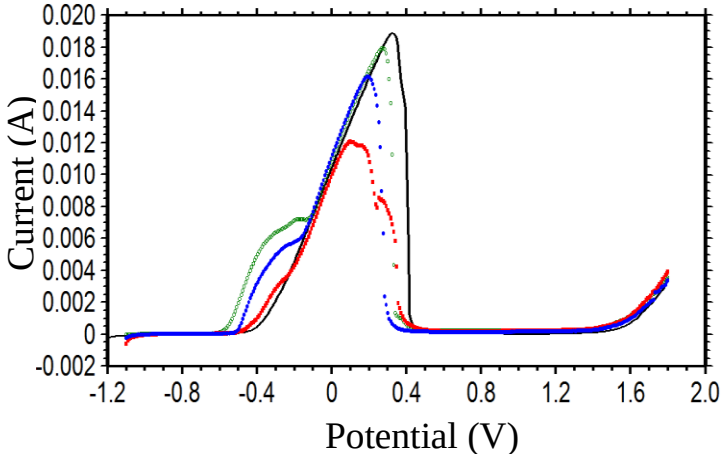

Fig. 3 Lineer Sweep voltametry recorded for MS (-), MS/ZnNi (o), MS/ZnNi/PANi (●) and MS/ZnNi/PANi/PPy (■) electrodes in 0.05 M EDTA containing 0.50 M sodium sulphate solution.

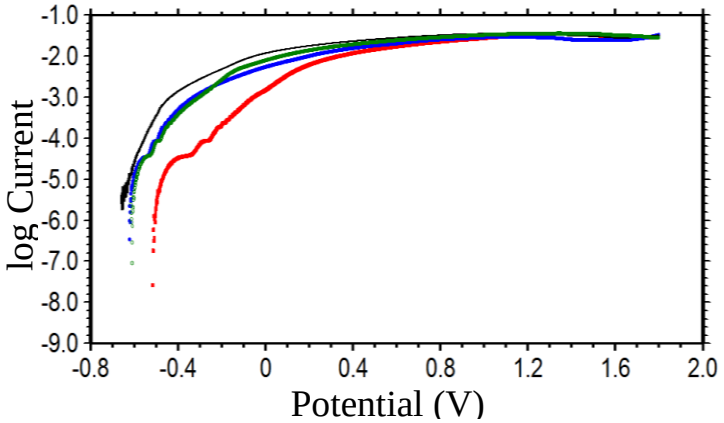

Fig. 4 Anodic polarization results recorded for MS (-), MS/ZnNi (o), MS/ZnNi/PANi (●) and MS/ZnNi/PANi/PPy (■) electrodes after 240 h of immersion time in 3.5% NaCl solution.

Figure 5 shows the Nyquist plots recorded for CS, CS/ZnNi, CS/ZnNi/PANi and CS/ZnNi/PANi|PPy electrodes after 72 and 240 h immersion times in 3.5% NaCl solution. After 72 h of exposure time, the E_{ocp} values of CS/ZnNi, CS/ZnNi/PANi and CS/ZnNi/PANi|PPy electrodes were found to be approx. -0.595, -0.599 and -0.576 V, respectively while that of bare CS electrode was −0.669 V. For the CS/ZnNi electrode, this value was significantly in the anodic direction compared to the CS electrode, despite the active zinc metal in the alloy. This behavior was the result of a stable oxide layer formed on the ZnNi alloy coating surface. On the other hand, appearance of more positive E_{ocp} value for CS/ZnNi/PANi|PPy electrode indicated prominent differences between dissolution behavior of ZnNi alloy plating and the corrosion reactions at the CS surface. This showed that PPy homopolymer film on CS/ZnNi/PANi surface exhibited an important passive film behavior against to corrosive products on carbon steel electrode. In Fig. 5(a), there were two depressed semicircles which could not be well resolved from each other from high and low frequency region, for CS/ZnNi, CS/ZnNi/PANi and CS/ZnNi/PANi|PPy electrodes, while the plot of bare CS electrode consisted of one depressed semicircle. The depressed semicircle obtained for bare CS electrode was equal to the polarization resistance (R_p) that including the total of the charge transfer resistance (R_{ct}) that is responsible for the anodic dissolution of bare metal and diffusion resistance (R_d), after 72 h of exposure time. Besides, there were R_{ct} at high frequency region and oxide layer resistance (R_o) + alloy plating resistance (R_{ZnNi}) at low frequency region for CS/ZnNi electrode, while the two depressed semicircles for CS/ZnNi/PANi and CS/ZnNi/PANi|PPy electrodes were equal to R_p including the total of R_{ct} + R_{ZnNi} + R_o + polymer film resistance (R_{pf}) ranging from high to low frequency region. The corrosion current (I_{corr}) and the protection efficiency values (E%) of PANi|PPy and PANI coatings on CS/ZnNi electrode were calculated as in our earlier work (Ozyilmaz et. al. 2006). The parameters calculated for CS, CS/ZnNi, CS/ZnNi/PANi and CS/ZnNi/PANi|PPy electrodes are presented in Table 1. In Table 1, R_p values, which were analyzed with the ZView2 software, were obtained from Stern-Geary equation for calculation of corrosion current (I_{corr}) using following equation (1). B value was equal to $(\beta_a x \beta_c)/((\beta_a + \beta_c)x2.303)$; β_c and β_a were cathodic and anodic Tafel slopes, respectively. The value of B was taken as 0.052 V for coated electrodes and 0.026 V for uncoated electrode.

$$Icorr = \frac{B}{Rp} \quad (1)$$

The protection efficiency values (E %) were calculated by using the following equation.

$$E\% = \frac{R^{-1}_{p(uncoated)} - R^{-1}_{p(coated)}}{R^{-1}_{p(uncoated)}} x100 \quad (2)$$

The R_p values obtained for CS/ZnNi/PANi|PPy electrode was found to be highest when compared with those of CS, CS/ZnNi and CS/ZnNi/PANi electrodes. Besides, I_{corr} value obtained for CS/ZnNi/PANi|PPy electrode was found to be 1.45 µA that the lowest value when compared with those of all electrodes. This case showed the barrier effect of PPy film as top coating, after 72h of immersion time in 3.5% NaCl solution. After 240 hours, the R_p values of the CS, CS/ZnNi/PANi and CS/ZnNi/PANi|PPy electrodes were lower than the values obtained after 72 hours of exposure, while the value of the CS/ZnNi electrode was higher. These results showed that the stable oxide layers formed on the ZnNi alloy coating surface over time. The R_p value increase of CS/ZnNi electrode was observed due to the formation of stable NiO and complex ZnO•H_2O on ZnNi plating surface. Nevertheless, the R_p values recorded for CS/ZnNi CS/ZnNi/PANi and CS/ZnNi/PANi|PPy electrodes were found to be higher when compared with those of uncoated CS metal, after 240 h of exposure time, while the highest R_p value was obtained for CS/ZnNi/PANi|PPy electrode. In addition, the E% value of CS/ZnNi/PANi|PPy electrode was 75.36% that it was relatively higher value than those of 17.92% for CS/ZnNi and 9.87% for CS/ZnNi/PANi electrodes. On the other hand, a decrease in the I_{corr} value of the CS/ZnNi/PANi|PPy electrode was observed after 240 hours compared to the 48 hour immersion times. After 240 hours of exposure, the decrease in R_p for the CS/ZnNi/PANi|PPy electrode was indicative of a small increase in the amount of electrolyte solution in the alloy coating and the homopolymer film surfaces. Nevertheless, I_{corr} value obtained for CS/ZnNi/PANi|PPy electrode was obtained as 1.52 µA that the lowest value than those of 3.49 for CS/ZnNi and 3.83 for CS/ZnNi/PANi electrodes. It was clear that PPy film exhibited an effective barrier property against corrosion products, whereby providing a decrease in diffusion rate of ions.

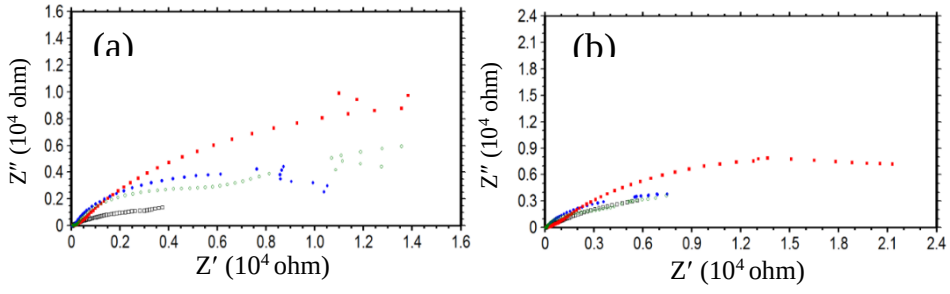

Fig. 5 The Nyquist plots recorded for MS (-), MS/ZnNi (o), MS/ZnNi/PANi (●) and MS/ZnNi/PANi/PPy (■) electrodes after 72h(a) and 240h(b) of immersion time in 3.5% NaCl solution.

Table 1. The E_{ocp}, R_p, I_{corr} and E% values recorded for CS, CS/ZnNi and CS/ZnNi/PANi and CS/ZnNi/PANi/PPy electrodes after various exposure times in 3.5% NaCl.

Electrode	t (h)	E_{ocp} (mV)	R_p (Ω)	I_{corr} (μA)	E%
CS	72	-648	9020	-	-
	240	-665	12232	-	-
CS/ZnNi	72	-595	14148	3.67	36.25
	240	-613	14903	3.49	17.92
CS/ZnNi/PANi	72	-599	13433	3.81	32.85
	240	-616	13571	3.83	9.87
CS/ZnNi/PANi|PPy	72	-576	35813	1.45	74.81
	240	-545	34259	1.52	64.30

4. Conclusions

As a result of the study, the CS surface can be successfully coated with ZnNi alloy from the citrate sulphate bath at 47 mA/cm^2 current density via galvanostatic technique. It was seen from the photograph that a homogeneous ZnNi alloy coating in blue-gray color was obtained. Then, PANi coating was successfully synthesized on CS/ZnNi electrode from neutral medium. It was found that the polarization of CS/ZnNi surface was necessary for homogenous PANi film synthesis prior to monomer oxidation and film growth. And then, PPy film was carried out on CS/ZnNi/PANi electrode surface in pyrrole containing acetonitrile + tetrabutyl ammonium perchlorate (TBAP) solution medium. The TBAP was found to be suitable as electrolyte in acetonitrile medium for homogeneous polypyrrole synthesis. As a result, the homogeneous and adherent PANi and top PPy films were synthesized on CS/ZnNi electrode surface. The corrosion performance of the bare CS electrode was compared with CS/ZnNi, CS/ZnNi/PANi and CS/ZnNi/PANi|PPy electrodes. The single ZnNi alloy coating and bilayer ZnNi/PANi coating did not show any significant barrier behavior on the CS electrode surface. On the other hand, the PPy coating as the top layer exhibited a significant physical barrier behavior on the CS/ZnNi/PANi electrode at longer exposure time.

Author Contributions:
IF performed the synthesis and corrosion measurements of the alloy and polymer coatings. ATO and IF evaluated the corrosion performance of the alloy and polymer films. IF wrote the manuscript.
ATO controlled the manuscript. All authors read and approved the final manuscript.

Conflict of interest disclosure:
The authors state that there are no conflicts of interest to disclose.

References

Akdağ A, Özyılmaz AT. 2017. Poly(N-methylpyrrole) Film on ZnNi Plated Carbon Steel Electrode. Acta Chim. Slov. 64(2):312–318. doi.org/10.17344/acsi.2016.3119

Ates M. 2016. A review on conducting polymer coatings for corrosion protection. J Adhes Sci Technol. 30(14):1510–1536. doi.org/10.1080/01694243.2016.1150662

Bhat RS, Shetty SM, Kumar, NA. 2021. Electroplating of Zn-Ni Alloy Coating on Mild Steel and Its Electrochemical Studies. J Mater Eng Perform. 30:8188–8195. doi.org/10.1007/s11665-021-06051-1

Chouia F, Chala A, Lakel A, Sahraoui T. 2021. Morphology and Corrosion Behavior of Zn-Ni Layers Electrodeposited on Low Alloy Carbon Steel Substrate. Ann Chim Sci Mat. 45(3):225–230. doi.org/10.18280/acsm.450305

El-Lateef HM, El-Sayed A, Mohran H. 2015. Role of Ni content in improvement of corrosion resistance of Zn–Ni alloy in 3.5% NaCl solution. Part I: Polarization and impedance studies. T Nonferr Metal Soc. 25(8):2807–2816. doi.org/10.1016/S1003-6326(15)63906-1

Hou B, Li X, Ma X, Du C, Zhang D, Zheng M, Xu W, Lu D, Ma F. 2017. The cost of corrosion in China. NPJ Mater Degrad. 1(1):4. doi.org/10.1038/s41529-017-0005-2

International Iron and Steel Institute. 1978. A handbook of world steel statistics 1978. https://worldsteel.org/steel-by-topic/statistics/steel-statistical-yearbook/

Kaliyannan GV, Velusamy MKK, Palaniappan SK, Anandraj MK, Rathanasamy R. 2020. Polymer Coatings for Corrosive Protection. Polymer Coatings: Technology and Applications, Wiley, pp 371–395. doi.org/10.1002/9781119655145.ch17

Kilinççeker G, Galip H. 2008. The effects of acetate ions (CH_3COO^-) on electrochemical behavior of copper in chloride solutions. Mater Chem Phys. 110(2-3):380-386. doi.org/10.1016/j.matchemphys.2008.02.026

Kilinççeker G, Demir H. 2013. The Inhibition Effects of Methionine on Corrosion Behavior of Copper in 3.5% NaCl Solution at pH = 8.5. Prot Met Phys Chem. 49(6):788-797. doi.org/10.1134/s2070205113060221

Koch GH, Brongers MPH, Thompson NG, Virmani YP, Payer JH. 2002. Cost of Corrosion Supplement. Corrosion Costs and Preventive Strategies in the United States. https://doi.org/FHWA-RD-01-156

Oxford Economics. 2019. The Role of Steel Manufacturing in the Global Economy: A Report for the World Steel Association. *https://www.worldsteel.org*

Ozyilmaz AT, Ozyilmaz G, Colak N. 2006. Novel synthesis medium for poly(aniline-co-o-anisidine). Surf Coat Technol. 201:2484-2490. doi:10.1016/j.surfcoat.2006.04.008

Ozyilmaz AT, Sangun MK, Filazi I, Surmelioglu C, Ozyilmaz G. 2020. A Novel Approach to the Synthesis of Alloy: PEG400 Containing ZnNi and ZnNiCr Alloy Coatings and Their Anticorrosion Performance. Metall Mater Trans A. 51(7):3638–3647. doi.org/10.1007/s11661-020-05766-5

Özyılmaz AT. 2005. The corrosion behavior of polyaniline top coat on nickel plated copper from neutral aqueous medium. Prog Org Coat. 54(2):127–133. doi.org/10.1016/j.porgcoat.2005.05.003

Sokolova MP, Smirnov MA, Kasatkin IA, Dmitriev IY, Saprykina NN, Toikka AM, Lahderanta E, Elyashevich GK. 2017. Interaction of Polyaniline with Surface of Carbon Steel. Int J Polym Sci. 2017:1–9. doi.org/10.1155/2017/6904862

Tozar A, Karahan IH. 2014. Structural and corrosion protection properties of electrochemically deposited nano-sized Zn–Ni alloy coatings. Appl Surf Sci. 318:15–23. doi.org/10.1016/j.apsusc.2013.12.020

Üneri S. 2011. Korozyon ve Önlenmesi (3rd ed.). Corrosion Association, Ankara

Winiarski J, Laszczyńska A, Szczygieł B. 2015. An electrochemical study on the influence of sodium molybdate on electrodeposition process and phase composition of ternary Zn–Ni–Mo alloy coatings. Trans IMF. 93(5):267–274. doi.org/10.1080/00202967.2015.1114728

World Steel Association. 2021. Global crude steel output decreases by 0.9% in 2020. World Steel Association Press Releases. *https://www.worldsteel.org*

RESEARCH ARTICLE
Eurasian J Bio Chem Sci, 5(1):22-28, 2022
https://doi.org/10.46239/ejbcs.1032007

EJBCS

Eurasian Journal of Biological and Chemical Sciences

Journal homepage: www.dergipark.org.tr/ejbcs

Real-Time Monitoring the Indoor Air Quality Parameters of Intensive Care Unit During the Pandemic Period

Sanaz Lakestani[1*], Mehmet Milli[2], İsa Yıldız[3], Abdullah Demirhan[3]

[1*] *Bolu Abant Izzet Baysal University, Scientific Industrial and Technological Application and Research Center, Bolu, Turkey.*
[2] *Bolu Abant Izzet Baysal University, Department of Computer Engineering, Faculty of Engineering, Bolu, Turkey.*
[3] *Bolu Abant Izzet Baysal University, Department of Anesthesiology and Reanimation, Faculty of Medicine, Bolu, Turkey.*

*Corresponding author : sanazlakestani@ibu.edu.tr
Orcid No: https://orcid.org/0000-0002-1661-7166

Received : 03/12/2021
Accepted : 10/05/2022

Abstract: People spend most of their time in enclosed spaces (e.g., hospital, houses, office buildings, public transportation, and schools). The coronavirus in late 2019 has rapidly spread throughout the world. After the pandemic, people started to spend more time in indoor environments, especially in hospitals. In this study, air quality monitoring was carried out in the Intensive Care Unit of a hospital in Bolu - Turkey. This is the first comprehensive study done in Turkey. In this study, $PM_{2.5}$, PM_{10}, temperature, and relative humidity parameters affecting indoor air quality were monitored instantly for one month with a Wireless Sensors Network-based system. By the results of the study, the maximum concentration of these parameters except relative humidity was higher than the limited by accepted values parameters by the United States Environmental Protection Agency (EPA), The American Society of Heating, Refrigerating and Air-Conditioning Engineers (ASHRAE), and the World Health Organization (WHO).
Keywords: Intensive Care Unit, PM, Indoor Air Quality, Monitoring, Wireless Sensor Network.

1. Introduction

Indoor air pollution has become a serious issue affecting public health, and indoor air quality monitoring system helps in the detection and improvement of indoor air quality. Air pollution is a major environmental hazard to human health and a leading cause of mortality and morbidity worldwide (Chen and Hoek, 2020). Indoor air quality monitoring in the healthcare environment has become a critical part of hospital management, especially in intensive care units. It is thought that air quality in intensive care units does not get the standard levels with routine preventions and requires additional measures. The indoor air quality monitoring system helps to determine and improve air quality.

Many studies have shown that particulate matters are higher indoors than outdoors (Karakas et al. 2013) PM is highly associated with the incidence of respiratory and cardiovascular diseases and mortality (Kim et al. 2015).

Average indoor PM concentrations reported in hospitals in developed countries, including European countries and Taiwan, are generally low(Heibati et al. 2021a). PM with aerodynamic diameter below 2.5 µm ($PM_{2.5}$) and 10 µm (PM_{10}) are < 20 µg/m^3 and < 25 µg/m^3, respectively (Baurès et al. 2018; Fernández et al. 2009; Loupa et al. 2016). However, those measured in China ($PM_{2.5}$, 98, and 124 µg/m^3) (Wang et al. 2006) and South Korea (PM_{10}, 57 µg/m^3) (Hwang et al. 2018) is substantially higher with levels up to 250 µg/m^3 (Heibati et al. 2021b).

After the SARS-CoV-2 pandemic was started to spread rapidly in the world, healthcare organizations and healthcare professionals were focused on the treatment processes and the infection risk rather than limiting the spread of the disease. However, the fact that the indoor air quality in the hospitals, which has been a great risk, is an important factor in determining the rate of spread of the disease has been ignored. The increased risk of occupational exposure of healthcare workers to SARS-CoV-2 is of particular concern (Stern et al. 2021).

After the SARS-CoV-2 virus emerged in China, it is started to be seen in almost all countries in a short time. The first official deaths caused by COVID-19 in Turkey have been reported by the Ministry of Health on March 18, 2020 (Interior Republic of Turkey Ministry of, 2020).

In the pandemic period, one of the important transmission of the disease was having a great impact on international human transport. As of March 21, 2020, the number of countries with a flight ban reached 46 in total (Against and Turan, 2020). Turkey is a transit point for international human transport when viewed from this angle ıt has a critical geopolitical position. Apart from the travel restrictions, with the advice of the Scientific Committee, about blocking entering of the virus into Turkey or delaying the disease to enter Turkey, serious steps were taken. One of these steps is to close the border gates with neighbor states.

In Turkey during the pandemic process, the treatment of critical patients in the intensive care unit was carried out. In this study, real-time monitoring of the ICU indoor air parameters and evaluation of the results will provide opinions about limiting the spread of the disease. As a result of the study, the physical conditions of the intensive care units used in the treatment of this disease will be discussed and concrete data will be revealed.

This is the first comprehensive study done during the COVID-19 in Turkey. In this study, indoor air quality levels were monitored in real-time using Wireless Sensor Networks from the intensive care unit. Indoor levels of PM_{10}, $PM_{2.5}$, temperature, and relative humidity were measured by using wireless sensor networks.

Reduction of hospital infections and other diseases due to environmental factors through real-time monitoring and communication system in a hospital environment will provide an extensive impact on society by reducing expenditures on health. It was formed an important database for more extensive projects to be carried out in the future.

2. Materials and Method

2.1. Study Area

This study was carried out in the Intensive Care Unit (ICU) of a hospital in Bolu, Turkey. The intensive care unit consisted of a nursing station, a washing stand, an isolated room, and 13 beds. The area of the ICU is approximately 250 m^2. High-Efficiency Particulate Air filters (HEPA) were installed above the 13 beds. The layout of the floor plan of the ICU is presented in Figure 1.

2.2. Sampling

Wireless Sensor Networks were installed on a flat and horizontal surface at about 1.5 meters above the floor. Continuously the changes indoor air quality levels in intensive care units were being monitored by using Wireless Sensor Networks (WSN). Data were collected by WSN from four different points for one month in the ICU;

a) Near the entrance door
b) Near the nursing station
c) Near the isolated room
d) Isolated room

Every sampling day, the number of persons, activities in the ICU, and the cleaning program were recorded and can be summarized as below:

a) In the morning; doctors, interns, and nurses examined the patients.
b) At 10:00 am, washing/transferring of patients, changing bedclothes, and cleaning the beds and floor were performed.
c) In the evening patients were asleep or resting and two or three nurses stayed in ICU.

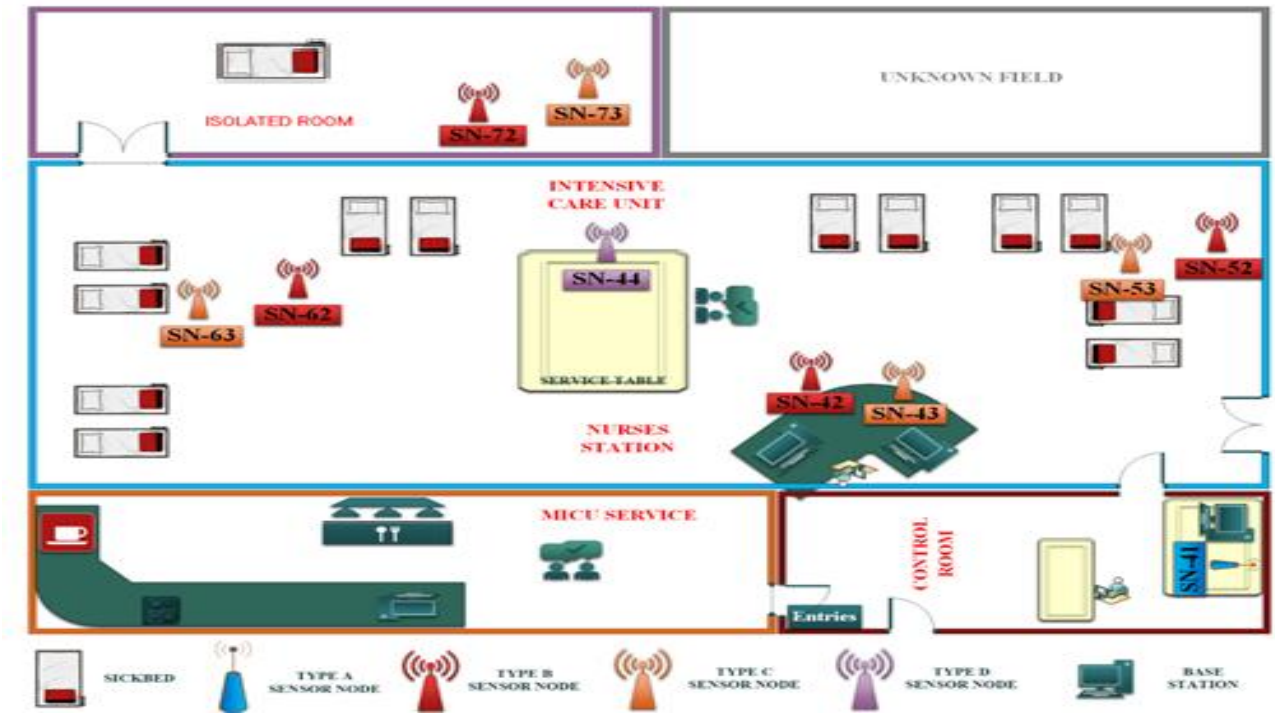

Fig. 1 Schematic layout of Intensive Care Unit (Not drawn to scale).

2.3. Creating Sensor Nodes and Establishing a Wireless Sensor Network

In the proposed study, 3 different nodes are designed. These are the Gateway node, Sensor node, and repeater node. The task of the sensor nodes is to measure the parameter in the physical environment and transmit it to the gateway node. Gateway node acts as a bridge for transmitting data from nodes which has measurement capability to the station. Repeater nodes, on the other hand, are responsible for strengthening the signal when the communication between sensor nodes and gateway nodes is disrupted due to distance or physical obstacles. Arduino Uno with ATmega328P microcontroller was used as a microcontroller board in all nodes. The circuit elements that make up the nodes are soldered using Proto Shield. Gateway node and Repeater Nodes consist of Arduino Uno and nRF24L01 communication Devices. The antenna has been added to increase the signal distances of the nRF24L01 communication modules. In sensor nodes, Arduino UNO consists of sensors that detect the parameters to be measured, as well as the NRF24L01 module. The sensors forming the sensor nodes are described in detail below. The technical components used in the nodes created within the scope of the study are explained in Figure 2.

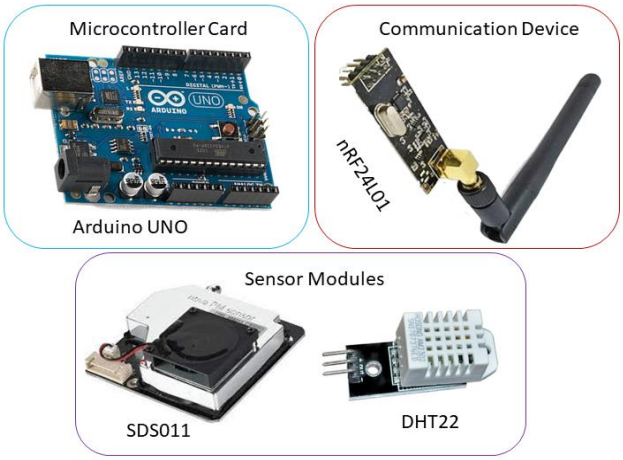

Fig. 2 Hardware components that makeup sensor nodes

Within the scope of the study, 4 different parameters were collected in the intensive care unit chosen as the measurement environment. These parameters are PM2.5, PM10, temperature, and humidity data. Two different sensors were used to collect these 4 parameters. For the measurement of temperature and humidity values, the DHT22 sensor module, which is frequently used by researchers, was used. The DHT22 sensor module is a low-cost, digital output active sensor. It is also an ideal sensor for recommended operation with low power consumption and a high degree of accuracy. Nova SDS011 sensor module was used to measure PM2.5 and PM10 values. This sensor module detects particles of 0.3-10 μm in the air with laser scanning technique. Particles in the scanning area are detected by laser scattering. The reflected light is converted into an electrical signal. The analyzed particle amount is transmitted to the microcontroller card by serial communication. Detailed information about the installation of the sensor nodes is found in the article previously published by the project team (AKTAŞ et al. 2020).

2.4. Deployment of Sensor Nodes and Collection of Data

Sensor nodes developed to measure indoor air parameters were distributed homogeneously in the measurement environment. A total of 6 nodes, including 4 sensor nodes, 1 gateway node, and 1 repeater node, were designed to perform healthy measurements in the Intensive Care Unit, which was determined as the measurement environment. After the sensor nodes were deployed to the measurement environment, the sensors were calibrated for 1 day, some technical problems were solved and more accurate measurements were tried to be obtained. After it was seen that all sensor nodes started to send healthy data, the process of saving to the database was started. Each sensor node is programmed to measure only one data per minute.

In the study, Microsoft Structured Query Language (MSSQL) Server platform was used as a database for storing sensor measurements. MSSQL-Server is a relational database management system (RDBMS) that supports a wide variety of transaction processing, business intelligence, and analytics applications widely used by researchers. Structured Query Language (SQL), on the other hand, is a query language that performs operations such as recording, editing, adding, deleting, and pulling records to the database. The hourly averages of the data coming to the Base Station through the Gateway have been recorded in the MSSQL-Server database to avoid unnecessary repetitions.

2.5. Monitoring

After the sensor nodes were placed in the 4 locations in the ICU, and the data was sent properly, the data collection process was started on 02.09.2020 at 11:03. Each sensor in the installed system is programmed to measure an average per minute and send it to the gateway. During the data collection process, the hourly average of the collected data was added to MSSQL, a relational database, to avoid unnecessary sensor repetitions. MSSQL is a client/server-based SQL database management system used to save data in many studies. MSSQL is used as a database in this study because it is a system that is consistent, easy to use, and familiar to the project team. In addition, MSSQL has been preferred as a relational database in this project as it provides a clear user interface for sensor data monitoring and management.

The date range of the data collection process performed in the intensive care unit is also the same time the Covidien-19 outbreak in Turkey corresponds to the second peak it reached in October. The data collection process in ICU was ended on 01.10.2020. A total of 30 days of uninterrupted data was collected at the 4 different selected measurement sites. Between these dates, each sensor made approximately 43,000 measurements, and a total of approximately 1,400,000 measurements were made. Within the scope of this project, in the ICU designated as the second measurement area, doctor controls were carried out between 09:00 and 11:00 am every day. Besides, every day between

12:00 and 14:00 is determined as visitor hours. These situations have been beneficial in terms of evaluating the results of the project to what extent the human density and human activities affect the environmental conditions during these hours.

The monitoring data were collected from 1 October to 2 November 2021. Data were recorded hourly by using WSN in the ICU.

3. Results

3.1. The concentration of Indoor the Environmental Parameters

Table 1. showed the mean, maximum, minimum concentrations, and standard deviations of temperature, relative humidity, $PM_{2.5,}$ and PM_{10} in the ICU and ısolated room.

The maximum concentration of PM_{10} 99.94 µg/m3 was measured by WSN near the entrance door in the ICU. The maximum concentration of $PM_{2.5}$ 81.71 µg/m3 and Relative humidity (RH) of 45.80 % was measured by WSN near the nursing station (Table 1).

Table 1. Maximum, Minimum, Standard Deviation, and Mean Concentrations of Data Were Collected by Wireless Sensor Networks (WSN) in the ICU

Sensors Near The Nursing Station				
	***N**	**Max.**	**Min.**	**Mean± SD**
Temperature °C	720	28,47	20,42	24,69±1,12
Relative Humidity %	720	45,80	18,68	30,83±5,43
$PM_{2.5}$ (µg/m^3)	720	81,71	0,01	4,86±5,89
PM_{10} (µg/m^3)	720	99,94	0,05	6,92±7,79
Sensors Near The Entrance				
	***N**	**Max.**	**Min.**	**Mean± SD**
Temperature °C	720	28,28	21,6	25,39±1,10
Relative Humidity %	720	44,68	19,15	30,83±4,77
$PM_{2.5}$ (µg/m^3)	720	64,29	0,01	5,37±6,62
PM_{10} (µg/m^3)	720	91,04	0,04	7,80±8,56
Sensors Near The Isolated Room				
	***N**	**Max.**	**Min.**	**Mean± SD**
Temperature °C	720	29,05	20,43	25,32±1,36
Relative Humidity %	720	44,87	17,49	30,82±5,46
$PM_{2.5}$ (µg/m^3)	720	76,26	0,01	4,75±6,38
PM_{10} (µg/m^3)	720	95,47	0,03	7,78±8,85
Sensors in The Isolated Room				
	***N**	**Max.**	**Min.**	**Mean± SD**
Temperature °C	718	27,35	20,89	24,44±1,13
Relative Humidity %	720	39,12	13,91	28,31±4,60
$PM_{2.5}$ (µg/m^3)	720	51,85	0,01	4,44±4,40
PM_{10} (µg/m^3)	720	73,79	0,01	6,08±7,58

***N**: Number of samples

3.2. Statistical Analysis

Statistical calculations were performed using the Stat graphics Centurion Statistical Software. The environmental parameters were initially investigated by descriptive statistics (mean and standard deviation). The ANOVA test was done between environmental parameters. The differences between the groups were determined at a 95% confidence interval for each parameter ($p < 0.05$) (Table 2).

Table 2. One-Way ANOVA comparison test of environmental factors

	Temperature °C	**Relative Humidity %**	**$PM_{2.5}$ (µg/m^3)**	**PM_{10} (µg/m^3)**
Temperature °C		0.00	0.92	0.99
Relative Humidity %	0.00		0.00	0.00
$PM_{2.5}$(µg/m^3)	0.92	0.00		0.00
PM_{10} (µg/m^3)	0.99	0.00	0.00	

Since the P-value of the F-test is less than 0.05 there is a statistically significant difference between the mean of temperature and RH%, $PM_{2.5}$ with PM_{10} and RH%, PM_{10} with $PM_{2.5}$ and RH% to another at the 95.0% confidence level.

The *p*-value was greater than 0.05 which demonstrates that there was not a statistically significant difference between the mean of temperature, $PM_{2.5,}$ and PM_{10}.

4. Discussion

4.1. Maximum Acceptable Levels for Measured Parameters

Accepted values parameters by the United States Environmental Protection Agency (EPA), The American Society of Heating, Refrigerating and Air-Conditioning Engineers (ASHRAE), and the World Health Organization (WHO), Guidelines on Energy Efficiency of Air Conditioning Installations (EMSD) and Indoor Air Quality guideline value for Japan and South Korea were shown in table 3 and table 4.

Table 3. The Acceptable Values of Parameters to be provided by WHO, EPA and ASHRAE Organization in Indoor Environment

Organization	**PM_{10} µg/m^3**	**$PM_{2.5}$ µg/m^3**
WHO		
EPA (Pickett and Bell, 2011)	50 (24 hours)	25 (24 hours)
ASHRAE (Tucker, 2002)	50 (24 hours)	25 (24 hours)

Table 4. The Acceptable Values of Parameters to be provided by EMSD Organization, Japan and South Korea in Indoor Environment

Organization	Temperature °C	Relative Humidity %
EMSD (*Guidelines on energy efficiency of cultural heritage - ScienceDirect*, 1998) (Guidelines on the energy efficiency of cultural heritage - ScienceDirect, 1998)	20 to <25.5 (8 hours) (Excellent class)	
EMSD (*Guidelines on energy efficiency of cultural heritage - ScienceDirect*, 1998) (Guidelines on the energy efficiency of cultural heritage - ScienceDirect, 1998)	<25.5 (8 hours) (Good class)	
Indoor Air Quality guideline value for Japan and South Korea (Jeong, 2012)		40 to <70 (8 hours) (Excellent class)

Limit values accepted by EPA and WHO for PM_{10} and $PM_{2.5}$ were set as the daily average (24 hours) respectively 50 µg / m^3 and 25 µg / m^3. Accepted values by ASHRAE for PM_{10} were shown in table 3.

The maximum concentration of PM_{10} and $PM_{2.5}$ in the ICU and the isolated room were measured higher than the accepted value by EPA, WHO, and ASHRAE's limited (Figure 3).

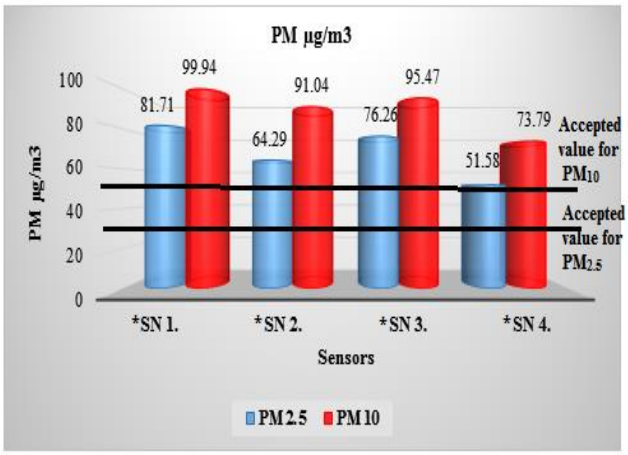

Fig. 3 The maximum concentration of PM_{10}, $PM_{2.5}$, and acceptable limited

***SN1:** Sensors Near The Nursing Station, ***SN2:** Sensors Near The Entrance Door, ***SN3:** Sensors Near The Isolated Room**, *SN4:** Sensors in The Isolated Room

It is important to note that temperature and RH will always relate to affect the survival of airborne viruses in aerosols. Temperature is one of the most major factors affecting virus survival, as it can affect the state of the virus genome. Virus survival decreases progressively at 20.5°C –24°C. The maximum temperature was recorded by sensors in the ICU and the isolated room was higher than the accepted limits (Wingate, n.d.) (Figure 4).

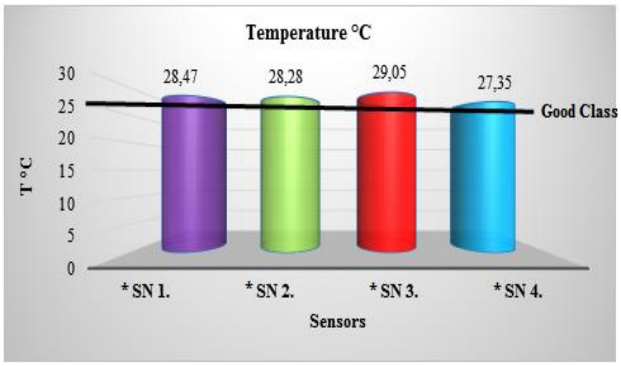

Fig. 4 The maximum concentration of temperature and acceptable limited

***SN1:** Sensors Near The Nursing Station, ***SN2:** Sensors Near The Entrance Door, ***SN3:** Sensors Near The Isolated Room**, *SN4:** Sensors in The Isolated Room

Relative humidity ranges about 55%–60% for more critical areas, such as operating theatres and recovery and the intensive care unit. Maximum percentages of relative humidity were measured in the ICU and the isolated room were lower than the acceptable value from the Indoor Air Quality guideline value for Japan and South Korea (Figure 5).

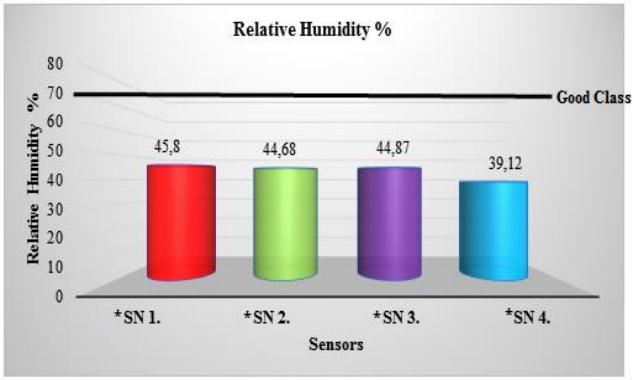

Fig. 5 The maximum concentration of RH and acceptable limited

***SN1:** Sensors Near The Nursing Station, ***SN2:** Sensors Near The Entrance Door, ***SN3:** Sensors Near The Isolated Room**, *SN4:** Sensors in The Isolated Room

5. Conclusion

In public places such as hospitals and schools, the level of indoor air quality is important for local administrators as social health is important.

However, poor indoor air quality in buildings can cause short and long-term health problems. Indoor air quality has been the outcome of diseases such as including deficits in lung function, chronic respiratory disease, lung cancer, heart disease, nervous system, liver, or kidneys(Lakestani et al. 2013).

Especially during the COVID-19 pandemic, it is thought that in critical areas like the intensive care units that will reduce the rate of spread of the diseases by the continuous monitoring of indoor air pollutants. Improving and increasing the indoor air quality in the hospitals for healthcare staff, patients, and visitors has been a part of the policies of hospital local governments.

The aim of this study, to provide real-time monitoring of indoor air quality levels by using wireless sensor networks in critical areas such as the intensive care units in hospitals and helping to take necessary measures. The results of this study include:

- Doctor controls of all the ICU services are done at approximately 10 o'clock. When the measured parameters were analyzed, it was seen that the increase usually at the doctor's control hours. To minimize the spread of the viruses, especially in cases such as the COVID-19 pandemic, the number of people in the indoor environment, such as the ICU, should be reduced as much as possible. Therefore, doctors' hours of control of the ICU patients should be spread throughout the day.
- According to the results, when the number of patients was more than 6 people, it is seen that the measured values, especially PM's values, sometimes exceed the maximum limits recommended by internationally accepted institutions.

The results have shown that the quality and quantity of HEPA filters were insufficient. Hospital management has been advised to review this situation.

After the COVID-19 pandemic, in the places where social public health is important and potential disease risk is high using new technologies that produce ozone, hydroxyl radicals, and emit UV light in addition to HEPA filets, can reduce environmental pollutants in the air to a minimum. Thus, in high-risk areas, it can use the negative pressure factor to minimize the connection of the potential virus with the outdoor.

To improve the maximum levels of indoor air quality in critical regions such as the ICU the following issues will be taken into consideration in future studies.

- By placing more sensor nodes in the ICU in which place the density of the parameters of indoor air quality is higher. In the ICU, a density map of indoor air quality in terms of parameters will be determined. It is thought by using this map will placement of HEPA filters and increase the efficiency of the filters. The increasing efficiency of the filters in the ICU affects the improvement of indoor air quality.
- When the indoor air parameters will be higher than the accepted level by worldwide, the relevant personnel will be automatically alerted with the instant messaging application and necessary measures will be taken urgently.

Acknowledgements

This study was supported by the Scientific Research Projects Department of Bolu Abant Izzet Baysal University (Grant NO: 2019.31.01.1421). The authors would like to thank the hospital management, and staff for the utilization of the Intensive Care Unit (ICU) which is a real-world use-case in the proposed real-time indoor air quality management system. Also, the authors are grateful to healthcare professionals for their contribution to the pandemic process that has been going on around the world since December 2019.

Authors' contributions:

SL: Project Design and management, Methodology and Data processing, Writing, Review & Editing. **ML:** Design of wireless sensor networks**,** Software and Data processing, Writing, Review & Editing. **İY:** Investigation & Literature Review **AD:** Investigation & Literature Review

Conflict of interest disclosure:

The authors declare no conflict of interests

References

Against F, Turan A. 2020. Türkiye ' de KOVİD - 19 ile Mücadele : Politikalar ve Aktörler 1–25.

Aktaş Ö, Milli Mehmet, Lakestani S, Milli Musa. 2020. Modelling sensor ontology with the SOSA/SSN frameworks: a case study for laboratory parameters. TURKISH J Electr Eng Comput Sci. 28:2566–2585. https://doi.org/10.3906/elk-1912-160

Baurès E, Blanchard O, Mercier F, Surget E, le Cann P, Rivier A, Gangneux JP, Florentin A.2018. Indoor air quality in two French hospitals: Measurement of chemical and microbiological contaminants. Sci Total Environ. 642:168–179. https://doi.org/10.1016/j.scitotenv.2018.06.047

Chen J, Hoek G. 2020. Long-term exposure to PM and all-cause and cause-specific mortality: A systematic review and meta-analysis. Environ Int. 143:105974. https://doi.org/10.1016/j.envint.2020.105974

Fernández E, Martínez C, Fu M, Martínez-Sánchez JM, López MJ, Invernizzie G, Ouranou A, Dautzenberg B, Nebot M. 2009. Second-hand smoke exposure in a sample of European hospitals. Eur Respir J. 34: 111–116. https://doi.org/10.1183/09031936.00180708

Guidelines on energy efficiency of cultural heritage - ScienceDirect, 1998.

Heibati B, Rivas I, Veysi R, Hoek G, Perez-Martinez PJ, Karimi A. 2021a. Evaluating size-fractioned indoor particulate matter in an urban hospital in Iran Environ Monit Assess. 193: 1–10. https://doi.org/10.1007/s10661-021-09327-0

Heibati B, Rivas I, Veysi R, Hoek G, Perez-Martinez PJ, Karimi A. 2021b. Evaluating size-fractioned indoor particulate matter in an urban hospital in Iran. Environ. Monit. Assess. 193, 1–10. https://doi.org/10.1007/s10661-021-09327-0

Hwang SH, Roh J, Park WM. 2018. Evaluation of PM10, CO2, airborne bacteria, TVOCs, and formaldehyde in facilities for susceptible populations in South Korea. Environ. Pollut. 242:700–708. https://doi.org/10.1016/j.envpol.2018.07.013

Interior Republic of Turkey Ministry of, 2020. Additional Circular on Markets in the Scope of Combating the Coronavirus Outbreak [WWW Document].

Jeong JY, 2012. Recently issues on Indoor air quality in Korea.

Karakas B, Lakestani S, Guler C, Dogan BG, Vaizoglu SA, Taner A, Sekerel B, Tıpırdamaz R, Gullu G. 2013. Indoor and Outdoor Concentration of Particulate Matter at Domestic Homes. World Acad. Sci. Eng. Technol. 7: 222–229.

Kim KH, Kabir E, Kabir S. 2015. A review on the human health

impact of airborne particulate matter. Environ. Int. 74:136–143. https://doi.org/10.1016/j.envint.2014.10.005

Lakestani S, Karakas B, Acar Vaizoglu S, Dgan GB, Cagatay G, Sekerel B, Taner A, Gullu G. 2013. Comparison of Indoor and Outdoor Air Quality in Children Homes at Prenatal Period and One Year Old. J Civil Environ Struct Constr Archit Eng 7.

Loupa G, Zarogianni AM, Karali D, Kosmadakis I, Rapsomanikis S. 2016. Indoor/outdoor PM2.5 elemental composition and organic fraction medications, in a Greek hospital. Sci Total Environ. 550:727–735. https://doi.org/10.1016/j.scitotenv.2016.01.070

Pickett AR, Bell ML. 2011. Assessment of indoor air pollution in homes with infants. Int J Environ Res Public Health 8, 4502–4520. https://doi.org/10.3390/ijerph8124502

Stern RA, Al-Hemoud A, Alahmad B, Koutrakis P. 2021. Levels and particle size distribution of airborne SARS-CoV-2 at a healthcare facility in Kuwait. Sci. Total Environ. 782: 146799. https://doi.org/10.1016/j.scitotenv.2021.146799

Tucker WG. 2002. ASHRAE® Standard: Ventilation for Acceptable Indoor Air Quality, ASHRAE Standard.

Wang X, Bi X, Sheng G, Fu J. 2006. Hospital indoor PM10/PM2.5 and associated trace elements in Guangzhou, China. Sci. Total Environ. 366: 124–135. https://doi.org/10.1016/j.scitotenv.2005.09.004

Wingate, n.d. Title: Importance of Monitoring and Controlling Temperature and Humidity in Hospitals [WWW Document]. URL https://blog.rotronic.com/2014/09/15/importance-of-monitoring-and-controlling-temperature-and-humidity-in-hospitals/

RESEARCH ARTICLE
Eurasian J Bio Chem Sci, 5(1):29-35, 2022
https://doi.org/10.46239/ejbcs.872104

EJBCS

Eurasian Journal of Biological and Chemical Sciences

Journal homepage: www.dergipark.org.tr/ejbcs

The effect of media ion and nitrogen gas dissolved in water on color removal with sonolysis, Fenton and sono-Fenton in the continuous flow ultrasonic reactor

Fadime Karaer Özmen[*1]

[*1] *Eskisehir Technical University, Engineering Faculty, Environmental Engineering Department, Eskisehir, Turkey*

*Corresponding author : fadimek@eskisehir.edu.tr
Orcid No: https://orcid.org/0000-0003-4423-205X

Received : 01/02/2021
Accepted : 02/02/2022

Abstract: Ultrasound has been researched as an alternative technique for color removal methods from water and wastewater. In this study the color removal from water using sonolysis, Fenton, and Sono-Fento was investigated and the effects of power intensity, media ions and nitrogen gas dissolved in water were investigated in model working solution with Basic Red 29 Dye in the continuous flow ultrasonic reactor. The experimentation was performed at 22 kHz ultrasonic frequency with different power intensity application in the ultrasonic system. The optimum color removal efficiency was achieved with 0.45 W/cm^2 power intensity. The color removal efficiency of Basic Red 29 was raised to two times with the coexistent effect of media ions while the media ions and dissolved gas increased to four times simultaneously. To conclude, the color removal efficiency followed from this order in sonolysis: N_2+ SO_4^{-2}+ HCO_3^-+NO_3^{-2} > HCO_3^-> SO_4^{-2}+ HCO_3^-+NO_3^{-2}> SO_4^{-2} >N_2> NO_3^{-2}. In Fenton process, the effects of Fe^{+2} and H_2O_2 concentration on system performance were examined obtaining 89% color removal efficiency by using 20 mg/L Fe^{+2} and 1000mg/L H_2O_2. With the hybrid Sono-Fenton process, the required Fe^{+2} amount decreased by 1/5, when the color removal efficiency increased to 98 % and there was no significant effects of media ions and dissolved gas on Fenton and Sono-Fenton treatment. As a result of toxicity studies, it was seen that the initial toxicity of wastewater decreased with treatment and the Sono-Fenton method was the most effective method on toxicity removal. It was determined that color removal using Sono-Fenton can be accomplished successfully, economically and environmentally friendly.

Keywords: sonolysis, Fenton, Sono-Fenton, color removal, media ions, nitrogen gas, toxicity

1. Introduction

Wastewater production of textile industry has recently gained great significance in environmental engineering in terms of synthetic dye content and toxic characteristic. The synthetic dyes are resistant to biological degradation (Tegli et al. 2014) and it remains a challenge to efficiently and accurately treat textile wastewater with conventinal metods due to its relatively high level of acidity, toxicity, and non-biodegredable organic load (Husain 2006). The textile industry wastewater is generally accepted as persistent, nonbiodegradable, photosynthesis limiting and toxic characteristics to the aquatic ecosystem (Weng et al. 2014).

The number of studies on alternative technologies aims to attain more effective color removal and reducing toxic effect of dyes has increased, although various conventional wastewater treatment methods have been used for color removal of these industries effluents to prevent their detrimental effects on aquatic ecosystem such as, adsorption (Khan et al. 2004), membrane processes (Sakoda et al. 1996) and ion exchange (Zhao et al. 2008), electrochemical treatment (Surme and Demirci 2014), advanced oxidation process (Lopez-Grimau et al. 2012), bio-sorption (Jin et al. 2014), nano-sized adsorption (Lin et al. 2015), and sonolysis (Zhang et al. 2013) can be listed among these alternative technologies.

Sonolysis has been used for various dyes with their different natures in the literature. Ai et al. developed sonolysis to remove Rhodamine B azo dye in aqueous solution in addition to methyl orange, methylene blue and Reactive Brilliant red X3-B with high removal efficiency (Ai et al. 2010). Zhang et al. demonstrated that sonolysis enhanced the reduction efficiency of C.I. Acid Orange 7 in the zero valent iron processes (Zhang et al. 2005). Sonolysis and their hybrid applications combined with other methods like sono-Fenton have been noticed to attain more efficient decolorization and reduce chemical and energy requirement. Fenton reaction can be improved by

combining UV (photo-Fenton, solar photo-Fenton), or ultrasound radiation (sono-Fenton), and electrical current (Electro-Fenton). The characteristics of the textile industry effluent is important for recent progress of the Fenton processes like sono-Fenton adressed as alternative to the treatment of textile effluents. (Ramos et al. 2021). Among advanced oxidation processes often used for treatment, sono-Fenton and photo-Fenton processes gain a lot of attention due to high pollutant degradation efficiency thanks to direct and synergistic effects of ultrasound and light which lead to the highest generation of reactive radicals such as •OH, •H and •OOH and thier catalytic role of ferrous ions (Moradi et al. 2020). Sayan and Edecan researched the removal of Reactive Blue 19 dye using sono-Fenton process. They reported that performing sonolysis with Fenton provided more efficient color removal because of accelerating synergetic effect of two systems (Sayan and Edecan 2008). The combination of the various advantages of these alternative methods such as, mass transfer accelerator, reaction rate acceletor, and catalyst effect the raise the removal efficiency, while the disadvantages such as, energy consumption, chemical requirement, and high cost are eliminated in the hybrid systems. Xu studied Reactive Brilliant red X3-B textile dye, which is persistent to UV radiation treatment, with different advanced oxidation process and he reached the highest decolorization efficiency in sono-photo-Fenton (US-Fe^{+2}–H_2O_2-UV) treatment (Xu 2001). Voncina and Majcen-Le-Marechal investigated six different reactive dyes with sono-oxidation (US-H_2O_2) treatment. They stated that advanced oxidation process related to sonolysis application combined with H_2O_2, UV, and ozone accelerated free radical formation efficiency. Since sonication improved mass transfer and chemical reaction speed (Voncina and Majcen-Le-Marechal 2003). Weng et al. studied with real textile wastewater and achieved successful decolorization efficiency using sono-Fenton process combined with 1 g/L zero valent iron dosage and 0.01 M hydrogen peroxide concentration applying 47 kHz sonic frequency while operating cost was estimated around 4.5 USD for 1 m^3 wastewater (Weng et al. 2014). Chu et al reported the results of the heterogeneous Fenton-like processes to remove organic dyes from water, and the synergistic effects of ultrasound (US) and Fenton with metalic biochar catalyst. The heterogeneous sono-Fenton-like triple (US–H_2O_2–catalyst) system exhibited a high dye-removal efficiency for methylene blue and orange (Chu et al. 2020). The main reason for using sonolysis together with other methods is that it requireshigh energy and cost to obtain effective removal efficiency. Zhang et al. reported that sonolysis did not enhance the colour removal of CI Reactive Black 8 combined application with Fenton process regarding to single Fenton treatment while improving COD removal (Zhang et al. 2007). The main disadvantage of other advanced oxidation methods (e.g., fenton) is the requirement of oxidizing chemicals and the possibility of forming toxic by-products as a result of treatment. An other study perfomed by same research team stated that ultrasound and Fenton process supported activated carbon system had 88% decolorization efficiency of Crystal Violet and acute toxicity of dye solution decreased after the treatment by Daphnia magna test (Zhang et al. 2013). The possibility of toxic by-products formation in Fenton treatment also depends on other ions being in the water. In addition, these ions can be effective in color removal by sonolysis eihter. The characteristics of the textile industry effluent is important for recent progress of the Fenton processes like sono-Fenton adressed as alternative to the treatment of textile effluents. There is no detailed study in which the effects of these characteristics on sonolysis, Fenton and hybrid sono-Fenton processes and efflux toxicity are examined in the literature.

The efficiency of such processes regarding the important characterization parameters (media ions, color, dissolved gas present in water) for model textile effluents was investigated in this survey.In this study the color removal from water using sonolysis, Fenton and sono-Fenton was researched in the continuous flow ultrasonic rector. The effect of media ions and dissolved nitrogen gases being in the water were investigated on the single and hybrid treatment processes by assessing toxicity.

2. Materials and Method

2.1. Sonolysis

The ultrasonic decolorization studies were performed in continuous flow reactor with 22 kHz frequency, applying 26 W power. The ultrasonic reactor was used in this study (refer to Fig. 1). A model wastewater was used in the treatment studies including Basic Red 29 (refer to Fig. 2) dye (Sigma Aldrich) with 40 mg/L initial concentration in the 100 mL volume.

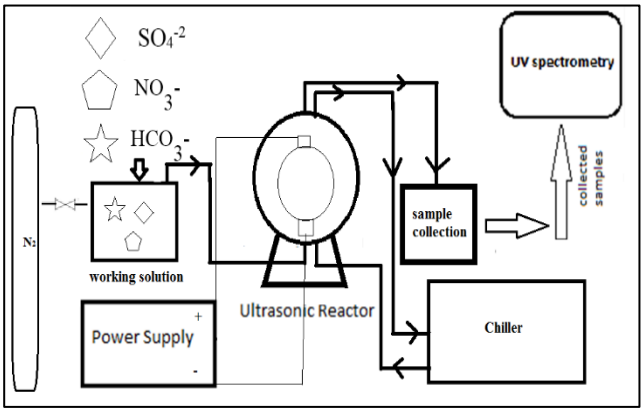

Fig. 1 Experimental setup

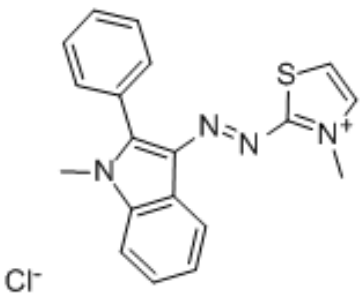

Fig. 2 Chemical formula of Basic Red 29

The reactor was performed at 5 mL/min flow rate to the ultrasonic reactor with 50 mL volume and the hydraulic retention time was determined as 10 minutes during decolorization treatment with sonolysis, Fenton, and Sono-Fenton processes. The absorbance of collected samples was obtained in UV-Vis spectrophotometer (Shimadzu UV-Vis 1600) at 506 nm and the decolorization efficiency calculated using Equation 1.

$$\text{Color removal efficiency (\%)} = \frac{C_i - C_e}{C_i} \times 100 \qquad \text{(Eqn. 1)}$$

Where,

C_i=influent Basic Red 29 concentration, mg/L

C_e =effluent Basic Red 29 concentration, mg/L

Each treatment was conducted with three independent experiments at the same conditions and the average results of all experiments was given in the result section.

2.2. Media ions effect on decolorization

In order to investigate effect of media ions present in water, SO_4^{-2}, HCO_3^-, and NO_3^{-2} ions were added to system in form of their water soluble sodium salt. Na_2SO_4 (Merck Millipore), $NaHCO_3$ (Merck Millipore), and $NaNO_3$ (Merck Millipore) were used to supply these ions to water with 0.1-0.2 M SO_4^{-2}, 4.1-8.2 mM HCO^{-3}, 4.0-8.0 mM NO_3^{-2} concentration added respectively to model wastewater considering their legally permissible concentrations in the surface waters as the quality parameters to examine their effect on decolorization.

2.3. Dissoved nitrogen gas effect on decolorization

Thedissolved nitrogen gas in water was determined in model wastewater solution in this study. The effect of dissolved nitrogen gas on decolorization was examined with 8 L/hour, 12 L/hour, and 16 L/hour nitrogen gases flowrates. The effect of three different nitrogen gases flowrate on ultrasonic color removal was determined during color removal from water using sonolysis and sono-Fenton.

2.4. Fenton and Sono-Fenton

Fenton (Fe^{+2}-H_2O_2) studies were conducted in a glass beaker. The $FeCI_2.4H_2O$ (Merck, 99% w/w) was used as Fe^{+2} source in Fenton treatment process. Firstly, The H_2O_2 concentrations were adjusted as 1000 mg/L in model solution and the effect of Fe^{+2} concentration was determined containing 2, 4, 6, 8, 10, 20, 40, 60, 80, and 100 mg/L Fe^{+2} using suitable primary $FeCI_2.4H_2O$ stock solutions.

Secondly, Sono-Fenton (US-Fe^{+2}-H_2O_2) studies were conducted in US reactor (refer to Fig. 1) using 1000 mg/L H_2O_2 (Merck, 35% w/w) concentrations and 20 mg/L Fe^{+2} concentrations. The effect of the media ions effect was determined with 0.2 M SO_4^{-2}, 8.2 mM $HCO_3^-$and 4.0 mM NO_3^{-2} concentration and the dissolved gas effect was investigated 16 L/hour nitrogen gas flowrates on Sono-Fenton processes.

2.5. Toxicity Asesment

Toxicity tests of effluent and influent samples were analyzed with Microtox Model 500 Analyzer (Azur Environmental, Carlsbad, CA) as cytotoxicity investigation. The lyophilized *Vibrio fischeri* bacterium (NRRL number B-11177, Microtox Acute reagent, Modern Water) with luminescence characteristics was used as a test microorganism. The *Vibrio fischeri* bacterium was incubated with reconstitution solution (nontoxic ultra-pure water, Modern Water) and osmatic adjuster solution (22% sodium chloride, Modern Water) at 15 °C during 15 min in glass cells. Four serial dilutions of the sample were prepared with dilution solution (2% sodium chloride, Modern Water). Toxic effects of the test result were recorded for each sample using Microtox calculation software (95% confidence) with light emission reduction percent value of 15 min exposure of *Vibrio fischeri to test sample.*

3. Results and Discussion

In this study the color removal from water using sonolysis, Fenton and Sono-Fenton technology was researched and the effects of media ions and dissolved nitrogen gas were determined in model synthetic Basic Red dye solution.

3.1. Sonolysis

The results of the experimentations process were given at 22 kHz frequency with different power intensity (W/cm^2) application to the system (refer to Fig. 3).

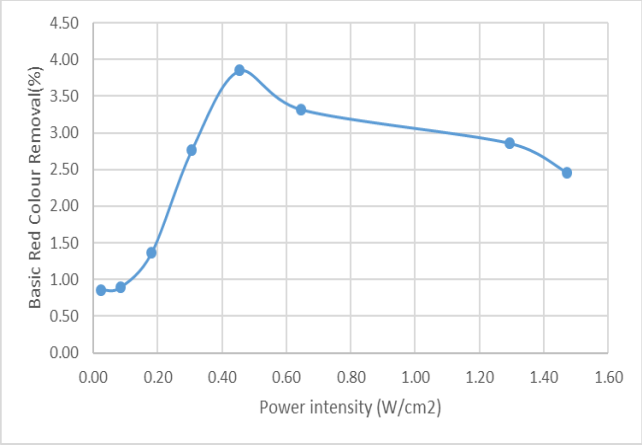

Fig. 3 Experimental setup

The optimum power intensity was determined as 0.45 W/cm^2, and raising the power intensity bigger than 0.45 W/cm^2 because the applied power is more than 0.45 W/cm^2 caused an increasement in heat or resonance of the ultrasonic system. The other sonolysis studies were performed this optimized power intensity with 0.45 W/cm^2. The results of the effect of sulphate ion on color removal were investigated for 0.1-0.2 M SO_4^{-2} (refer toFig. 4).

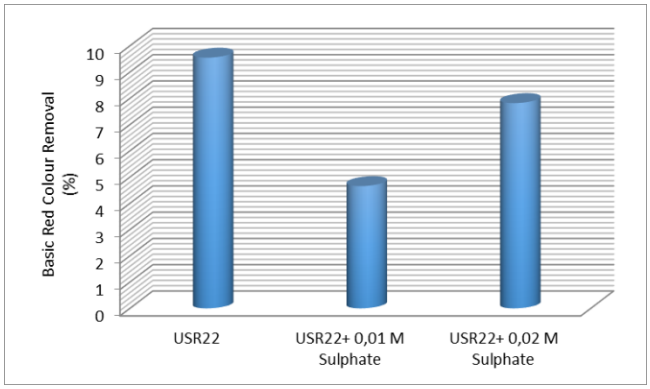

Fig. 4 The effect of sulphate ion on color removal

Another parameter considered in the color removal with sonolysis is the presence of media ions such as sulphate, bicarbonate, and nitrate presented in the liquid. According to Fig. 4, it was determined that suphate ion had negative effect on color removal efficiency of sonolysis. Dissolved ions accompanying in water can lead to the formation of ultrasonic cavitations, but they can have a negative effect as they can also cause an additional reactions such as conversion of the sulphate to sulfite or persulphate (Gayathri et al. 2010).

H_2O + ultrasonication→ H• + OH• (Eqn. 2)

SO_4^{-2} + H• + OH•→ $SO_4^{\bullet-}$ + H_2O (Eqn. 3)

SO_4^{-2} + $SO_4^{\bullet-}$ → $S_2O_8^{-2}$ (Eqn. 4)

Sonolyses catalyzes the production of persulphate, by activating sulphate with formation of hydroxyl radical by ultrasonication. If persulfate reaction in Eqn.4 has faster kinetics than Eqn. 3, the degradation rate of Basic Red 29 was enhanced by the US activated persulphate. Thus, its negative effect on color removal in the case of sulphate ion addition (refer to Fig. 4) could be explained by Eqn 2-4. The results of the effect of nitrate ion on color removal were investigated for 4.0-8.0 mM NO_3^{-2} (refer to Fig. 5).

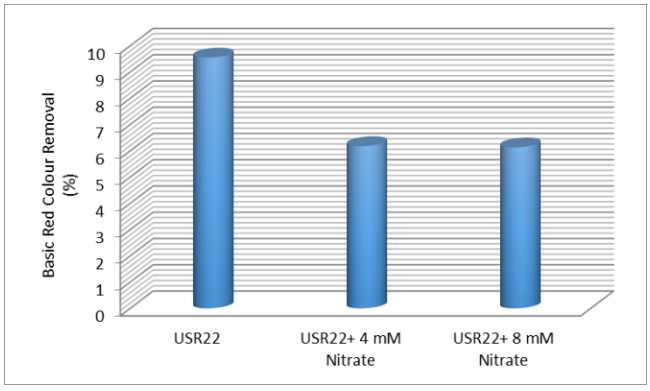

Fig. 5 The effect of nitrate ion on color removal

The nitrate ion addition affected the color removal adversely in parallel with the sulphate ion results. Similarly, it causes an additional reactions such as conversion of the nitrate to nitrogen and ammonia (Koparal and Ogutveren, 2002). The ultrasonical reduction of nitrate ions to nitrogen and ammonia could be explained as following reactions (Govindan et al. 2015).

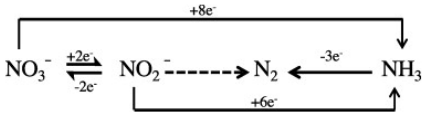

(Eqn. 5)

The formation of additional reaction of nitrite, nitrogen gas, and ammonia could be decreased the ultrasonic color removal efficiency. The results of the effect of bicarbonate ion on color removal were investigated for 4.1-8.2 mM HCO_3^- (refer to Fig. 6).

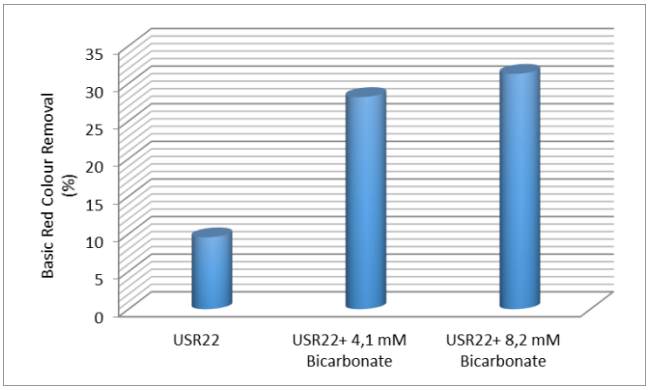

Fig. 6 The effect of bicarbonate ion on color removal

The addition of bicarbonate ion raised the color removal efficiency of Basic Red 29 three times unlike sulphate and nitrate ions. Bicarbonate ions could be identified as accelerator agents in the sonoysis because the rate constants of bicarbonate ions with sulfate and hydroxyl radicals are relatively high. Hence the presence of bicarbonate ions can eventuate in a competition for reaction with free radicals (Feizi et al. 2019). The results of the effect of nitrogen gas on color removal were investigated for 8, 12 and 16 L/h gas flowrate (refer to Fig. 7).

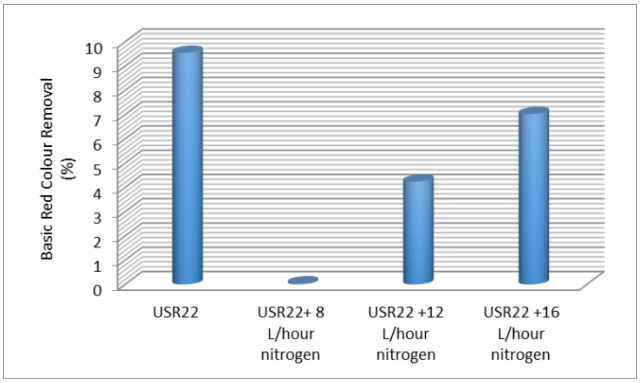

Fig. 7 The effect of nitrogen gas on color removal

The gas dissolved in the liquid affects the physical and chemical properties of acoustic cavitation bubbles and variation of the amount of dissolved gas in the liquid alters the production of collapse. The change of the type of dissolved gas modifies adiabatic rate, thermal transmission, the surface tension of the liquid, and the hot spot temperature of micro-bubbles. For these reasons the effect of dissolved gas on color removal with ultrasound must be investigated. After the nitrogen gas studies, it was observed

that the addition of nitrogen gas did not have a significant effect on sonolysis. The simultaneous effect of media ions (0.2 M SO_4^{-2}, 8.2 mM HCO^{-3} and 4.0 mM NO_3^{-2} and dissolved nitrogen gas (16 L/hour) on color removal in sonolysis is given in Fig.8.

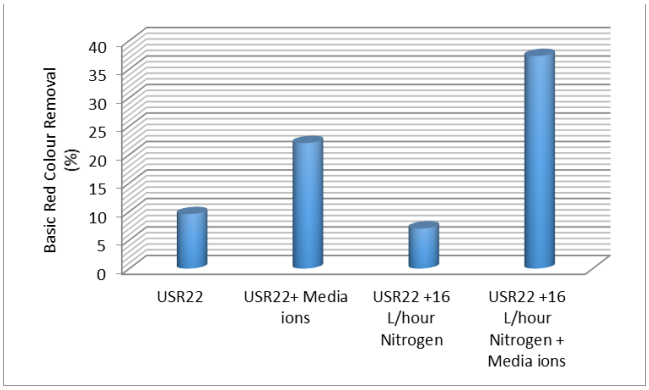

Fig. 8 The simultaneous effect of media ions (0.2 M SO_4^{-2}, 8.2 mM HCO_3^- and 4.0 mM NO_3^{-2} and dissolved nitrogen gas (16 L/hour) on color removal

The color removal efficiency of Basic Red 29 was raised to two times with the coexistent effect of media ions while the media ions and dissolved gas increased four times simultaneously. To conclude, the color removal efficiency followed from this order in sonolysis: N_2+ SO_4^{-2}+ HCO^{-3}+NO_3^{-2} > HCO_3^-> SO_4^{-2}+ HCO_3^-+NO_3^{-2}> SO_4^{-2} >N_2> NO_3^{-2}.

3.2. Fenton and Sono-Fenton

The effects of different Fe^{+2} concentrations on color removal were given in Fig. 9 in Fenton (Fe^{+2}-H_2O_2) studies to show the single effect of Fenton on Basic Red 29 removal.

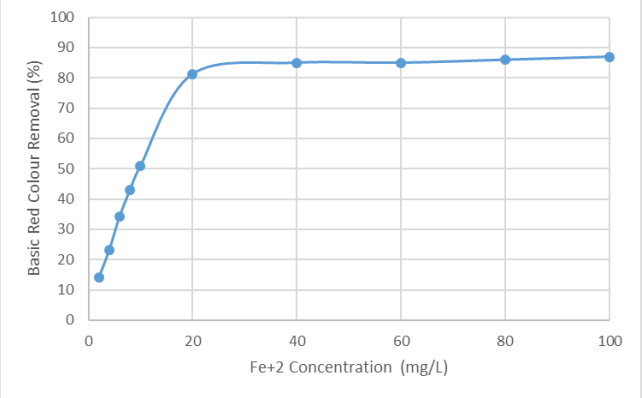

Fig. 9 The effect of Fe^{+2} concentration on Fenton (H_2O_2 concentration is 1000 mg/L and pH:3.96)

When the H_2O_2 concentration was set as 1000mg/L, the colorremoval efficiency raised to 12.0 % from 89 % as the concentration of Fe^{+2} was raised from 2 to 100 mg/L. It was determined that the applied Fe^{+2} concentrations showed same color removal trend between 20 and 100 mg/L Fe^{+2} concentration. Hybrid Sono-Fenton studies were carried out in an ultrasonic reactor by setting Fe^{+2} concentration to 20 mg/L and H_2O_2 concentration to 1000 mg/L. As in sonolysis studies, the effects of media ions and nitrogen gas on the Sono-Fenton were also investigated. The comparative graph of these studies is given in Fig.10.

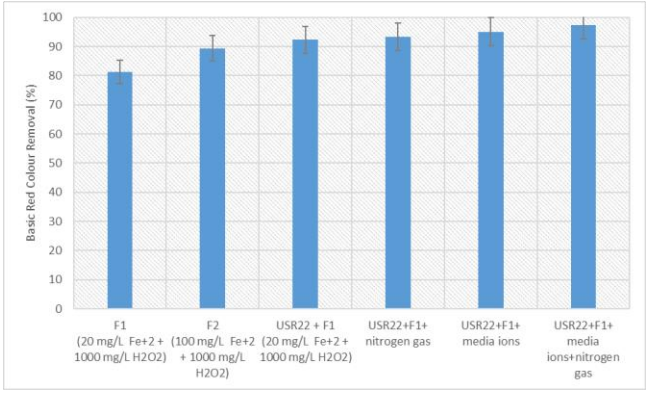

Fig. 10 The simultaneous effect of media ions

Comparing these results with literature, Weng et al. examined the effect of their anions by adding NaCl, Na_2SO_4, Na_2HPO_4, $NaNO_3$, and $NaClO_4$ salts while examining the removal of RS5 dye with Sono-Fenton at the end of the study, it was seen that Cl-, SO_4^{-2}, NO_3^- and ClO_4^- anions did not havesignificant effect, but $H_2PO_4^-$ anion suppressed the system (Weng et al. 2013). In another study, the effect of Cl^- and SO_4^{-2} ions was investigated. Accordingly, Cl^- ion was negative for the destruction of Blue2B (B54) and Red12B (R31) dyes; It has been observed that SO_4^{-2} ion does not have effect on destruction (Malik and Saha, 2004). After the nitrogen gas studies, it was observed that the addition of nitrogen gas did not have a significant effect on Fenton and US/Fenton reactions, as in the study of Saravanan and Sivasankar, 2015. They reported that the maximum decolourization occurs at acidic pH of 3.0, Argon gas bubbling, 8.82 mmol/L hydrogen peroxide, 10 g/L NaCl addition and the colour removal are the highest for Fenton's reagent-treated Reactive Black 5 dye solution which followed pseudo-first-order rate kinetics.

3.3. Toxicity assessment

The toxicity reduction of Basic Red 29 containing synthetic wastewater was illustrated in Fig. 11.

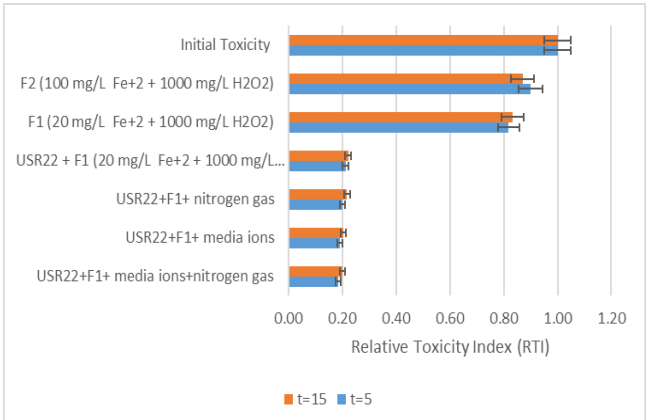

Fig. 11 The simultaneous effect of media ions

Toxicity assessment showed that 40 mg/L Basic Red 29 containing wastewater had a high toxic effect on *Vibrio fischeri* bacteria. The phenol solution was used as control according to Microtox Test Procedure with 50 mg/L concentration. The LC50 concentration of untreated wastewater was calculated as 20 mg/L (2%). In this paper, even if the sonolysis, Fenton, and Sono-Fenton treatment slightly reduced the toxicity of untreated wastewater in parallel with color removal, the toxicity of wastewater was significantly decreased with Sono-Fenton (US-Fe^{+2}-H_2O_2) treatment. However, the wastewater treated with Sono-Fenton (US-Fe^{+2}-H_2O_2) still showed toxic characteristic after 99% Basic Red 29 removal.

4. Conclusion

In this study the color removal from water using ultrasound technology was researched and the effect of applied power intensity, media ions, and nitrogen gas in water was determined with ultrasonic color removal of Basic Red 29 dye in the continuous flow reactor. The optimum color removal efficiency was achieved with 0.45 W/cm^2 power intensity. As a result of the study, it was determined that color removal from water using ultrasound technology can be accomplished successfully. The color removal efficiency of Basic Red 29 was raised to two times with the coexistent effect of media ions while the media ions and dissolved gas increased four times simultaneously. To conclude, the color removal efficiency followed from this order in sonolysis: N_2+ SO_4^{-2}+ HCO_3^-+NO_3^{-2} > HCO_3^-> SO_4^{-2}+ HCO_3^-+NO_3^{-2}> SO_4^{-2} >N_2> NO_3^{-2}. In Fenton process, the effects of Fe^{+2} and H_2O_2 concentration on system performance were examined obtaining 89% color removal efficiency by using 20 mg/L Fe^{+2} and 1000 mg/L H_2O_2. With the hybrid Sono-Fenton process, the required Fe^{+2} amount decreased by 1/5, when the color removal efficiency increased to 98 %. As a result of toxicity studies, it was seen that the initial toxicity of wastewater decreased with treatment and the Sono-Fenton method was the most effective method for toxicity removal.

Acknowledgment

This research did not receive any specific grant from funding agencies in the public, commercial, or not-for-profit sectors.

Authors' contributions:

FKÖ: Conceptualization, Methodology, Software, Data Curation, Validation, Formal Analysis, Writing- Original Draft Preparation, Visualization, Investigation.

Conflict of interest disclosure:

The author declares that they have no known competing financial interests or personal relationships that could have appeared to influence the work reported in this paper.

References

Ai ZH, Li JP, Zhang L.Z, Lee SC. 2010. Rapid decolorization of azo dyes in aqueous solution by an ultrasound-assisted electrocatalytic oxidation process. Ultra Sonochem. 17(2):370-375.

Chu JH, Kang JK, Park SJ, Lee CG. 2020. Application of magnetic biochar derived from food waste in heterogeneous sono-Fenton-like process for removal of organic dyes from aqueous solution. J of Water Pro Eng. 37: 1-11.

Feizi R, Ahmad M, Jorfi S, Ghanbari F. 2019. Sunset yellow degradation by ultrasound/peroxymonosulfate/CuFe2O4: Influential factors and degradation processes. Korean J of Chem Eng. 36(6):886-893.

Gayathri P, Praveena R, Dorathi J, Palanivelu K. 2010. Sonochemical degradation of textile dyes in aqueous solution using sulphate radicals activated by immobilized cobalt ions. Ultra Sonochem. 17(3):566-571.

Govindan K, Noel M, Mohan R. 2015. Removal of nitrate ion from water by electrochemical approaches. J Water Proc Eng. 6:58-63.

Husain Q. 2006. Potential applications of the oxidoreductive enzymes in the decolorization and detoxification of textile and other synthetic dyes from polluted water: A review. Crit Rev in Biotech. 26(4):201-221.

Jin YP, Wu YW, Cao JL, Wu YY. 2014. Optimizing decolorization of Methylene Blue and Methyl Orange dye by pulsed discharged plasma in water using response surface methodology. J of the Taiwan Inst of Chem Eng. 45(2):589-595.

Khan TA, Singh VV, Kumar D. 2004. Removal of some basic dyes from artificial textile wastewater by adsorption on Akash Kinari coal. J of Sci and Ind Res. 63(4): 355-364.

Koparal AS, Öğütveren ÜB. 2002. Removal of nitrate from water by electroreduction and electrocoagulation. J of Haz Mat. 89(1):83-94.

Lin KYA, Yang HT, Lee WD, Tsao KY. 2015. A magnetic fluid based on covalent-bonded nanoparticle organic hybrid materials (NOHMs) and its decolorization application in water. J of Mol Liq. 204:50-59.

Lopez-Grimau V, Gutierrez-Bouzan MD, Valldeperas J, Crespi M. 2012. Reuse of the water and salt of reactive dyeing effluent after electrochemical decolorisation. Colo Technol. 128(1):36-43.

Malik PK, Saha SK. 2004. Oxidation of direct dyes with hydrogen peroxide using ferrous ion as catalyst. Sep Purif Technol. 31:241-250.

Moradi M, Elahinia A, Vasseghian, Y, Dragoi EN, Omidi F, Khaneghah AM. 2020. A review on pollutants removal by Sono-photo-Fenton processes. J Environ Chem Eng 8(5):1-20.

Sakoda A, Nomura T, Suzuki,M. 1996. Activated carbon membrane for water treatments: Application to decolorization of coke furnace wastewater. J Int Ads Soci 3(1):93-98.

Saravanan S, Sivasankar T.2015. Ultrasound-assisted Fenton's treatment of reactive black 5 dye: effect of system parameters, kinetics and mechanism. Desalin and Water Treat. 56:492-501.

Sayan E, Edecan ME. 2008. An optimization study using response surface methods on the decolorization of Reactive Blue 19 from aqueous solution by ultrasound. Ultra Sonochem. 15(4):530-538.

Ramos MDN, Santana CS, Velloso CCV, Da Silva AHM, Magalhães F, Aguiar A. 2021. A review on the treatment of textile industry effluents through Fenton processes. Pro. Safety and Environ. Protect., 155:1-21.

Tegli S, Cerboneschi M, Corsi M, Bonnanni M, Bianchini R. 2014. Water recycle as a must: decolorization of textile wastewaters by plant-associated fungi. J Basic Microbio. 54(2): 120-132.

Xu Y. 2001. Comparative studies of the $Fe^{3+/2+}$-UV, H_2O_2-UV, TiO_2-UV/vis systems for the decolorization of a textile dye X-3B in water. Chem. 43(8):1103-1107.

Voncina DB, Majcen-Le-Marechal A. 2003. Reactive dye decolorization using combined ultrasound/H2O2. Dyes and Pigm. 59(2):173-179.

Weng C, Lin Y, Yuan, H.2013. Rapid decoloration of Reactive Black 5 by an advanced Fenton process in conjunction with ultrasound. Sep Purif Technol. 117:75–82.

Weng CH, Lin YT, Liu N, Yang HY. 2014. Enhancement of the advanced Fenton process by ultrasound for decolorisation of real textile wastewater. Colo Technol. 130(2):133-139.

Zhao ZS, Liu JF, Tai C, Zhou QF, Hu JT, Jiang GB. 2008. Rapid decolorization of water soluble azo-dyes by nanosized zero-valent iron immobilized on the exchange resin. Sci in China Series B-Chem. 51(2):186-192.

Zhang H, Duan LJ, Zhang Y, and Wu F. 2005. The use of ultrasound to enhance the decolorization of the CI Acid Orange 7 by zero-valent iron. Dyes and Pigm. 65(1):39-43.

Zhang H, Gao H, Cai C, Zhang CY, Chen L. 2013. Decolorization of Crystal Violet by ultrasound/heterogeneous Fenton process. Water Sci and Technol. 68(11):2515-2520.

Zhang H, Zhang Y, Zhang D.B. 2007. Decolorisation and mineralisation of CI Reactive Black 8 by the Fenton and ultrasound/Fenton methods. Colo Technol. 123(2):101-105.

REVIEW ARTICLE
Eurasian J Bio Chem Sci, 5(1):36-44, 2022
https://doi.org/10.46239/ejbcs.1049566

EJBCS

Eurasian Journal of Biological and Chemical Sciences

Journal homepage: www.dergipark.org.tr/ejbcs

Kamkatın muhafazası ve çeşitli gıdaların üretiminde kullanımı

Nuray Can[1*], Meryem Badayman[2]

*[*1]İstanbul Aydın Üniversitesi, Anadolu Bil Meslek Yüksekokulu, Gıda Kalite Kontrolü ve Analizi Programı, İstanbul, Türkiye*
[2]İstanbul Aydın Üniversitesi, Anadolu Bil Meslek Yüksekokulu, Gıda Teknolojisi Programı, İstanbul, Türkiye

*Corresponding author: nurayc@aydin.edu.tr
Orcid No: https://orcid.org/0000-0002-2410-9487

Received : 28/12/2021
Accepted : 10/04/2022

Özet: Rutaceae familyasının *Fortunella* cinsine ait olan kamkat, küçük meyveleri olan bir ağaçtır. Kamkat, anavatanı olan Çin'in yanı sıra Japonya, Amerika, Avustralya, Güney Afrika, Porto Riko, Guatemala, Kolombiya, Brezilya ve Hindistan'da yetiştirilmektedir. Meiwa (*Fortunella crassifolia*), Hong Kong (*F. hindsii*), marumi (*F. japonica*), nagami (*F. margarita*), *F. obovata* ve *F. polyandra* gibi türleri bulunmaktadır. Çapı 2 cm, ağırlığı 10 g olan kamkat meyvesinin şekli yuvarlak veya oval olup tadı ekşidir. Rengi turuncu sarı kabuğu ise tipik bir aromaya sahip, tatlı ve yenilebilirdir. Lif, şeker ve mikroelementler yönünden zengin olan kamkat meyvesinin hasat sonrası raf ömrü, *Penicillium*'un etkisinden dolayı nispeten kısadır ve bu da yüksek düzeyde çürüme ile sonuçlanmaktadır. Ticari soğuk depolarda 2-4°C'de 1-2 ay, ev tipi buzdolabında ise 2-3 hafta, kalitede önemli kayıp olmadan muhafaza edilebilmekte, oda sıcaklığında ise yalnızca birkaç gün dayanmaktadır. Kamkatın kalitesini korumak ve raf ömrünü artırmak için çeşitli teknolojiler uygulanmaktadır. Bu uygulamalar, düşük sıcaklık, kurutma, modifiye atmosfer paketleme ve kaplama gibi bazı yöntemlerdir. Kamkat taze olarak tüketilebildiği gibi reçel, marmelat, jöle, sos, şurup, likör, şarap, turşu, şekerleme, sorbe, sufle gibi çeşitli yiyecek tariflerinde kullanılmaktadır. Literatür incelendiğinde kamkat meyvesinin taze veya kurutularak kullanılması, püre veya toz haline getirilerek kullanılması gibi uygulamaların çeşitli gıdaların aroma, renk, tekstürel özellikler ve besin değerine etkilerinin araştırıldığı görülmektedir. Kamkat meyve tozunun bisküvi, kek; püresinin dondurma, yoğurt ve fonksiyonel içecek eldesinde kullanıldığı çalışmaların yanı sıra kamkattan meyve suyu, reçel, sirke, likör ve şarap gibi ürünlerin üretimi ve üretim parametrelerinin belirlenmesine yönelik çalışmalar bulunmaktadır. Bu derlemede kamkat meyvesi ile ilgili bilgilere yer verilmiş olup muhafazası ve gıda üretimindeki kullanım alanlarından bahsedilmiştir.

Anahtar Kelimeler: Kamkat, kamkatın muhafaza yöntemleri, kamkat ürünleri

Preservation of kumquat and its uses in the production of various foods

Abstract: Kumquat, which belongs to the *Fortunella* genus of the Rutaceae family, is a tree with small fruits. Kumquat is grown in Japan, America, Australia, South Africa, Puerto Rico, Guatemala, Colombia, Brazil and India as well as its homeland of China. There are species such as Meiwa (*Fortunella crassifolia*), Hong Kong (*F. hindsii*), marumi (*F. japonica*), nagami (*F. margarita*), *F. obovata* and *F. polyandra*. The kumquat fruit, which has a diameter of 2 cm and a weight of 10 g, is round or oval in shape and has a sour taste. Its color is orange-yellow and the peel, which has a typical aroma, is sweet and edible. The post-harvest shelf life of kumquat fruit, which is rich in fiber, sugar and microelements, is relatively short due to the effect of *Penicillium*, and this causes a high level of rot. It can be stored for 1-2 months in commercial cold stores at 2-4°C, 2-3 weeks in domestic refrigerators, without significant loss in quality, and only a few days at room temperature. Various technologies are applied to preserve the quality of kumquat and increase its shelf life. These applications are some methods such as low temperature, drying, modified atmosphere packaging, and coating. Kumquat can be consumed fresh as well as used in various food recipes such as jam, marmalade, jelly, sauce, syrup, liqueur, wine, pickles, candy, sorbet, soufflé. When the literature is examined, it is seen that the effects of applications such as using kumquat fruit fresh or dried, using it as puree or powdered, on the aroma, color, textural properties and nutritional value of various foods. There are studies in which kumquat fruit powder is used in the production of biscuits and cakes, and kumquat fruit puree is used in the production of yogurt and functional beverage. In addition, studies have been carried out to determine the production and production parameters of products such as fruit juice, jam, vinegar, liquor and wine from kumquat. In this study, information about kumquat fruit is given and its storage and usage areas in food production are mentioned.

Keywords: Kumquat, preservation methods of kumquat, kumquat products

1. Giriş

Rutaceae familyasının *Fortunella* cinsine ait olan kamkat, Rutaceae familyasının bir başka üyesi *Citrus* cinsi ile akrabadır (Sadek ve ark. 2009). *Fortunella japonica, Fortunella margarita, Fortunella crassifolia* ve *Fortunella hindsii* tarımı yapılan başlıca türleridir (Lou ve Ho 2017). Bunlardan meiwa kamkat olarak adlandırılan *Fortunella crassifolia,* nagami kamkat olarak adlandırılan *Fortunella margarita* Hawai'de en yaygın yetiştirilen türler iken sırasıyla Hong Kong vahşi kamkat ve marumi kamkat olarak bilinen *Fortunella hindsii* ve *Fortunella japonica* ile birlikte *F. obovata,* ve *F. polyandra* Güneydoğu Asya'dan Japonya'ya kadar yetişen diğer türlerdir (Love ve ark. 2007). Uzun yıllardır meyvesinden faydalanmak veya süs bitkisi olarak ve hediye paketi ticaretinde kullanılmak üzere Çin, Japonya, Amerika, Avustralya, Güney Afrika, Porto Riko, Guatemala, Kolombiya, Brezilya ve Hindistan'da yetiştirilmektedir (Citrus pages 2021).

Kökleri iyi gelişmediğinden kamkat nadiren tohumdan yetiştirilmekte, genellikle portakal ve greyfurt ağaçlarına aşılama yoluyla yetiştirilmektedir. Kamkat ağacı subtropikal bir ağaç olarak kabul edilmekte ve düşük irtifadan 5000 ft'e kadar yüksekliklerde yetişebilmektedir. Yavaş büyüyen bir ağaçtır ve kış mevsiminde dinlenme dönemine girmektedir. Kuraklığa hassas, fakat geniş bir sıcaklık aralığına toleranslıdır (Love ve ark. 2007). Sıcaklık gereksinimi 26-37ºC olmakla birlikte 10-15ºC gibi düşük sıcaklıklara da, hasara uğramadan karşı koyabilmektedir. Deniz kenarı koşullarına uyum sağlayabildiği gibi iklimin pek çok turunçgil için çok soğuk sayılabileceği bölgelerde de yetişebilmektedir. Ancak daha sıcak bölgelerde daha iyi yetişmekte ve daha büyük ve tatlı meyveler vermektedir (Abobatta 2016).

Bolca güneş ışığına ihtiyaç duyan kamkat ağaçları, toprak iyi drene edilmiş olduğu sürece çoğu toprak tipine ve pH'a uyum göstermektedir (Abobatta 2016). Her 4 ayda bir, çok amaçlı narenciye gübresi ile gübrelenmesi ve kurak dönemlerde sulama yapılması kamkat ağacının sağlıklı ve üretken kalmasını sağlamaktadır (Love ve ark. 2007).

Boyu 1-2,5 m yüksekliğe ulaşabilen kamkat ağacı vazo şeklinde veya yuvarlak bir izdüşüme sahiptir. Ağacın açık yeşil renkli dalları dikensiz veya az dikenli olabilmektedir. Üst yüzeyi parlak koyu yeşil, alt yüzeyi ise açık yeşil renkli olan basit ve mızraksı yaprakları 3,25-8,6 cm uzunluğa sahiptir. İlkbaharda hoş kokulu beyaz çiçekler açmaktadır. Kış mevsiminin ortasında veya sonuna doğru kamkat meyveleri olgunlaşmaktadır (Abobatta 2016). Tamamen olgun ve turuncu olduğunda hasat edilen meyvelerde kusur olmamalı ve meyve sinekleri tarafından zarara uğratılıp uğratılmadığı dikkatle incelenmelidir (Love ve ark. 2007).

Ağırlığı yaklaşık 10 g, genişliği 1,6-4 cm olabilen kamkat meyvesi küresel, oval, yuvarlak veya yumurtamsı şekle sahiptir. Küçük meyve içi 3-6 parçadan meydana gelmektedir ve asitli veya yarı asitli ve ekşi tatta olup fazla sulu değildir. Kabuğu orta kalınlıkta, pürüzsüz yapıda ve meyveye sıkıca bağlıdır. Rengi turuncu sarı olan kabuk, içerdiği flavonoid ve terpenoidler nedeniyle tipik bir aromaya sahip, tatlı ve yenilebilirdir. Meyve çekirdeği, küçük, sivri uçlu ve olgunlaşmanın başında yeşil renkli olup bazı meyvelerde bulunmamaktadır (Anonim 2021; Wang ve ark. 2012; Yıldız Turgut ve ark. 2015).

Vitaminler ve polifenoller gibi antioksidan ve antimikrobiyal aktivite sergileyen çeşitli besin öğesi ve fitokimyasalları içerdiği bilinen kamkat meyvesi çürümeye karşı çok hassastır. Genellikle *Penicillium digitatum* başta olmak üzere küflerin etkisiyle depolama sırasında oldukça çabuk bozulmaktadır (Schirra ve ark. 1995; Li ve ark. 2022). Soğuk depolama, meyve kalitesini korumak ve patojen gelişimini önlemek için iyi bir araç iken, çürüme gelişimini tamamen engelleyememektedir. Kamkatın kalitesini korumak ve raf ömrünü artırmak için çeşitli hasat sonrası teknolojiler uygulanmaktadır (Palma ve D'Aquino 2018). Genellikle kamkat meyvesi, çekirdekleri hariç olmak üzere kabuğu ile birlikte taze olarak tüketilmektedir. Bunun yanı sıra reçel, marmelat, jöle, sos, şurup, likör, şarap, turşu, şekerleme, sufle, sorbe ve Moğol eti yemeği yapımında kullanılabilmektedir (Love ve ark. 2007; Sadek ve ark. 2009; Wang ve ark. 2012; Yıldız Turgut ve ark. 2015; Pinheiro-Sant'Ana ve ark. 2019). Literatürde kamkat meyvesinin taze veya kurutularak ya da püre ve toz haline getirilerek çeşitli gıdaların üretiminde kullanılmasına ve bu gıdaların bazı özellikleri üzerine etkilerinin incelenmesine yönelik çalışmalar bulunmaktadır. Bu derlemede kamkatın muhafazası ve gıda üretimindeki kullanımına yönelik yapılmış çalışmaların bir araya getirilmesi amaçlanmıştır.

2. Materyal ve Metot

Bu çalışmada kamkatın farklı yöntemlerle muhafazası ve çeşitli gıdaların üretiminde kullanımı ile bu gıdaların bazı özellikleri üzerine etkisi konusunda yapılan ulusal ve uluslararası bilimsel çalışmalar derlenmiştir.

3. Bulgular ve Tartışma

3.1. Kamkatın Kimyasal Bileşimi

Turunçgil meyveleri, birbirlerinden önemli düzeyde farklı kimyasal profil sergilemektedir (Kim ve ark. 2021). Bunlar arasında kamkat, gerek besin öğeleri gerekse fitokimyasallar açısından mükemmel bir kaynak olması ile ön plana çıkmaktadır. Lif, şeker ve mikroelementler yönünden zengin ve besleyici bir meyve olan kamkatın besin içeriği ve sekonder metabolitlerinin nitelik ve niceliği, farklı kültürel uygulamalar, üretim alanları, iklim koşulları, genetik çeşitlilik gibi faktörlere bağlı olarak değişiklik göstermektedir (Palma ve D'Aquino 2018). 100 g taze kamkatın besin öğeleri ve miktarları tablo 1'de gösterilmiştir.

Kamkatın karbonhidrat içeriği 12,42 g/100 g sukroz, 10,36 g/100 g fruktoz ve 9,47 g/100 g glukozdan oluşmaktadır (Shanmugavelan ve ark. 2013). Kamkat meyve suyunda baskın organik asit sitrik asit olup onu malik, tartarik ve maleik asit izlemektedir (Koh ve ark. 1993).

Tablo 1. Kamkatın besin öğeleri miktarı (USDA 2021)

Besin öğesi	Miktar	Besin öğesi	Miktar
Su	80,8 g	Kalsiyum	62 mg
Enerji	71 kcal	Demir	0,86 mg
Protein	1,88 g	Magnezyum	20 mg
Toplam lipid (yağ)	0,86 g	Fosfor	19 mg
Kül	0,52 g	Potasyum	186 mg
Karbonhidrat	15,9 g	Sodyum	10 mg
Diyet lif	6,5 g	Çinko	0,17 mg
C vitamini	43,9 mg	Bakır	0,095 mg
Tiamin	0,037 mg	Kolin	8,4 mg
Riboflavin	0,09 mg	A vitamini	15 µg
Niasin	0,429 mg	α-karoten	155 µg
Pantotenik asit	0,208 mg	β-kriptoksantin	193 µg
B6 vitamini	0,036 mg	Lutein + zeaksantin	129 µg
Folat	17 µg	E vitamini (α tokoferol)	0,15 mg

Çoklu doymamış yağ asidi miktarı, tekli doymamış ve doymuş yağ asidi miktarından fazla olan kamkatın lipit miktarı %0,26 ile %0,37 arasında değişmektedir. Yapısında en fazla bulunan doymuş yağ asitleri palmitik ve stearik asittir. Kamkatın tekli doymamış yağ asidi miktarı %19,28-%25,01 düzeyindedir ve en yüksek miktarda bulunan tekli doymamış yağ asidi oleik asittir. Doymuş ve tekli doymamış yağ asidi miktarı birbirine yakın olmasına rağmen çoklu doymamış yağ asidi miktarı bunların iki katı seviyesinde olan kamkat, %46,59-%52,03 oranında çoklu doymamış yağ asidi içermektedir. Bunun da %34,08 gibi önemli kısmını α-linoleik asit oluşturmaktadır. α-linolenik asit ve eikosapentaenoik asit de kamkatta bulunan çoklu doymamış yağ asitleri arasında yer almaktadır (Güney ve ark. 2015).

Kamkatın uçucu yağları turunçgillerde olduğu gibi kabukta yoğunlaşmıştır. Uçucu yağ kompozisyonunu 90'dan fazla bileşiğin oluşturduğu bildirilmektedir. Bunların arasında terpenler en tipik bileşik olup limonen en fazla bulunan terpendir ve tüm yağın %90'ından fazlasını oluşturmaktadır. Diğer önemli bileşenler ise mirsen (~%1,84), linalool (~%1,4) ve etil asetattır (~%1,13). Kabuk yağındaki ana bileşen limonen olmakla birlikte kabuk yağının karakteristik aromasını veren bileşiğin sitronelil asetat olduğu ifade edilmektedir. Kamkat esansiyel yağları, terpenil alkol ve esterlerin daha fazla çeşidini ve seskiterpenleri daha yüksek miktarda içermesi ile turunçgillerden ayrılmaktadır (Palma ve D'Aquino 2018). Gıda endüstrisinde kamkat esansiyel yağları, aroma vermek, antioksidan ve antimikrobiyal etkisinden yararlanmak üzere kullanım imkanına sahiptir. Bu bağlamda ekstraksiyon yöntemi önem taşımakta olup kamkat esansiyel yağlarının hidrodistilasyon yöntemiyle ekstraksiyonunda ultrason ve mikrodalga önişlemleri, esansiyel yağ kimyasal bileşimini belirgin bir şekilde etkilememekle birlikte ekstraksiyon verimini ve 2,2-difenil-1-pikrilhidrazil (DPPH) radikal süpürme aktivitesini artırmaktadır (Yu ve ark. 2021).

Kamkatın kabuğu, meyve etine göre fenolik bileşik ve flavonoid içerik yönünden daha zengindir. Olgunlaşmaya bağlı olarak meyvenin fenolik bileşik ve flavonoid içeriği azalmaktadır. Olgunlaşmış kamkat kabuk ve meyve etinde toplam fenolik bileşik miktarı kuru ekstraktta gallik asit eşdeğeri (GAE) olarak sırasıyla 1362 mg GAE/100 g ve 799 GAE mg/100 g'dır. Olgunlaşmamış kamkat kabuk ve meyve etinde toplam fenolik bileşik miktarı sırasıyla 3000 GAE mg/100 g ve 1540 GAE mg/100 g (kuru ekstrakt)'dır (Lou ve ark. 2016). Kamkat meyve etindeki başlıca fenolik bileşikler ponsirin, didymin, isorhoifolin, hesperidin, narirutin olarak bildirilmiştir (Ramful ve ark. 2011). Kamkat kabuğundaki fenolik bileşikleri oluşturan temel gruplar *C*-glikolize flavonlar, *O*-glikolize flavonlar, *C*-glikolize flavanonlar, *O*-glikolize flavanonlar, flavonoller, kalkonlar, fenolik asitler ve türevleridir (Sadek ve ark., 2009). İçerdiği flavonoid ve uçucu yağ gibi bileşenler sayesinde kamkat antioksidan kapasiteye sahiptir (Palma ve D'Aquino 2018). DPPH radikal süpürme aktivitesi ve demir iyonu indirgeyici antioksidan güç yöntemleri ile elde edilen sonuçlar, kamkat meyve kabuğunun farklı turunçgil kabukları ile kıyaslandığında en güçlü antioksidan kapasiteyi sergilediğini göstermiştir (Chen ve ark. 2021).

Meyvesi ekşi olan kamkatın tatlı olan kabuğu, terpenoid ve flavonoidler nedeniyle tipik bir aromaya sahiptir (Wang ve ark. 2012). Bu sayede çeşitli gıdaların üretiminde aroma verici etkisinden yararlanmak üzere kullanımına yönelik çalışmalar yapılmıştır (Mousa ve ark. 2011; He ve ark. 2015; Aamer ve ark. 2017).

Kamkatta 11 karotenoid saptanmış olup bunların toplam miktarının 2185,16 µg/100 g olduğu bildirilmektedir. Bunlardan β-karoten, β-kriptoksantin, lutein ve zeaksantin serbest halde, sitraurin-kaproat, sitraurin-laurat, sitraurin-miristat, sitraurin-palmitat, kriptoksantin-laurat, kriptoksantin-miristat, kriptoksantin-palmitat esterleşmiş halde bulunmaktadır. β-sitraurin-laurat ve β-kriptoksantin-laurat kamkatta en fazla bulunan karotenoidlerdir (Pinheiro-Sant'Ana ve ark. 2019). Kamkat meyve eti oldukça az miktarda karotenoid içermesine rağmen, kabuk meyveye göre fazla miktarda karotenoid içermektedir. β-sitraurin (%16,6), (9*Z*)-violaksantin (%16,9), β-kriptoksantin (%11,4) ve violaksantin (%9,8) kabuktaki başlıca karotenoidlerdir (Agócs ve ark. 2007). Çeşitli meyve ve sebzelerde sarı, turuncu, kırmızı gibi renklerden sorumlu olan karotenoidler, kamkatta bulunan sağlığa faydalı ikincil metabolitler arasında yer almaktadır. Karotenoidlerin sağlığa faydalı etkileri arasında pro A vitamini aktivitesi göstermesi, antioksidan etkisi olması, kanser oluşumunu engellemesi yer almaktadır. Sağlık üzerine olumlu etkilerinin bulunmasının yanı sıra karotenoidlerin gıdalarda renklendirici olarak doğal ve yapay formları kullanılmaktadır (Ötleş ve Atlı 1997). Bu durum, karotenoid içeriği yüksek olan kamkatın gıda formülasyonlarında kullanılmasıyla ürünün rengini olumlu yönde etkileyeceği yönündeki görüşlere dayanak oluşturmaktadır. Nitekim kamkat ilavesinin bisküvi, kek, yoğurt, dondurma gibi ürünlerin rengini olumlu yönde etkileyebileceği gösterilmiştir (Mousa ve ark. 2011;

Çakmakçı ve ark. 2015; Aamer ve ark. 2017; Olcay 2019; Yıldız Turgut ve ark. 2019).

Yangılanma önleyici, antibakteriyal, antifungal, antiülser ve antitümör etkilerinin olduğu ifade edilen fitosteroller de kamkatın bileşiminde yer almaktadır (Ateş ve Velioğlu 2005). Kamkatın 12,56 µg/g fitosterol içerdiği, bunun da kuru ağırlıkta 1,02 µg/g kampesterol, 1,33 µg/g stigmasterol, 7,04 µg/g sitosterol, 10,45 µg/g amirin, 8,43 µg/g lupenon'dan oluştuğu bildirilmektedir (Chen ve ark. 2017).

3.2. Kamkatın Muhafazası ve Depolanması

Amerika ulusal gıda kompozisyonu veri tabanına göre, 100 g taze kamkatın 80,8 g'ı sudan oluşmaktadır (USDA 2021). Bu da su oranı yüksek diğer meyve sebzeler gibi kamkatın kısa sürede bozulmasına neden olabilmektedir. Ayrıca turunçgil grubundaki meyvelerden biri olan kamkatın hasat sonrası raf ömrünün nispeten kısa olmasının bir nedeni de yüksek oranda *Penicillium* gibi patojenik bir mikroorganizmanın etkisiyle çürümesidir (Ladaniya 2008; Youssef ve ark. 2014). Günümüzde kamkatın depolanması sırasında amaçlanan yalnızca mikrobiyolojik ve kimyasal bozulmaları önlemek değil aynı zamanda faydalı bileşenlerin yüksek oranda korunmasını sağlamaktır (Yıldız Turgut ve Topuz 2020). Taze kamkat 2-4°C'de depolandığında, ticari depolarda 1-2 ay, ev tipi buzdolaplarında ise 2-3 hafta bozulmadan kalabilmektedir. Oda sıcaklığında ise 1-2 gün dayanabilmektedir (Love ve ark. 2007).

Hasat sonrası depolama ve nakliye sürecinde su kaybı, esmerleşme, çürüme ve mekanik yaralanmalar nedeniyle besin değeri, aroma ve görünüş gibi niteliklerde bozulmalar meydana gelmekte ve depolama süresi kısalmaktadır (Hosseini ve ark. 2019). Bundan dolayı kamkatın raf ömrünü uzatabilecek çeşitli muhafaza yöntemleri üzerine araştırmalar yürütülmüş olup soğukta muhafaza, kurutma, UV-C uygulaması, bitki ekstraktları ve dezenfektan kullanımı ve kaplama bunlar arasında yer almaktadır.

Muhafaza yöntemlerinden biri olan kurutma işlemi ile meyvenin sahip olduğu su oranı ve su aktivitesi (a_w) değeri düşürülerek depolama esnasında mikrobiyolojik, kimyasal veya biyokimyasal yollarla bozulmasının ve kalitesini kaybetmesinin önlenmesi amaçlanmaktadır (Cemeroğlu 2011).

Farklı kurutma yöntemlerinin kamkatın bazı özellikleri üzerine etkisini incelemek amacıyla yapılan bir çalışmada, kamkat dilimlerinin bir kısmı kurutma öncesi haşlama işlemine tabi tutulmuş, bir diğer kısım ise herhangi bir ön işleme tabi tutulmadan kurutulmuştur. Kamkat meyvesi, sıcak hava, mikrodalga destekli sıcak hava kurutma, ultrason destekli ozmotik ön kurutma sonrası sıcak hava ile tamamlayıcı kurutma ve vakum olmak üzere 4 ayrı kurutma işlemi uygulanarak nem oranı yaş baza göre %12±1 oluncaya kadar kurutulmuştur. Kurutma sonrası, düşük yoğunluklu polietilen torbalar içerisinde 100 g'lık kamkat dilimleri 4 ay boyunca 22-24°C oda sıcaklığında depolanmıştır. Depolama süresi boyunca her ay ürünlerin nem miktarı, a_w, renk değerleri (L*, a*, b*, kroma, hue açısı, toplam renk değişimi), 5-hidroksimetilfurfural (HMF) ve askorbik asit içerikleri bulunarak, bunlardaki değişim gözlemlenmiştir. Depolamanın sonunda nem içeriği ve a_w değerinde en yüksek artışın sırasıyla ön işlemli ultrason destekli ozmotik ön kurutma sonrası sıcak hava ile tamamlayıcı kurutma ve sıcak hava ile kurutma yöntemleri ile kurutulan örneklerde belirlendiği bildirilmiştir. Örneklerin HMF değerleri incelendiğinde en yüksek artışın ön işlemsiz ultrason destekli ozmotik ön kurutma sonrası sıcak hava ile tamamlayıcı kurutma ve en düşük artışın ise ön işlemsiz mikrodalga destekli sıcak hava kurutma yönteminde gerçekleştiği araştırmacılar tarafından belirlenmiştir. Çalışma sonucunda en yüksek askorbik asit kaybının ön işlemli ultrason destekli ozmotik ön kurutma sonrası sıcak hava ile tamamlayıcı kurutma, en düşük askorbik asit kaybının ise ön işlemsiz ultrason destekli ozmotik ön kurutma sonrası sıcak hava ile tamamlayıcı kurutma yönteminde tespit edildiği ortaya konmuştur (Yıldız Turgut ve Topuz 2020).

Kamkatın depolama süresine etki eden bir diğer uygulama meyvenin klor ile muamele edilmesidir. Sıcaklığı 22°C olan klor çözeltisine 30 saniye daldırılarak klorlanan meyvede 0. ve 7. günde görünür bir küf gelişimi gözlenmediği, 14. günde, yüzey alanının %4,48'inde küf oluşumunda dikkate değer bir artış olduğu ve 28. günde ise küf yayılımının yüzey alanının %13,62'sine ulaştığı tespit edilmiştir (Kassim ve ark. 2016). Klor çözeltileri kamkatta küflenmeyi geciktirmesi, az maliyetli ve uygulamasının kolay olması sebebiyle kullanılsa da olası kanserojenik bileşiklerin oluşumu gibi insan sağlığını etkileyen bir durum söz konusu olduğu için klora alternatif uygulamaların araştırıldığı ifade edilmektedir (Korkmaz ve Tiryaki Gündüz 2018). Bu uygulamalardan biri olan UV-C ışığın germisidal etkisini inceleyen çalışmalar bulunmaktadır. UV-C ışığı uygulamasının hasat sonrası turunçgillerde görülen ve bozulmalara neden olan *P. digitatum* ve *Penicillium italicum* mikroorganizmalarını inaktif hale getirip depolama ömrünü uzatmak amacıyla kullanılabileceği gösterilmiştir (Gündüz ve Pazır 2013; Gündüz ve ark. 2015). Gündüz ve Pazır (2013) UV-C işlemi uyguladıktan sonra 6 gün boyunca 25°C'de depoladıkları turunçgillerde küf gelişiminin 3 kat daha düşük olduğunu belirlemiştir.

Bitki ekstraktlarından elde edilen bazı doğal bileşenlerin antimikrobiyal ve antioksidan aktivite göstererek meyvenin tazeliğini koruyabileceği ve raf ömrünü artırabileceği ifade edilmektedir. Bu bileşenlerden biri olan ellagik asit uygulamasının fizyolojik ve biyokimyasal fonksiyonlarındaki azalmayı ve doku hasarını engelleyerek kamkat meyvesinin kalitesini önemli ölçüde koruduğu tespit edilmiştir. Bu sayede meyvenin raf ömrünü 14-16°C'de 2 ila 6 gün arasında bir süre uzatarak 13 güne çıkardığı bildirilmektedir. Söz konusu çalışmada ellagik asit uygulanmamış kontrol örnekleri ile karşılaştırıldığında ellagik asit uygulamasının meyve çürümesi oranını %22,63'e indirdiği, meyve sertliği, toplam suda çözünür kuru madde, titre edilebilir asitlik ve C vitamini içeriği

seviyelerindeki düşüşü yavaşlattığı gösterilmiştir (Liu ve ark. 2018).

Yenilebilir kaplamaların uygulanmasının fiziksel hasarı önlemek, görünümü iyileştirmek ve meyve çürümesini azaltmak için uygun maliyetli bir yaklaşım olabileceği ifade edilmektedir. Nitekim sater otu ve tarhun otu esansiyel yağları kullanılarak hazırlanan kitosan bazlı kaplamaların kamkatın depolanması sırasında ağırlık kaybını azaltmada ve titre edilebilir asitlik ile C vitamini içeriğini korumada etkili olduğu gösterilmiştir. İlaveten 30 günlük depolamanın sonunda duyusal yönden kabul edilemez olarak değerlendirilen kaplanmamış kontrol örneklerine kıyasla kaplanmış olan kamkatın duyusal yönden kabul edilebilirliğinin çok daha yüksek olduğu ortaya konmuştur (Hosseini ve ark. 2019).

3.3. Kamkatın Gıdaların Üretiminde Kullanımı

Kamkat meyvesinin tatlı bir aromaya sahip olan kabuğu, meyvenin en tatlı kısmıdır. Merkezi ekşi olan meyve, kabuğu ile birlikte yenildiğinde alışılmadık ferahlatıcı bir lezzet vermektedir (Abobatta 2016). Bu nedenle taze olarak tüketimi tercih edilebildiği gibi kamkat meyvesinin çeşitli gıdaların üretiminde taze veya kurutularak kullanılması, püre veya toz haline getirilerek kullanılması gibi uygulamalar da mevcuttur.

Farklı yöntemlerle elde edilen kamkat tozlarının fonksiyonel özelliklerinin belirlenmesi amacıyla gerçekleştirilen bir çalışmada kamkat meyveleri blender kullanılarak püre haline getirildikten sonra %10 maltodekstrin ilave edilerek ve maltodekstrinsiz olarak sıcak havada ve dondurarak kurutma yöntemleri ile kurutmanın ardından öğütülerek toz haline getirilmiştir. Toplam fenolik madde, flavonoid ve karotenoid miktarı, antioksidan aktivite ve flavonoid kompozisyonu gibi fonksiyonel özellikler açısından karşılaştırıldığında dondurarak kurutulan maltodekstrinsiz kamkat tozunun diğerlerinden üstün olduğunu ve maltodekstrin ilavesinin dondurarak kurutma yöntemiyle elde edilen toz üründe askorbik asit içeriğini, sıcak hava ile kurutma yönteminde ise flavonoid bileşenlerin miktarını olumlu etkilediğini belirleyen araştırmacılar, kamkat tozlarının kek, pasta, puding, ekmek, meyveli içecek gibi ürünlerde aroma verici, renklendirici ve fonksiyonel katkı maddesi olarak kullanılma imkanı bulabileceğini vurgulamıştır (Yıldız Turgut ve ark. 2019). Nitekim Olcay (2019) ve Olcay ve Demir (2021) tarafından yapılan çalışmalarda, konveksiyonel, mikrodalga ve vakumlu kurutma uygulanan kamkat meyveleri öğütücüden geçirilerek meyve tozu haline getirilmiş ve buğday unu ağırlığının %10, 20 ve 30'u olacak şekilde kamkat tozu ikameli bisküvi ve kek üretiminde kullanılmıştır. Kamkat tozu ilave edilen bisküvi ve kek örneklerinin renginin koyulaştığı, bunun istenmeyen bir durum olmakla birlikte kamkat tozunun kendine has rengi ile sarılık ve kırmızılığın da artmasının ürünlerin albenisini artırdığı ve en iyi renk değerlerinin mikrodalga yönteminin kullanıldığı ürünlerden elde edildiği ifade edilmiştir. Araştırmacılar tarafından, kamkat tozu ikamesinin, örneklerin fenolik bileşik içeriğinde yüksek miktarda artış, fitik asit içeriğinde ise büyük oranda düşüş sağlaması nedeniyle kamkat tozlu kek ve bisküvilerin mineral emilimi fazla, antioksidan kapasitesi yüksek fonksiyonel ürünler olarak düşünülebileceği belirtilmiştir. Kamkat tozu ilave edilmesinin bisküvilerin fiziksel özelliklerini geliştirdiği ve kamkat tozu ikameli bütün örneklerin beğenilerinin yüksek ve kabul edilebilir nitelikte oldukları tespit edilmiştir. Kamkat meyvesinin kurutulmasında mikrodalga kurutmanın en uygun yöntem olduğu belirlenen çalışmalar sonucunda, %10 kamkat meyve tozu ikamesinin duyusal kabul edilebilirlik açısından en uygun oran olduğu ve kurutulmuş kamkat meyve tozlarının bisküvi ve kek üretiminde kullanımı ile bu ürünlerin kimyasal ve besinsel özelliklerinin geliştirilebileceği ve fonksiyonelliğinin artırılabileceği ortaya konmuştur. Kamkat meyvelerinin kek üretiminde kullanıldığı bir başka çalışmada He ve ark. (2015), taze kamkat meyvelerini kullanarak selenyumca zengin kek üretimi gerçekleştirmiştir. Organik selenyum katkısı için selenyumca zengin mayanın tespit edildiği araştırmada, en uygun jel ajanları formülasyonunun agar: karragenan: pektin=2:2:1 şeklinde olduğunu tespit eden araştırmacılar, optimum kamkat meyve keki formülasyonunu, kamkat meyve püresi: beyaz toz şeker: malt şurubu: jel ajanları: sitrik asit=40:20:40:3:0,4 olarak bildirmiştir. Tabaka kalınlığı 8 mm olacak şekilde hazırlanan kek karışımının, 60°C sıcaklıkta 20 saat pişirilmesi ile elde edilen kekin, zengin kamkat aroması, tekdüze doku, iyi bir tat ve esneklik gösterdiği ortaya konmuştur. Toplam selenyum içeriğinin 229 µg/kg'a ve organik selenyum içeriğinin 198 µg/kg'a ulaşması nedeniyle, meyveli kekin selenyum açısından zengin bir ürün olarak kabul edilebileceği bildirilmiştir. Kamkat meyvesi kullanımının, keklerin yanı sıra çeşitli ürünlerin tat, aroma, renk gibi duyusal özelliklerini iyileştirdiğini ortaya koyan çalışmalar mevcuttur. Çakmakçı ve ark. (2015), kamkatı dondurma üretiminde kullanarak dondurmanın kalite özellikleri üzerine etkisini incelemiştir. Bu amaçla meyveler çekirdekleri çıkartıldıktan sonra blender kullanılarak ezme haline getirilmiş ve elde edilen kamkat ezmesi bir dondurma karışımına ağırlıkça %5, 10 ve 15 oranında ilave edilerek kamkatlı dondurmalar üretilmiştir. İlave edilen kamkat ezmesi oranı arttıkça, potasyum ve magnezyum mineralleri, C vitamini, toplam fenolik ve flavonoid bileşik miktarı ve hacim artışı değerinde artma meydana geldiği ve %10 ve 15 kamkat ezmesi ilavesinin ilk damlama süresini ve tam erime süresini artırdığı tespit edilmiştir. En yüksek lezzet puanına %10 kamkat ezmesi ilavesi, en yüksek renk puanına %15 kamkat ezmesi ilavesi ile üretilen dondurmaların sahip olduğu bildirilen çalışma sonucunda, kamkat ezmesi ilave edilmesinin dondurmanın duyusal özelliklerini olumlu etkilediği ve bu nedenle dondurma üretiminde doğal renk ve aroma maddesi kaynağı olarak kullanılabileceği bildirilmiştir. İlave olarak elde ettikleri bulgulara göre araştırmacılar, kamkat ezmesinin doğal antioksidan kaynağı olarak değerlendirilebileceğini ifade etmiştir. Kamkat püreli düşük kalorili yoğurt üretimi yapan Mousa ve ark. (2011), blenderdan geçirerek püre haline getirdikleri meyveyi, sakkaroz, fruktoz, stevia ve bunların karışımları ile tatlandırdıkları yoğurt örneklerine ilave etmiştir. Yoğurtlara üretimden sonra ve 7 ile 14 gün depolamanın ardından

kimyasal, fiziksel ve mikrobiyolojik analizler yapılmıştır. Buna göre 14 gün depolamanın ardından en yüksek protein oranına sakkaroz ile hazırlanan kamkatlı yoğurdun, en yüksek β-karoten oranına sakkaroz-stevia karışımı ile tatlandırılan kamkatlı yoğurdun sahip olduğu belirlenmiştir. Yapılan duyusal değerlendirme sonucu, sakkaroz ile hazırlanan kamkatlı yoğurdun tat-aroma, tekstür ve renk yönünden en yüksek değerlere, stevia ile hazırlanan yoğurdun ise en düşük değerlere sahip olduğu ortaya konmuştur. Peynir endüstrisi yan ürünleri, yoğurt kültürü ve kamkat kullanılarak fonksiyonel içecek üretiminin yapıldığı bir çalışmada Aamer ve ark. (2017), çekirdekleri çıkartılan meyvelerin blenderdan geçirildikten sonra cam kavanozlarda 10 dk süreyle 90°C'de ısıtılmasıyla hazırlanan kamkat püresi ve bu pürenin %43-44 kuru madde olacak şekilde şeker ilave edilerek kaynatılmasıyla hazırlanan kamkat ezmesininin, kalsiyum, potasyum ve magnezyum gibi mineraller, β-karoten, C vitamini, toplam fenolik asitler ve flavonoidler yönünden iyi birer kaynak olduklarını ve yüksek antioksidan kapasitesine sahip olduklarını bildirmiştir. Aynı çalışmada, kamkat püresi ve ezmesi ile peynir endüstrisi yan ürünlerinin farklı oranlarda karıştırılması ile hazırlanan tüm içeceklerin, yalnızca peynir endüstrisi yan ürünleri kullanılarak hazırlanan içeceklerden toplam fenol, flavonoid, askorbik asit, β-karoten miktarı ve antioksidan aktivite yönünden daha zengin oldukları ve kamkat püresi ve ezmesinin ilave edilmesinin içeceklerin kabul edilebilirliğini arttırdığı ortaya konmuştur. Bu verilerden yola çıkan araştırmacılar, kamkat püresi ve ezmesinin kolay erişilebilir bir antioksidan kaynağı ve potansiyel bir gıda takviyesi olarak kullanılabileceğini, peynir endüstrisi yan ürünleri kullanılarak üretilen içeceklerde aromayı, besin değerini ve doğal rengi geliştirmek üzere kullanılabileceğini bildirmiştir.

Literatürde kamkat meyve suyuna yönelik yapılan çalışmalar da bulunmaktadır. Olgunlaşmış ve olgunlaşmamış kamkat meyvelerinden elde edilen meyve suyunun flavonoid bileşen içeriği ve antioksidan özelliklerinin incelendiği bir çalışmada, 13 flavonoid bileşen tanımlanmış ve olgunlaşmamış kamkat meyvelerinden elde edilen meyve suyunun, olgun meyvelerin suyundan, flavonoidlerce daha zengin olduğu saptanmıştır. En yüksek miktarda bulunan bileşiğin, olgunlaşmış ve olgunlaşmamış meyvelerden elde edilen meyve suyunda sırasıyla 19,94±0,29 mg/L ve 62,49±0,50 mg/L düzeyinde bulunan ploretin 3′,5′-di-C-β-glukozid olduğu tespit edilmiştir. Tanımlanan diğer bileşiklerin 3,0 mg/L'den daha düşük miktarlarda bulunduğu ve bunların birçoğunun, özellikle olgun meyvelerin suyunda, yalnızca eser miktarlarda (<0,1 mg/L) var olduğu belirlenmiştir. Olgunlaşmış ve olgunlaşmamış meyve sularının DPPH radikaline karşı anlamlı antioksidan etki gösterdiği ve olgunlaşmış meyvelerden elde edilen meyve sularının en yüksek etkinliğe sahip olduğu bildirilmiş olup kamkat suyunun antioksidan aktiviteyi güçlendirmeye yönelik diyetlere önemli katkı sağlayabileceği ifade edilmiştir (Barreca ve ark. 2011). Zeng ve Huang (2011), elde ettikleri kamkat suyunun acılığını gidermek amacıyla naringinaz enzim muamelesi uygulamış ve bu işlem için ideal koşulların, enzim dozajı 1,4 g/L (enzim aktivitesi 414 U/g), enzim uygulama sıcaklığı 41°C ve uygulama süresi 101 dakika şeklinde olduğunu tespit etmiştir. Söz konusu koşullar altında acılık giderme oranının %48,23'e ulaştığı bildirilmiştir. Koh ve ark. (1993), kamkat suyunun organik asit kompozisyonunun %58,27 sitrik asit, %32,49 malik asit, %9,14 tartarik asit ve %0,08 maleik asitten oluştuğunu ve malik asit içeriği yönünden ülkemizde Rize mandalinası olarak bilinen Satsuma mandarininden oldukça farklı olduğunu ortaya koymuştur. Aynı çalışmada kamkat suyu ve portakal suyunun farklı oranlarda kullanılmasıyla hazırlanan reçellerin bazı kalite özellikleri de incelenmiştir. Kamkat suyu kullanılmadan hazırlanan reçelde 1,294 g-force olan sertlik değeri, reçeldeki kamkat suyu oranı arttıkça düşmüş ve %100 oranında kamkat suyu ile hazırlanan reçelde 355 g-force olarak belirlenmiştir. Reçelde kullanılan kamkat suyu oranının artmasının diğer tekstürel özelliklerde ise çok büyük değişikliklere yol açmadığını ifade eden araştırmacılar, duyusal değerlendirme yapıldığında %40-60 oranında portakal suyu içeren kamkat reçelinin panelistler tarafından portakal reçeline göre daha üstün olarak değerlendirildiğini bildirmiştir. Kamkat meyvesinin reçel üretiminde kullanılabilirliğinin ve kamkat reçelinin bazı fiziksel ve kimyasal özelliklerinin incelendiği bir başka çalışmada çekirdekleri uzaklaştırılan ve 3 parçaya bölünen meyveler, kabuktaki acılık maddelerini uzaklaştırmak amacıyla kaynar suda 15 dakika haşlanmalarının ardından açık kazanda pişirme tekniği ile reçel üretiminde kullanılmışlardır. Titrasyon asitliği, pH, suda çözünür kuru madde, toplam kuru madde, CIE L, a*, b* renk değerleri, toplam kül ve bazı mineral madde analizleri yapıldığında, elde edilen reçellerin Türk Gıda Kodeksi Reçel, Jöle, Marmelat ve Tatlandırılmış Kestane Püresi Tebliği'nde verilen kriterlere uygun olduğu tespit edilmiştir. Taze meyve ile kıyaslandığında reçeldeki mineral maddelerin miktarında düşüş gözlemlenmekle birlikte miktar yönünden çoktan aza doğru sırasıyla potasyum, kalsiyum magnezyum, fosfor ve demir içeren kamkat reçelinin insan sağlığı ve beslenmesinde önemli bazı mineral maddeler bakımından da iyi bir kaynak olduğu belirtilmiştir (Yıldız Turgut ve ark. 2015).

Kamkatın sirke, likör, şarap gibi ürünlerin eldesinde değerlendirilmesi de söz konusudur. Liu (2011), kamkat sirkesi üretiminde alkol ve asetik asit fermantasyonlarının optimum koşullarını belirlediği çalışmasında, alkol fermantasyonu için optimum koşulların başlangıç şeker konsantrasyonunun %17, aktif kuru maya inokülasyon oranının %0,2 ve fermantasyon sıcaklığının 32°C olması ile elde edildiğini tespit etmiştir. Optimum asetik asit fermantasyon koşullarını ise, asetik asit bakterilerinin inokülasyon oranı %10, başlangıç alkol içeriği hacmen %7 ve fermantasyon sıcaklığı 32°C şeklinde bildirmiştir. Araştırmacı tarafından bu koşullar altında, kamkat sirkesinin asetik asit içeriğinin 4,7 g/100 mL'nin üzerinde olduğu ortaya konmuştur. Wang ve ark. (2009a), AS1.41 asetik asit bakteri suşunu kullanarak sıvı hal fermantasyon koşullarında kamkat sirkesi üreterek fermantasyon sürecini incelemiştir. En uygun fermantasyon koşularını, başlangıç inokülasyon oranı %7 ve fermantasyon süresi 8 gün şeklinde tespit eden araştırmacılar, bu koşullarda kamkat

sirkesi asetik asit düzeyinin %4,69'a ulaştığını bildirmiştir. Wang ve ark. (2009b), kamkat sirkesi durultulmasında kitosan kullanımını incelemiştir. Optimum durultma koşulları, kitosan miktarı 1,25 g/L, durultma sıcaklığı 50°C ve durultma süresi 3 saat olarak belirlenmiştir. *Fortunella margarita* türüne ait kamkat meyve yağından geleneksel bir Yunan likörünün elde edilerek uçucu bileşenlerinin incelendiği bir çalışmada Kontaratou ve ark. (2007), meyve likörünün uçucu bileşenlerini ağırlıklı olarak sırasıyla %40,2 ve %10,3 oranında bulunan linalol ve limonenin oluşturduğunu ortaya koymuştur. Summo ve ark. (2016), kamkat kabukları ve kabuklu kamkat meyvesinden yaptıkları likörlerin uçucu bileşen kompozisyonunu, kabul edilebilirlik ve tercih edilirlik durumlarını belirleyerek greyfurt kabuğu likörü ve İtalyan limon likörü olan limoncello ile karşılaştırmıştır. Çalışmada kamkat kabuğu likörünün uçucu bileşen sayısı yönünden diğerlerinden daha zengin olduğu belirlenmiştir. Kabuklu kamkat meyvesi likörünün diğerlerinden daha az uçucu bileşen içermesinin nedeninin, yalnızca kabukların kullanılmasının kabuk ile alkol arasında yüksek temas alanı yaratması ve tahrip olan hücrelerin uçucu bileşiklerin daha iyi ekstrakte edilmesine imkan vermesi olabileceği ifade edilmiştir. Karbonil, alkol ve esterlerin oksijenli bileşiklere oranının likörde aroma kalitesinin önemli bir göstergesi olduğunu belirten araştırmacılar, kamkat likörlerinin limoncellodan daha düşük oksijenli bileşik içeriğine sahip olmasına rağmen kabul edilebilirliklerinin yüksek olduğunu ve yüksek seskiterpen alkol içeriği sayesinde kabuklu kamkat meyve likörünün umut vaat ettiğini bildirmiştir. Zhang ve Liu (2010), şeker ve bal gibi yardımcı maddeler de kullanarak oval kamkat kabuğu likörü üretmiştir. Çalışmada 10 g oval kamkat kabuğu liksiviasyonu için 50 mL Luzhou aromalı likör kullanılmış ve liksiviasyon 4 gün sürmüştür. Bu işlemin ardından alkol oranı hacimce %20 ve şeker içeriği %15 olana kadar tatlandırıcı ile karıştırılmış ve tekrar oval kamkat kabuğu ilave edilerek 2 gün liksiviasyon uygulanmıştır. β-siklodekstrin %0,04 oranında kullanılarak acılığın giderilmesinin ve %0,04 jelatin uygulamasının ardından elde edilen likörün parlak, yarı saydam ve hoş bir tat ve aromaya sahip olduğu ortaya konmuştur. Chen ve ark. (2014), kamkat kabuk yağının fazla miktarda uçucu yağ içeriği nedeniyle fermantasyonu engellemesi ve pektinaz kullanımının neden olduğu fazla metanol oluşumu durumlarının önüne geçmek için şıra eldesinde bir ısı ekstrakt yöntemi uygulamıştır. Isıl işlemin fermantasyon oranını artırabileceğini ve bu şekilde elde edilen ürünün %10,29-13,20 (v/v) etanol içerdiğini ortaya koymuştur. Fermantasyon sürecinde değerlerde azalma olmakla birlikte, ısıl işlem uygulanmayan ve pektinaz ile muamele edilen şıra ile kıyaslandığında, ısıl işlem uygulamasının polifenol bileşik içeriğini ve antioksidatif aktiviteyi artırabileceği belirlenmiştir. Pektinaz kullanılan ve ısı ekstrakt yöntemi uygulanan ürünlerin 3 ay olgunlaştırılmasının ardından etanol içerikleri (%13) karşılaştırıldığında fark olmadığı görülürken, metanol içeriklerinin ise anlamlı farklılık gösterdiği belirlenmiş ve ısı ekstrakt yönteminin kamkat şarabının metanol içeriğini önemli ölçüde azaltabileceği bildirilmiştir. İlaveten araştırmacılar uçucu asitliğin 1,5 g/L (asetik asit cinsinden) olarak bildirildiği yasal düzenleme göz önüne alındığında şarabın uçucu asitliğinin bu değerin altında ve toplam asitliğinin 4,5-4,7 g/L olduğunu ortaya koymuş ve esmerleşme reaksiyonunun 200 ppm kükürt dioksit ile önlenebileceğini ifade etmiştir.

4. Sonuç

Kamkat meyvesi, vitamin, mineral, karotenoid, flavonoid ve uçucu yağ içeriğince zengin ve önemli antioksidan aktivitesi olan bir meyvedir. Yararlı bileşenler içeren bu meyve sağlık alanında eskiden beri Çin halkı tarafından terapötik olarak kullanılmıştır. Kabuğuyla birlikte tüketilebilmesi biyoaktif maddelerin alımı yönünden kamkatı, turunçgillere kıyasla önemli hale getirmektedir. Taze olarak tüketilmesinin yanında çeşitli yiyecek tariflerinde de kullanılabilen kamkatın raf ömrü depolama koşullarına bağlı olarak değişmektedir. Kalite kaybını azaltmak ve raf ömrünü artırmak amacıyla soğukta muhafaza, kurutma, modifye atmosfer paketleme, kaplama, UV-C, bitki ekstraktları ve dezenfektan ile muamele gibi uygulamalar kullanılabilmektedir. İçerdiği bileşenlerin sağlık üzerine olumlu etkilerinden yararlanmak ve gıdaların duyusal özelliklerini geliştirmek amacıyla kullanılabilirliğini incelemeye yönelik çalışmalar yapılmış olup taze olarak, kurutularak, püre, ezme veya toz haline getirilerek kamkatın bisküvi, kek, dondurma, yoğurt ve fonksiyonel içecek gibi çeşitli gıda formülasyonlarına katılması yoluyla ürünlerin fonksiyonelliğinin artırılmasını, renk, aroma ve besin değeri gibi özelliklerinin iyileştirilmesini sağlayabileceği gösterilmiştir. Buna ek olarak meyve suyu, reçel, sirke, likör ve şarap gibi ürünlerin üretiminde değerlendirilmesinin mümkün olduğu araştırmacılar tarafından yapılan çalışmalar ile ortaya konmuştur. Bu alanda araştırmaların sürdürülmesi ürün çeşitliliğinin artmasına ve potansiyel fonksiyonel ürünlerin ortaya çıkmasına imkan tanıyacaktır. Hem gıda güvenliği hem de tüketiciye ulaşmadan önce ve ulaştıktan sonra yaşanan meyve kayıplarının yarattığı ekonomik zarar göz önüne alındığında uygun depolama koşulları ve muhafaza yöntemlerinin önemi ortaya çıkmaktadır. Bundan dolayı kamkatın taşınması ve depolanması esnasında gereksinim duyduğu koşullar sağlanmalı ve ihtiyaç halinde uygun muhafaza yöntemlerinden yararlanılmalıdır. Bu kapsamda kamkatın muhafazasına yönelik olarak yapılacak yeni ve ayrıntılı çalışmaların farklı alternatifler yaratması açısından önem arz ettiği düşünülmektedir.

Kaynaklar

Aamer RA, El-Kholy WM, Mailam MA. 2017. Production of functional beverages from whey and permeate containing kumquat fruit. Alex J Fd Sci & Technol. 14(1):41-56.

Abobatta W. 2016. Kumquat trees *Fortunella* sp. https://www.researchgate.net/publication/322775804_Kumquat_Tree. Erişim tarihi 3 Ekim 2021.

Agócs A, Nagy V, Szabó Z, Márk L, Ohmacht R, Deli J. 2007. Comparative study on the carotenoid composition of the peel and the pulp of different citrus species. IFSET. 8:390-394.

Ateş J, Velioğlu S. 2005. Kolesterole karşı yeni silahımız: bitki sterolleri. Gıda Mühendisliği Dergisi. 20:55-58.

Barreca D, Bellocco E, Caristi C, Leuzzi U, Gattuso G. 2011. Kumquat (*Fortunella japonica* Swingle) juice: flavonoid distribution and antioxidant properties. Food Res Int. 44:2190-2197.

Cemeroğlu BS. 2011. Meyve ve Sebze İşleme Teknolojisi. Nobel Akademik Yayıncılık, Ankara.

Chen LC, Ye RA, Dai KF, Lin SB. 2014. Characteristics and antioxidative properties of the kumquat wine produced from heat-extracted must. Taiwan. J Agric Chem Food Sci. 52(4, 5, 6):143-153.

Chen MH, Yang KM, Huang TC, Wu ML. 2017. Traditional small-size citrus from Taiwan: essential oils, bioactive compounds and antioxidant capacity. Medicines. 4(2):28.

Chen Y, Pan H, Hao S, Pan D, Wang G, Yu W. 2021. Evaluation of phenolic composition and antioxidant properties of different varieties of Chinese citrus. Food Chem. 364:1-10.

Citrus pages. 2021. Kumquats and kumquat hybrids *Citrus japonica* Thunb. (formerly *Fortunella* Swingle). http://citruspages.free.fr/kumquats.php. Erişim tarihi 3 Ekim 2021.

Çakmakçı S, Topdaş EF, Çakır Y, Kalın P. 2015. Functionality of kumquat (*Fortunella margarita*) in the production of fruity ice cream. J Sci Food Agric. 96:1451-1458.

Gündüz GT, Juneja VK, Pazır F. 2015. Application of ultraviolet-C light on oranges for the inactivation of postharvest wound pathogens. Food Control. 57:9-13.

Gündüz GT, Pazır F. 2013. Inactivation of *Penicillium digitatum* and *Penicillium italicum* under *in vitro* and *in vivo* conditions by using UV-C light. J Food Prot. 76(10):1761-1766.

Güney M, Öz AT, Kafkas E. 2015. Comparison of lipids, fatty acids and volatile compounds of various kumquat species using HS/GC/MS/FID techniques. J Sci Food Agric. 95:1268-1273.

He XM, Sun J, Li L, Sheng JF, Zheng FJ, Li JM, Liu GM, Li CB. 2015. Study on production process of selenium-rich kumquat fruit cake. Southwest China Journal of Agricultural Sciences. 28(6):2736-2741.

Hosseini S, Ivanov D, Dolgui A. 2019. Review of quantitative methods for supply chain resilience analysis. TRANSPORT RES E-LOG. 125:285-307.

Kassim A, Workneh TS, Laing MD, Basdew IH. 2016. The effects of different pre-packaging treatments on the quality of kumquat fruit. CYTA J Food. 14(4): 639-648.

Kim DS, Lee S, Park SM, Yun SH, Gab HS, Kim SS, Kim HJ. 2021. Comparative Metabolomics Analysis of Citrus Varieties. Foods. 10: 1-15.

Koh JS, Kim CS, Ko MS, Yang YT. 1993. Manufacture of processed foods and its quality characteristics from kumquats, a citrus variety produced in *Cheju*. Korean J Food Sci Technol. (25)1:33-38.

Kontaratou V, Graikou K, Chinou I. 2007. Chemical analyses of the essential oils of three *Fortunella* cultivars and a Greek traditional kumquat liqueur. In: Abstracts of the 55th International Congress and Annual Meeting of the Society for Medicinal Plant Research, Graz, Austria, 2-6 September 2007.

Korkmaz A, Tiryaki Gündüz G. 2018. Meyve ve sebzelerde UV-C ışık uygulamaları ile küf inhibisyonu. Akademik Gıda. 16(4):58-469.

Ladaniya MS. 2008. Citrus fruit. Biology, Technology and Evaluation. London, UK, Elsevier.

Li X, Meenu M, Xu B. 2022. Recent development in bioactive compounds and health benefits of kumquat fruits, Food Rev. Int. 1-21.

Liu J. 2011. Production technology of kumquat vinegar. China, Brewing, 12.

Liu Y, Liu Y, Liu Y, Liu H, Shang Y. 2018. Evaluating effects of ellagic acid on the quality of kumquat fruits during storage. Sci Hortic. 227:244-254.

Lou SN, Ho CT. 2017. Phenolic compounds and biological activities of small-size citrus: Kumquat and calamondin. J Food Drug Anal. 25:162-175.

Lou SN, Lai YC, Hsu YS, Ho CT. 2016. Phenolic content, antioxidant activity and effective compounds. Food Chem. 197:1-6.

Love K, Bowen R, Fleming K. 2007. Twelve fruits with potential value-added and culinary uses. University of Hawai'i College of Tropical Agriculture and Human Resources, Hawai.

Mousa RAS, Abd El-Rahman HAA, El-Massry FHM. 2011. Effect of some natural sweeteners on yoghurt with fruit (kumquat) during storage. Egypt J Agric Res. 89(3):1039-1051.

Olcay N. 2019. Farklı teknikler ile kurutulmuş kamkat meyvesinin, bisküvi ve kek üretiminde kullanım imkânları. Yüksek Lisans Tezi. Konya: Necmettin Erbakan Üniversitesi Fen Bilimleri Enstitüsü.

Olcay N, Demir MK. 2021. Effect of kumquat (*Fortunella margarita*) powders dried by different methods on some physical and chemical properties of cake. J. Food Meas. Charact. 15:5360-5368.

Ötleş S, Atlı Y. 1997. Karotenoidlerin insan sağlığı açısından önemi. Pamukkale Univ Muh Bilim Derg. 3(1):249-254.

Pinheiro-Sant'Ana HM, Anunciação PC, Souza CS, Paula Filho GX, Salvo A, Dugo G, Giurida D. 2019. Quali-Quantitative profile of native carotenoids in kumquat from brazil by HPLC-DAD-APCI/MS. Foods. 8(166):1-10.

Ramful D, Tarnus E, Aruoma OI, Bourdon E, Bahorun T. 2011. Polyphenol composition, vitamin C content and antioxidant capacity of Mauritian citrus fruit pulps. Food Res Int. 44:2088-2099.

Sadek ES, Makris DM, Kefalas P. 2009. Polyphenolic composition and antioxidant characteristics of kumquat (*Fortunella margarita*) peel fractions. Plant Foods Hum Nutr. 64:297-302.

Schirra M, Agabbio M, Continella G, D'Aquino S. 1995. Extension of kumquat fruit storage life by postharvest hot dip treatments in water and freshening agent. Adv Hort Sci. 9:83-86.

Shanmugavelan P, Kim SY, Kim JB, Kim HW, Cho SM, Kim SN, Kim SY, Cho YS, Kim HR. 2013. Evaluation of sugar content and composition in commonly consumed Korean vegetables, fruits, cereals, seed plants, and leaves by HPLC-ELSD. Carbohydr Res. 380:112-117.

Summo C, Trani A, Faccia M, Caponio F, Gambacorta G. 2016. Volatiles and acceptability of liqueurs from kumquat and grapefruit. Ital J Food Sci. 28:258-270.

USDA 2021. Fooddata central kumquat, raw. https://fdc.nal.usda.gov/fdc-app.html#/food-details/1102593/nutrients. Erişim tarihi 15 Kasım 2021.

Wang D, Shangguan XC, Jiang Y. 2009a. A study on the technique for fermentation of kumquat vinegar. Acta Agric Univ Jiangxi. 31(1):114-118.

Wang D, Shangguan XC, Jiang Y. 2009b. Clarification technology of kumquat vinegar. China, Brewing. 2009-04.

Wang YW, Zeng WC, Xu PY, Lan YJ, Zhu RX, Zhong K, Huang YN, Gao H. 2012. Chemical composition and antimicrobial activity of the essential oil of kumquat (*Fortunella crassifolia* Swingle) peel. Int J Mol Sci. 13:3382-3393.

Yıldız Turgut D, Çınar O, Seçmen T. 2019. Farklı yöntemlerle elde edilen kamkat (*Fortunella margarita* Swing.) tozlarının fonksiyonel özelliklerinin belirlenmesi. Gıda. 44(4): 605-617.

Yıldız Turgut D, Gölükcü M, Tokgöz H. 2015. Kamkat (*Fortunella margarita* Swing.) meyvesi ve reçelinin bazı fiziksel ve kimyasal özellikleri. Derim. 32(1):71-80.

Yıldız Turgut D, Topuz A. 2020. Depolama süresinin farklı kurutma yöntemleri ile kurutulmuş kamkat dilimlerinin bazı kalite özelliklerine etkisi. YYÜ Tar Bil Derg. 30(1):44-56.

Youssef K, Sanzani SM, Ligorio A, Ippolito A, Terry LA. 2014. Sodium carbonate and bicarbonate treatments induce resistance to postharvest green mould on citrus fruit. Postharvest Biol Technol. 87:61-69.

Yu F, Wan N, Zheng Q, Li Y, Yang M, Wu Z. 2021. Effects of ultrasound and microwave pretreatments on hydrodistillation extraction of essential oils from kumquat peel. Food Sci Nutr. 9:2372-2380.

Zeng LL, Huang HH. 2011. Optimization of debitterizing of kumquat juice by naringinase with response surface method. Food Sci Technol. 5:315-318.

Zhang P, Liu XW. 2010. Development of oval kumquat liqueur. Liquor-Making Science & Technology. 2.

EJBCS